R82-34

INFILTRATION AND EVAPORATION AT INHOMOGENEOUS LAND SURFACES

by
P. CHRISTOPHER D. MILLY
and
PETER S. EAGLESON

Ralph M. Parsons Laboratory
Hydrology and Water Resource Systems

Report Number 278

This material is based upon work supported by the National Science Foundation under Grant Numbers ATM-7812327 and ATM-8114723

June 1982

MIT

DEPARTMENT
OF
CIVIL
ENGINEERING

SCHOOL OF ENGINEERING
MASSACHUSETTS INSTITUTE OF TECHNOLOGY
Cambridge, Massachusetts 02139

R82-34

INFILTRATION AND EVAPORATION AT INHOMOGENEOUS LAND SURFACES

by

P. Christopher D. Milly

and

Peter S. Eagleson

Ralph M. Parsons Laboratory

Hydrology and Water Resource Systems

Report Number 278

This material is based upon work supported by
the National Science Foundation under
Grant Numbers ATM-7812327 and ATM-8114723

June 1982

INFILTRATION AND EVAPORATION AT
INHOMOGENEOUS LAND SURFACES

Abstract

The local response of the land surface to atmospheric forcing is determined by the surface parameters, the surface state, and the forcing. Because these factors are highly variable at length scales smaller than those of many hydrologic analyses, and because they enter nonlinearly into the hydrologic response functions, the calculation of areal average response in terms of real physical parameters is non-trivial. Treating an inhomogeneous soil surface as a battery of independent, parallel soil columns, we calculate the areal average infiltration that results from a spatially variable storm event. The spatial variability of soil and storm properties turns out to be critical in shaping the infiltration function for an inhomogeneous basin. A particular feature of the average response is that increased spatial variability of soil type or of storm depth almost invariably leads to decreased infiltration and increased surface runoff.

The calculation of the areal average evapotranspiration rate is complicated by atmospheric advection, which provides a feedback mechanism whereby the downstream evaporation is influenced by the upstream. The upstream influence may persist over a fetch of hundreds of kilometers. A conceptual model of the atmospheric boundary layer is developed and applied to the analysis of evapotranspiration from a surface whose supply of water and energy may be characterized by spatially variable canopy resistances and available energies (net radiation minus heat flux into the ground). The surface roughness is also considered to be variable in space. An explicit dependence of areal average evapotranspiration upon the patch size -- the characteristic length of the variability -- is derived. The effect of local advection is shown to be most significant when there is a great variation of the canopy resistance between patches. Otherwise, the individual patches behave in a relatively independent manner. This points to the importance of spatial variability of the water supply in the analysis of areal average evapotranspiration.

ACKNOWLEDGEMENTS

This work was performed with the support of the National Science Foundation under research grants Numbers ATM-7812327 and ATM-8114723, and under its Graduate Fellowship program.

This document is essentially Part B of the doctoral thesis submitted by P. Christopher D. Milly to the Department of Civil Engineering at M.I.T. Its completion was supervised by Dr. Peter S. Eagleson, Professor of Civil Engineering.

TABLE OF CONTENTS

LIST OF FIGURES

Figure No.		Page No.

LIST OF TABLES

NOTATION

NOTE: Most of the symbols used are listed here. Some minor symbols that are used infrequently are not listed. Occasionally, a single symbol takes two meanings when confusion seems unlikely.

Symbol	Description
A	a dimensionless A_o
A_o	constant term in Philip's cumulative infiltration equation
a	$Z_w n(1-s_o)$
a_i	relative proportion of area having patch type i
B	maximum water table depth
CV	coefficient of variation of α
c	$d\ell nK/d\ell ns$
c_p	specific heat of air at constant pressure
D	dimensionless soil storage capacity
d	height in atmosphere above which u and K_z are approximated as constants
d	$c-1-1/m$
E	evaporation rate
E_i	evaporation rate at patch type i
E_i'	normalized E_i
$\overline{E}$	average E over all patches
$\overline{E}'$	normalized $\overline{E}$
e	vapor pressure of water
e_f	free-stream vapor pressure, height h'
e_h	vapor pressure at height h

Symbols	Description
e_i	vapor pressure in atmosphere, at ground level, above patch type i.
e_m	$e_s(\theta_m)$
e_s	saturation vapor pressure
e_{sf}	$e_s(\theta_f)$
e_{sh}	$e_s(\theta_h)$
e_z	vapor pressure at height z
e_o	vapor pressure at evaporation source
e_{oi}	$e_s(\theta_{oi})$
F_i	cumulative depth of infiltration
f_i	actual infiltration rate
f_i^*	infiltration capacity
f_{s_o}	p.d.f. of s_o
f	p.d.f. of α
F_1	c.d.f. of u_1
F_2	c.d.f. of u_2
G	heat flux into the ground
g	acceleration of gravity
H	sensible heat flux into atmosphere
H_i	sensible heat flux from patch type i
h	storm depth
h	average height of internal boundary layer
h'	average height of boundary layer associated with length ℓ'
h_o	maximum storm depth
h_o	height at which $K_z = \frac{1}{2} K_o$
$\bar{h}$	average storm depth
I	$F_i(t_r)/\bar{h}$

Symbol	Description
$\bar{I}$	areal average of I
i	rainfall intensity
K(1)	saturated hydraulic conductivity
$\bar{K}$	$K\alpha^{-2}$
$\underset{\approx}{K}$	turbulent diffusivity tensor
K_y	principal component of $\underset{\approx}{K}$ in y direction
K_z	principal component of $\underset{\approx}{K}$ in the vertical direction
K_o	maximum value of K_z
L	latent heat of vaporization of water
ℓ	typical patch dimension in wind direction
ℓ'	streamwise length of modeled evaporation area
m	$-(d\ell n\psi/d\ell ns)^{-1}$
N	number of patch types
n	porosity
q	$\rho c_p\ u_{*e}(e_{sf} - e_f)/\Delta\bar{R}$
R	radius of area modeled for infiltration
R	Rn - G
R_i	Rn - G at patch type i
R_s	surface runoff rate
R_v	gas constant for water vapor
$\bar{R}$	areal average of Rn - G
Rn	net radiation
r	distance from storm center
r_o	$r/\ell n(h_o/h)$
r_a	aerodynamic diffusion resistance

Symbol	Description
r_{ai}	aerodynamic diffusion resistance between patch type i and height h
r_c	canopy resistance
r_{ci}	r_c at patch type i
r_1	$(\sum^{N} a_i/r_{ai})^{-1}$
r_2	aerodynamic diffusion resistance between heights h and h'
S	dimensionless sorptivity
$\bar{S}$	$d(Rn - G)/dT_o$
S_i	sorptivity
s_o	initial soil moisture saturation for infiltration
T	temperature
T_f	temperature in free stream, height h'
T_z	temperature at height z
T_o	temperature at evaporation source
t	time
t_r	storm duration
t_o	time at which surface saturates due to Horton mechanism
t_1	time at which surface saturates due to Dunne mechanism
t'	apparent start of storm when f_i is in the falling stage
U	approximate windspeed above height d
u	windspeed
u_1	$h/\bar{h}$
u_2	Z_w/B

Symbol	Description
u_*	friction velocity
u_{*i}	u_* above patch type i
u_{*e}	effective u_* of modeled area
$\underset{\sim}{u}$	wind vector
Z_w	water table depth
z	height coordinate
z_o	surface roughness height
z_{oi}	z_o for patch type i
z_{oe}	effective z_o of modeled area
α	soil scaling factor
γ	psychrometric constant
Δ	slope of saturation vapor pressure curve
θ	potential temperature
θ_f	θ in free stream, height h'
θ_h	θ at height h
θ_m	typical temperature, for linearization of e_s
θ_{oi}	θ at patch type i
μ_n	mean of logarithm of α
μ_s	mean of s_o
μ_α	mean of α
ρ	density of air
σ_n	standard deviation of logarithm of α
σ_s	standard deviation of s_o
σ_α	standard deviation of α

Symbol	Description
Φ	advection decay function
ϕ_i	dimensionless infiltration sorptivity
ϕ_1, ϕ_2	functions used to approximate ϕ_i
Ψ_i	$-\rho c_p K_z \; \partial\psi_i/\partial z$
ψ	matric potential
ψ_1	$\gamma\theta + e$
ψ_2	$-\Delta\theta + e$
$\psi(1)$	bubbling potential
$\bar{\psi}$	$\alpha\psi$

Chapter 1

INTRODUCTION

1.1 An Overview

In many physically-based analyses of land surface hydrology, it is expedient, and therefore common, to employ a vertical, one-dimensional framework for modeling a finite area. This is the approach taken, for instance, by Milly and Eagleson (1982) in the development of a simple parameterization of the ground hydrology for use in an atmospheric general circualtion model (GCM). In the present work, we deal with the spatial variability of infiltration and evaporation within an inhomogeneous area, in particular with its effect upon the mean response. Simplified frameworks for analysis are adopted in order to obtain representative results without resorting to complex simulation models. After a general discussion of spatial variability (this chapter), we consider the problem of infiltration and surface runoff from a single storm, where storm quantities and soil properties vary spatially (Chapter 2). We then analyze the spatial variability of evapotranspiration, when a canopy resistance model applies, in Chapter 3. Chapter 4 is a summary of our conclusions.

1.2 Spatial Variability of Atmospheric Forcing and of Land Surface Parameters and States

The local response of the land surface to atmospheric forcing is determined by the surface parameters and by the forcing. Because these factors are highly variable at length scales smaller than, for example, the GCM grid scale, and because land surface processes are nonlinear, the analysis of the areal-average response is non-trivial.

The most non-uniform atmospheric forcing variable is apparently precipitation, with horizontal length scales as small as a few kilometers. Clearly, one inch of rain on ten percent of a region will not have the same hydrologic effect as one-tenth of an inch over the entire region. It is therefore necessary that information on the spatial (and possibly temporal) structure of a given storm be available for the parameterizations of land surface hydrology. Sensitivity studies using realistic models of the land surface are necessary in order to determine precisely what data are required.

A second inhomogeneity of atmospheric forcing results from the feedback effect of surface fluxes on downwind conditions due to advection. Thus, even over a perfectly homogeneous surface receiving a constant radiative input, evaporation and surface temperature would vary spatially downwind of a discontinuity in surface properties (Yeh and Brutsaert, 1971). On the basis of a very simple conceptual model, McNaughton (1976a,b) estimates a horizontal length scale of the order of ten kilometers for the re-establishment of a quasi-equilibrium Bowen ratio downwind of such a discontinuity. As we shall see, a more realistic estimate would be several hundred kilometers. Thus, although the driving force for evaporation - solar radiation - is fairly uniform in space, other convenient measures of atmospheric forcing, such as potential evaporation, may be highly variable due to advection and the variability of surface parameters.

The spatially variable atmospheric inputs are modulated further by the large variety of surface soil, vegetal, and geomorphological types. For example, even on relatively small, "homogeneous" plots of land, the hydraulic conductivity of the soil, which is critical in dividing rainfall into surface runoff and soil moisture storage, may range over a few orders of magnitude (Nielsen et al., 1973).

Geomorphology exerts control locally over the variations in soil, vegetation, and depth to the water table. Vegetation is important not only directly in the surface heat and water balances, but also indirectly through its influence on the turbulent boundary layer and its transport characteristics.

Due to the spatial variability of the water balance that results from all of the effects mentioned above, the amount of moisture stored in the soil at the beginning of an infiltration or evaporation period is itself spatially variable. Since infiltration and evaporation are sometimes sensitive to the moisture content, this is another source of inhomogeneity for them.

1.3 Lateral Interactions at the Land Surface

An extensive, inhomogeneous land surface may be viewed as a battery of parallel, vertical cells having varying characteristics. The behavior of the battery is complicated by the existence of several connections among the cells, which prevent any individual cell from operating independently. The cell corresponds to our one-dimensional soil system, and the connections are the various pathways for horizontal water flow.

Horizontal flow in the saturated zone averages the spatial variations in recharge and forms a relatively smooth water table. The depth to the water table at a given location is thus dependent upon recharge at other locations. Water flows laterally also in the unsaturated layers if there is a pronounced anisotropy or layering of the soil, if the surface slope is very steep, or if large lateral moisture gradients exist.

The surface drainage network conveys any rejected rainwater away from its point of impact. It therefore provides coupling between different locations by making the excess water available for infiltration elsewhere, either on the hillslope or in a channel.

The final avenue for lateral interaction is atmospheric advection, which was mentioned in the previous section. Atmospheric advection links different locations on the land surface by transporting air (with the contained heat and water vapor) from one surface to another. Upwind evaporation thus affects downwind evaporation.

Chapter 2

SPATIAL VARIABILITY OF INFILTRATION AND OF STORM SURFACE RUNOFF

2.1 Available Methods of Analysis

In order to approach the question of spatial variability, we must work with some kind of an areally distributed (as opposed to point) hydrologic model. Such a model will serve as an experimental apparatus. The conditions of the various experiments are defined by the specification of the spatial and temporal distributions (or the statistics) of atmospheric forcing and of the internal system parameters. Experimental results are obtained as model outputs. In this section we review a hierarchy of increasingly simplified distributed modelling alternatives, arriving eventually at the approach to be used later in this section. We consider here only the response to rainfall and thus ignore the atmospheric side of the problem that is important for evaporation. The role of vegetation is also neglected.

The most general physically-based approach to the analysis of spatial variability is by means of simulation, accounting for the full three-dimensional equations of porous media and pipe flow - flow through discrete subsurface channels, as described, for instance, by Atkinson (1978) - in the saturated and unsaturated zones and including the dynamics of overland and channel flow. Even if a computational model were available for such a system, the problem of specifying how soil properties and surface geometry vary and the problem of analyzing the impact of those variations on the system behavior would be immense.

One rather general alternative is the two-dimensional cross-sectional model, which is capable of simulating all of the processes mentioned above and has the added advantage of decreased dimensionality. Already, however, there is a loss of the representation of topographic hollows, which may be prime sites for the production of overland flow (Chorley, 1978), and of other geometrical effects. A computational model of this system, neglecting pipe flow, has been presented recently by Zaslavsky and Sinai (1981), who studied the effect of a surface transition layer of soil properties on the mechanism of lateral flow. Lateral variability of soil properties was not addressed.

If the further simplification is made that lateral flow in the unsaturated zone is negligible, the problem becomes more manageable computationally. The cross-sectional problem of parallel, vertical moisture flow beneath a surface experiencing overland sheet flow has been modeled by Smith and Woolhiser (1971a,b) and by Hillel and Hornberger (1979). The latter considered the sensitivity of storm surface runoff to the relative areal proportions of clay and loam soil and to their relative locations on the slope. For the assumed topography and storm, the first factor was more important, though the second was also significant, demonstrating the ability of overland flow to transport excess runoff to more permeable areas. The neglect of lateral flow in the unsaturated zone limits the generality of these results, although it could be argued that the near-surface throughflow, important in many catchments, is similar in character to overland flow.

In a similar study, Smith and Hebbert (1979) abandoned the one-dimensional partial differential equation governing moisture flow in favor of an infiltration equation. They modeled the areal response of a catchment with spatially variable soil properties during a storm event and found that surface runoff was significantly affected by both random and deterministic (i.e., having a trend) variations of soil properties. (Here, a "significant effect" means that the mean soil properties fail to reproduce the response observed with varying soil properties.)

The next step in conceptual simplification of the watershed models is to ignore the feedback effect of overland flow on infiltration. Precipitation that cannot infiltrate where it falls is assumed to enter and remain in the surface drainage network. Separate one-dimensional "soil columns" then remain only weakly coupled by the relatively static water table.

Sharma and Luxmoore (1979) used such a model, together with a vegetation parameterization, to study the effect of soil spatial variability on the monthly water balance of a small watershed. They found the effect to be most significant during the months when runoff-producing rainfall was frequent.

They speculate that the relatively small effect calculated for the evapotranspiration component may be attributable to their neglect of variation in vegetal type in the model.

In the same parallel, one-dimensional framework, Freeze (1980) was able to carry out a fairly extensive study of storm surface runoff from a hillslope, including an analysis of the temporal distribution of storm runoff. Stochastic fields for soil parameters, storm parameters, and topography were employed. Various sensitivity runs demonstrated the strong influence of spatial variability.

The last three analyses cited above employed computationally burdensome Monte-Carlo simulation techniques. It is reasonable to expect, however, that a similar, but simpler, approach dealing directly with the statistics of parameters, states, and forcing would capture the essential features of spatial variability and its effect on regional water and heat balances. For instance, such an approach has been applied successfully to the problem of averaging in time for the long-term mean components of the water balance (Eagleson, 1978).

2.2 A One-Dimensional Model of Infiltration

We shall employ the simplest of the modelling alternatives described above - the decoupled battery of parallel cells - in order to model spatial variability of infiltration and surface runoff. Two distinct mechanisms are considered to be active in preventing the infiltration of precipitation at a point (Freeze, 1980). The first, the so-called Horton mechanism, is the gradual increase of surface soil moisture and decrease of infiltration capacity that would occur during a storm when the water table is deep enough to have no influence. If the infiltration capacity decreases to less than the rainfall intensity, surface runoff from that point on the surface will occur. The second, the Dunne mechanism, is related to the finite storage capacity of the soil column. Since discharge from the saturated zone is slow relative to the storm time scale, total infiltration into a column has an upper bound given approximately by the initial air content of the medium between the surface and either the water table or a relatively impermeable soil layer. When this column becomes saturated, infiltration virtually ceases and all precipitation goes into surface runoff. Either or both of these mechanisms may be active at a given location during the course of a single storm. We shall proceed to quantify these mechanisms using infiltration theory. This development is essentially an extension of the work done by Eagleson (1978).

Philip (1957) has proposed a series approximation for the time-varying infiltration rate that results when a semi-infinite soil column at constant initial water content is subjected to saturation at the surface. For many purposes, it has been found that the first two terms of that series yield an adequate representation of the process. Thus,

$$f_i^*(t) = \frac{1}{2} S_i t^{-\frac{1}{2}} + A_o \qquad (2.1)$$

in which $f_i^*(t)$ is the infiltration rate, t is time elapsed, S_i is the infiltration sorptivity, and A_o is another infiltration parameter. From Eagleson's (1978) work, we may express the two infiltration parameters in terms of soil physical parameters and moisture content as

$$S_i = 2\left[\frac{5n\ K(1)\ \psi(1)}{3\pi m}\right]^{1/2} \phi_i\ (d, s_o)(1 - s_o) \tag{2.2}$$

and

$$A_o = \frac{1}{2}\ (1 + s_o^c)\ K(1) \tag{2.3}$$

in which ϕ_i is the dimensionless infiltration diffusivity, n is the effective porosity, K(1) is the value of hydraulic conductivity at full water saturation, and s_o is the initial moisture saturation of the soil. In the derivation of (2.2) and (2.3), the hydraulic characteristics of the soil are assumed to be given by the following expressions:

$$\psi(s) = \psi(1)s^{-1/m} \tag{2.4}$$

$$K(s) = K(1)s^c \tag{2.5}$$

In these equations, ψ is the matric potential, K is hydraulic conductivity, s is the saturation with respect to effective porosity, and c and m are constants related to the soil type.

The constant d in (2.2) is the exponent of s in the soil moisture diffusivity. Through the dependence of soil moisture diffusivity upon K and ψ, it is given by

$$d = c - 1 - 1/m \tag{2.6}$$

The dimensionless infiltration diffusivity is (Eagleson,1978)

$$\phi_i(d,s_o) = (1 - s_o)^d \sum_{n=o}^{d} (d + \tfrac{5}{3} - n)^{-1} \binom{d}{n} \left(\frac{s_o}{1 - s_o}\right)^n \tag{2.7}$$

for integer values of d. In order to separate the influence of s_o and d, we shall employ the following approximation to this function:

$$(1 - s_o)\ \phi_i(d,s_o) \cong (1 - s_o)\ \hat{\phi}_i(d,s_o) = \phi_1(d)\ \phi_2(s_o) \tag{2.8}$$

where

$$\phi_1(d) = \frac{4 + 5/3}{d + 5/3} \tag{2.9}$$

$$\phi_2(s_o) = (1 - s_o)\ \phi_i(4,s_o) \tag{2.10}$$

Figure 2.1 illustrates the error involved in this approximation. For small s_o, the approximation is good, while there is considerable error for some d when s_o is large. The overall behavior of the function is fairly well represented, however.

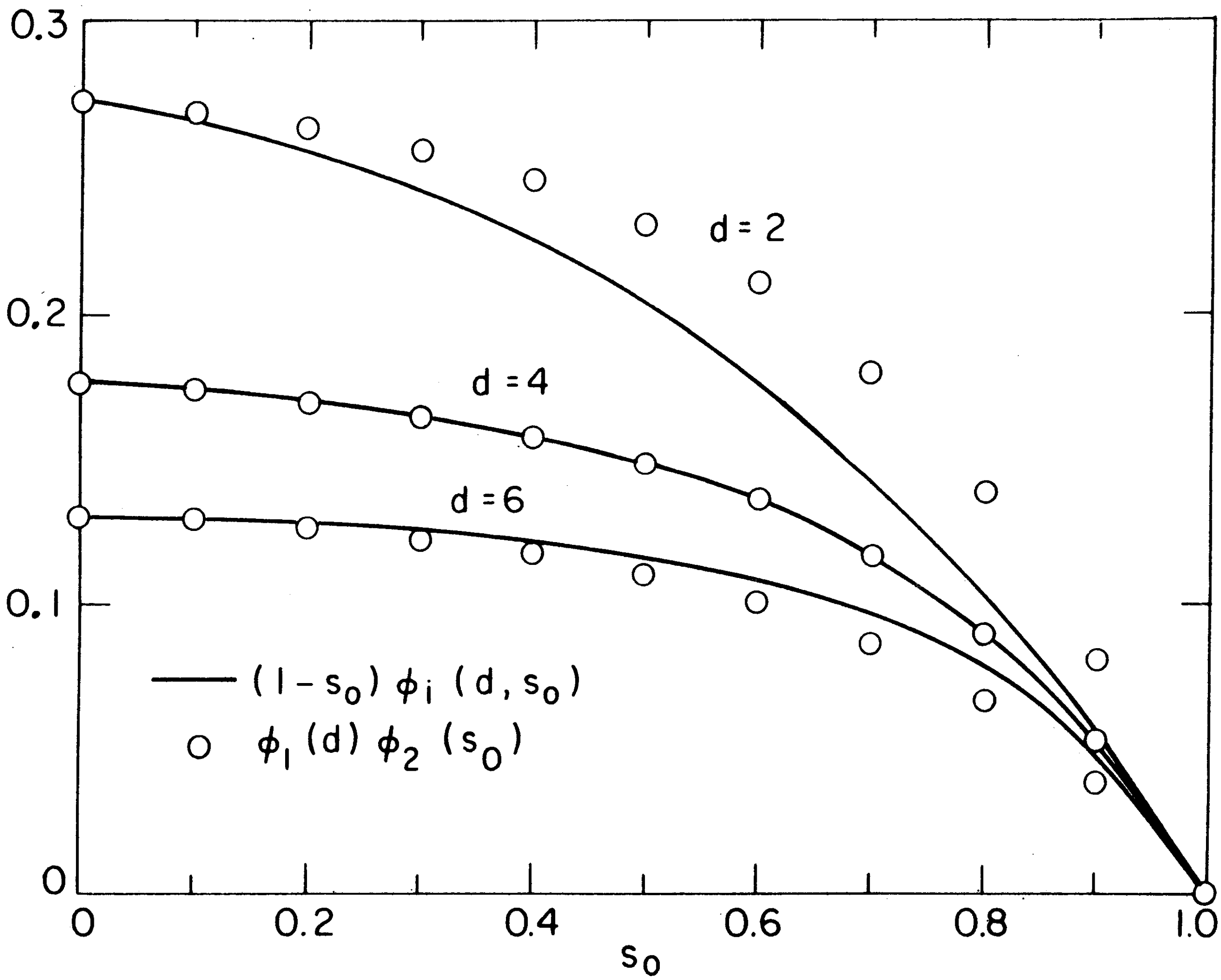

Figure 2.1

PLOT OF $(1-s_o)\phi_i(d,\ s_o)$ AGAINST s_o. CIRCLES INDICATE THE APPROXIMATE REPRESENTATION.

Furthermore, s_o will ordinarily have a small value at the end of an interstorm evaporation period.

Equation (2.1) applies to a fully saturated surface and predicts an infinite infiltration rate at t=0. At early times, the rate will actually be limited by the precipitation rate. We thus modify (2.1) in the following way:

$$f_i(t) = \begin{cases} i & 0 < t \leq t_o \\ f_i^*(t - t') & t_o < t \leq t_r \end{cases} \tag{2.11}$$

in which f_i is the actual infiltration rate, i is the constant precipitation rate during the storm of duration t_r, t_o is the time at which saturation of the surface occurs, and t' is the equivalent time origin assuming saturation conditions from the beginning. This model is pictured in Fig. 2.2. The approximate validity of (2.11) relies on the time-compression assumption, which has been justified theoretically (Reeves and Miller, 1975). The times t_o and t' may be calculated by imposing the conditions that the rate and cumulative depth of infiltration given by (2.11) be continuous at time t_o:

$$i = f_i^*(t_o - t') \tag{2.12}$$

$$it_o = \int_{t_o}^{t'} f_i^*(t - t')dt \tag{2.13}$$

Using the definition of f_i^* given in (2.1), we may solve

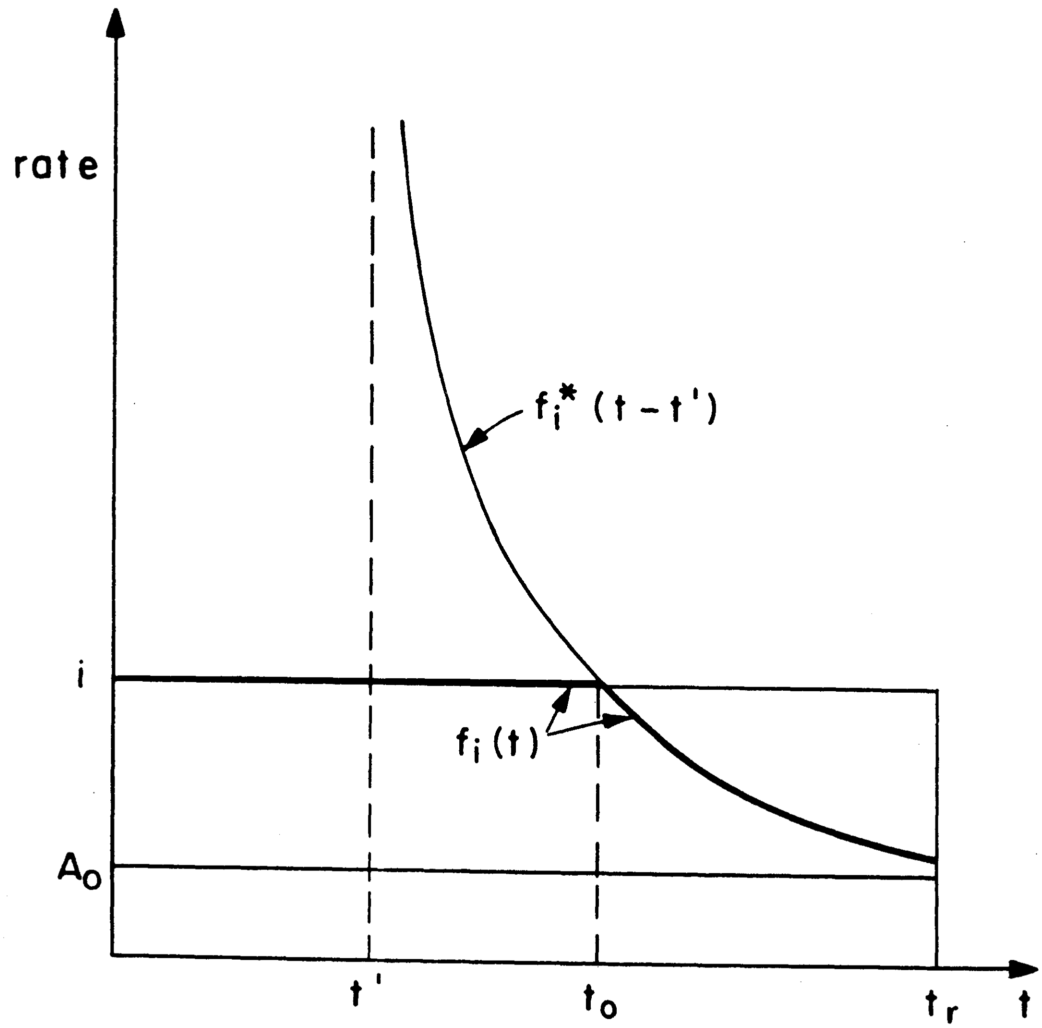

Figure 2.2

INFILTRATION RATE AS A FUNCTION OF TIME DURING A PRECIPITATION EVENT. MODIFIED AFTER EAGLESON (1978).

(2.12) and (2.13) for t_o and t'. The result is

$$t_o = \begin{cases} \dfrac{S_i}{2i(i-A_o)}\left[1 + \dfrac{A_o}{2(i-A_o)}\right] & i>A_o \\ \infty & i\leq A_o \end{cases} \tag{2.14}$$

$$t' = t_o - \frac{S_i}{4(i-A_o)^2} \tag{2.15}$$

where $t_o = \infty$ means that f_i^* is always greater than i, no matter how large t is.

Equation (2.11) is based on the assumption that moisture can infiltrate unimpeded by any subsurface obstacles. If a relatively impervious layer or a water table is present at some shallow depth, then the cumulative infiltration depth cannot exceed the depth-integrated air content above the barrier at the beginning of the event. We thus modify (2.11) to the form

$$f_i(t) = \begin{cases} i & 0 < t < \min(t_o, t_1, t_r) \\ f_i^*(t-t') & t_o < t < \min(t_1, t_r) \\ 0 & \min(t_1, t_r) < t \end{cases} \tag{2.16}$$

in which t_1 is the time at which the column becomes fully saturated. Equation (2.16) is a correct modification of (2.11) given the approximation that the surface infiltration rate is not affected by the lower barrier until full saturation occurs. This approximation seems reasonable when the water table is not too close to the surface. The errors introduced by it are probably no greater than those associated with the assumptions of constant initial saturation and time compression. For any given event, the second or third stage in (2.16), or both, may be absent, depending on the relative magnitudes of t_o, t_1, and t_r. The set of possibilities is depicted in Figure 2.3. In general, the value of t_1 may be expressed implicitly as

$$\int_{-Z_w}^{0} n(1-s_o)\, dz = \int_{0}^{t_1} f_i(t)dt \tag{2.17}$$

in which Z_w is the depth to the water table or to a relatively impervious layer. For a uniform initial soil moisture saturation, s_o,

$$Z_w\, n(1-s_o) = \int_{0}^{t_1} f_i(t)dt \tag{2.18}$$

Defining the cumulative infiltration, F_i, we have

$$F_i(t) = \int_{0}^{t} f_i(\tau)d\tau \tag{2.19}$$

or, applying (2.16),

$$F_i(t) = \int_{o}^{\min(t_o,t_1,t_r,t)} i\, d\tau + \int_{t_o}^{\max[t_o,\min(t_1,t_r,t)]} f_i^*(\tau - t')d\tau$$

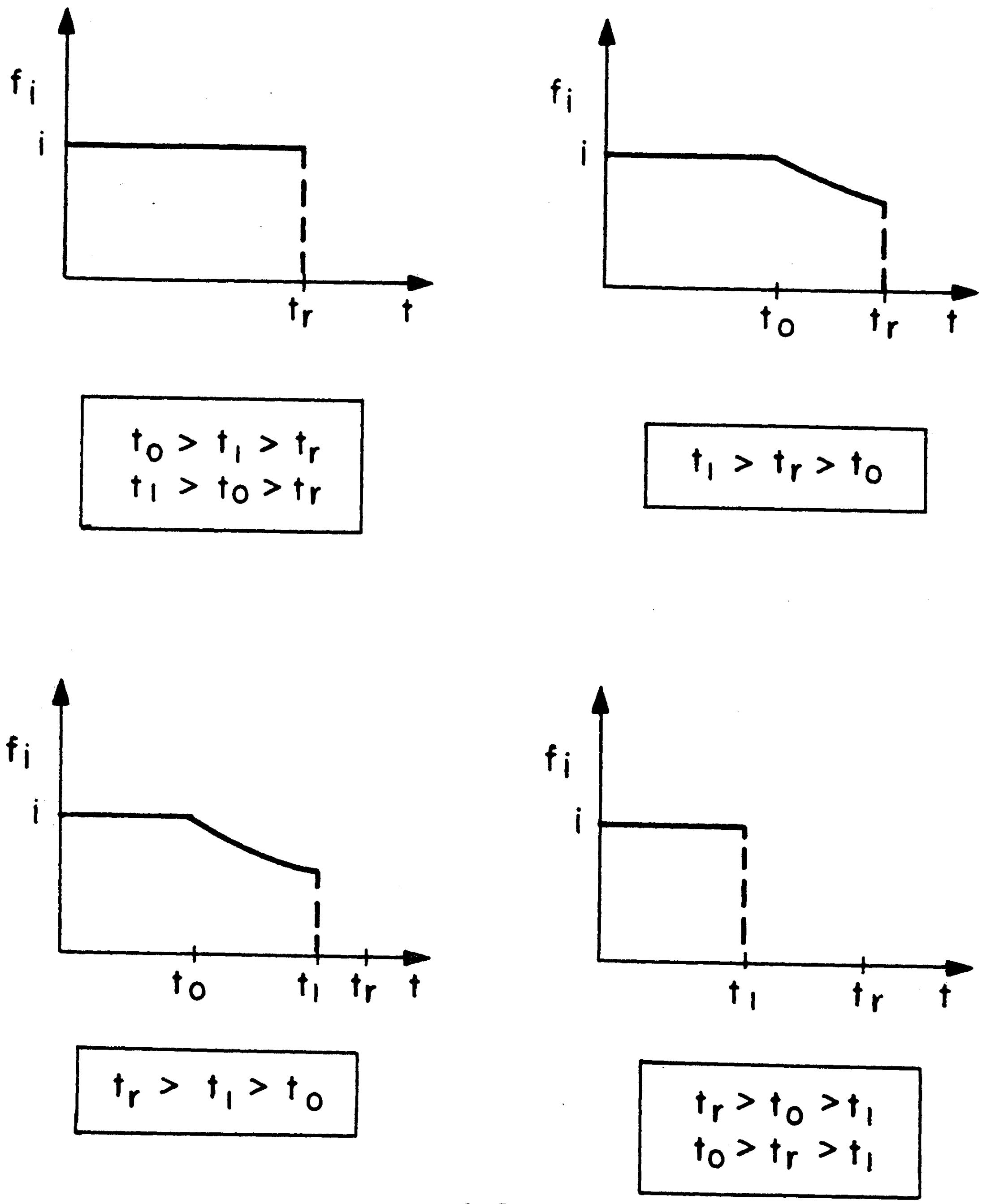

Figure 2.3

INFILTRATION RATE AS A FUNCTION OF TIME FOR THE VARIOUS RELATIVE MAGNITUDES OF THE CHARACTERISTIC TIMES.

$$= i \min(t_o, t_1, t_r, t)$$

$$+ \left[S_i(\tau - t')^{\frac{1}{2}} + A_o(\tau - t')\right]_{t_o}^{\max[t_o, \min(t_1, t_r, t)]} \qquad (2.20)$$

Thus, (2.18) may be reformulated as

$$Z_w\, n(1-s_o) = F_i(t_1) = i \min(t_o, t_1, t_r)$$

$$+ [S_i(\tau - t')^{1/2} + A_o(\tau - t')]_{t_o}^{\max(t_o, t_1)} \quad t_1 < t_r \qquad (2.21)$$

The solution of (2.21) for t_1 is

$$t_1 = \begin{cases} a/i & t_o > a/i \\ t' + \dfrac{S_i^2}{2A_o^2}\left[1 + \dfrac{2A_o a}{S_i^2}\left(1 + \dfrac{4A_o a}{S_i^2}\right)^{1/2}\right]; & t_o < a/i \end{cases} \qquad (2.22)$$

in which

$$a = Z_w\, n(1-s_o) \qquad (2.23)$$

Rather than study the temporal distribution of infiltration (and, hence, of runoff), we shall instead concentrate on the behavior of total storm infiltration, as given by

$F_i(t_r)$. This may be expressed as

$$F_i(t_r) = \min \left\{ a,\ i \min(t_o, t_r) + [S_i(\tau - t')^{1/2} + A_o(\tau - t')]_{\tau = t_o}^{\tau = \max(t_o, t_r)} \right\} \qquad (2.24)$$

or

$$F_i(t_r) = \begin{cases} \min(a,\ it_r) & t_r \leq t_o \\ \min\{a,\ it_o + S_i\left[(t_r - t')^{1/2} - (t_o - t')^{1/2}\right] + A_o(t_r - t_o)\} & t_o < t_r \end{cases} \qquad (2.25)$$

The total surface runoff, R_s, is given by

$$R_s = it_r - F_i(t_r) \qquad (2.26)$$

2.3 Stochastic Models of the Factors Determining Total Infiltration

Equations (2.25) and (2.26), together with (2.2), (2.3), (2.6), (2.14), (2.15), and (2.23), specify total infiltration and runoff as functions of the following variables:

$$i,\ t_r,\ K(1),\ n,\ c,\ m,\ \psi(1),\ s_o,\ Z_w$$

The parameters m and $\psi(1)$ may be expressed as functions of the other soil parameters using (Eagleson, 1978)

$$m = \frac{2}{c-3} \tag{2.27}$$

and

$$\psi(1) = \sigma\left(\frac{n}{\mu\gamma}\right)^{1/2}\left(10^{.66 + \frac{.55}{m} + \frac{.14}{m^2}}\right)^{-1/2} \tag{2.28}$$

in which σ is surface tension, μ is viscosity, and γ is specific weight of water. Then the following seven parameters remain:

storm . . . . i, t_r
soil type . . . . $K(1)$, n, c
soil state. . . . . s_o
water table/topography. . . . Z_w

Given that these parameters may all vary from point to point within an area of interest, infiltration and runoff will also be non-uniform. We shall study this non-uniformity by applying (2.25) in conjunction with probability density functions for the parameters.

2.3.1 Precipitation Parameters

The internal space-time structure of a precipitation event is complex and dependent on storm type. In this study, we are concerned primarily with spatial variability, and have therefore adopted the temporally constant intensity model employed in Section 2.2. In fact, the percentage mass curve (cumulative rainfall percentage versus percentage duration) is not a straight line and has a shape dependent on the storm type (Eagleson, 1970). If we ignore temporal variations in point intensity, then a storm is fully described by specifying i and t_r. Our description of spatial variability will then be embodied by the chosen spatial distributions for i and t_r.

At a given time during the storm, rainfall intensity varies widely in space. A discussion of the observed behavior is given by Gupta and Waymire (1979), and is briefly summarized here. Figure 2.4 illustrates the hierarchichal structure of a storm. Convective cells are the smallest recognizable features, typically 10 to 30 km^2 in area, and produce the most intense rainfall. Convective cells usually occur in cell clusters and small mesoscale areas (SMSA's). In the latter, the rainfall intensity outside, but close to, the cells is greater than in the surrounding area. In the former, there is no such region of intermediate intensity. Cell clusters and SMSA's are embedded in larger areas (10^3 - 10^4 km^2) called large mesoscale areas (LMSA's), in which the precipitation rate is relatively low. The LMSA is considered to be the largest common structural feature among a variety of storm types. In the case of synoptic scale ($>10^4$ km^2) storms, one or more LMSA's may be imbedded in the synoptic area. Rainfall intensities inside the LMSA's are higher than outside.

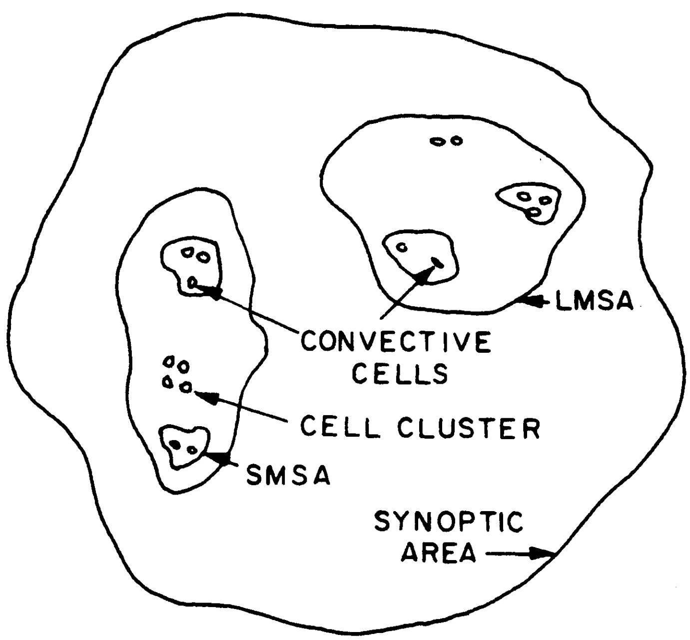

Figure 2.4

INSTANTANEOUS SPATIAL STRUCTURE OF A SYNOPTIC RAINSTORM

(from Gupta and Waymire, 1979).

Lifetimes of the various features range from several minutes for convective cells, to a few hours for an SMSA or LMSA, to a few days for a synoptic area. During their lives, they travel not only with respect to the ground, but also relative to each other. The average intensity (or total depth) at a point during a storm is thus determined by the chance passage overhead of the various storm features. The hierarchical range of intensity described above is smoothed out by the motion of the individual features.

A number of empirical studies indicate that total storm depth tends to have a single maximum in space, and that storm depth decreases uniformly with distance from this storm center. Many of these studies have been reviewed by Court (1961). A representative model is that of Boyer (1957). For storms of circular shape, it may be written as

$$h = h_o \exp(-r/r_o) \qquad (2.29)$$

in which h is the local total storm depth, h_o is its maximum, r is the distance from the storm center, and r_o is a characteristic horizontal dimension of the storm. For simplicity, we shall employ this model regardless of the lateral scale of the storm. In fact, the reduction of h with distance in convective storms is sharper than predicted by (2.29) (Eagleson, 1970), which therefore underestimates the spatial variability of depths generated by such events.

Using, (2.29), a distribution function for h can be defined over a specified area when the location of the storm center is known. We consider here a circular region of radius R whose center coincides with the storm center. The cumulative distribution function of storm depth is

$$F_H(h) = \frac{\text{area with storm depth less than h}}{\text{total area}}$$

$$= \frac{\pi R^2 - \pi (r_o \ln \frac{h_o}{h})^2}{\pi R^2}$$

$$= 1 - \left(\frac{r_o}{R}\right)^2 \left(\ln \frac{h_o}{h}\right)^2 \qquad h_o e^{-R/r_o} < h < h_o \quad (2.30)$$

The average storm depth within the modelled area is

$$\bar{h} = \frac{1}{\pi R^2} \int_o^{2\pi} \int_o^R h_o \, e^{-r/r_o} \, r dr d\theta$$

$$= 2 \, h_o \left(\frac{r_o}{R}\right)^2 \left[1 - e^{-R/r_o} \left(1 + \frac{R}{r_o}\right) \right] \qquad (2.31)$$

Defining a normalized storm depth,

$$u_1 = h/\bar{h} \qquad (2.32)$$

we obtain an alternative to (2.30),

$$F_1(u_1) = 1 - \left(\frac{r_o}{R}\right)^2 \left[\ln \left(\frac{h_o}{\bar{h}} u_1^{-1}\right)\right]^2; \quad \frac{h_o}{\bar{h}} e^{-R/r_o} < u_1 < \frac{h_o}{\bar{h}} \quad (2.33)$$

This function is plotted in Figure 2.5 for various values of the relative storm radius, r_o/R. For a GCM grid square, we have $R \sim 200$ km. The large value of $r_o/R=1$ then corresponds to a relatively uniform, synoptic scale storm. A lower limit of $r_o/R=10^{-2}$ would correspond to a small, isolated convective cell. For this case, the upper curve in Figure 2.5 reflects the concentration of most of the rainfall volume in a very small proportion of the area.

The frequency distribution proposed here is useful for characterizing the variability of h when the modelled area is large relative to the storm size. When the area is relatively small, this model incorrectly implies negligible variance of total storm depth. In fact, there will still be a random component resulting from the stochastic, cellular nature of true storms. The current model therefore underestimates the spatial variability of rainfall when the modelled area is small relative to the storm size but large compared to the square of the autocorrelation length of total rainfall depth.

The storm depth is the product of the two storm parameters introduced earlier, i and t_r, both of which will vary in space. We shall assume that t_r is constant, so that all variation of h is due to variation of i. This assumption is consistent with our neglect of temporal variations of storm intensity, since the latter allows us to "smear" the intensity over its highs and lows in time. The smaller values of point duration can thus be enlarged by adding on a zero-intensity

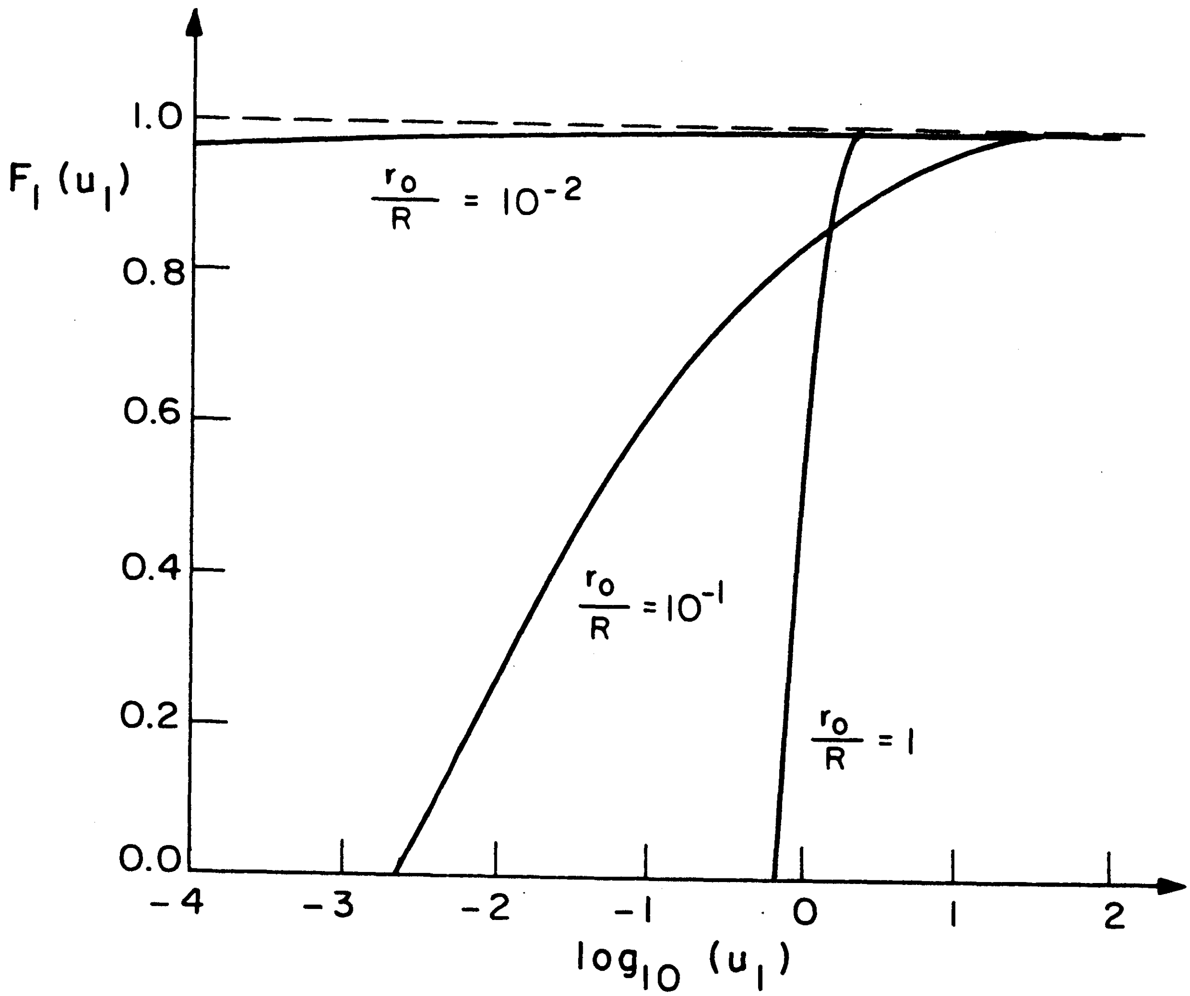

Figure 2.5

CUMULATIVE DISTRIBUTION FUNCTION OF THE LOGARITHM

OF NORMALIZED STORM DEPTH.

period of rainfall at the end of the storm. The constant t_r may be viewed as a mean point storm duration. Given this constant value of t_r, the cumulative distribution function of i is determined directly by (2.32) and (2.33), with it_r substituted for h.

2.3.2 Soil Type

If we classify soils according to their hydraulic characteristics - moisture retention curve, saturated and relative hydraulic conductivity - then we shall find that soil type varies enormously even in small, apparently homogeneous, plots. A theoretical concept that has provided a framework for recent analyses of soil spatial variability is that of similar media, introduced by Miller and Miller (1956). Two similar media are geometrically similar and differ only in their characteristic length scale (e.g., average grain diameter). For practical purposes, the definition can be extended to require only statistical similarity. Then the internal pore geometries need not be exactly similar, but the pore size distributions for representative elementary volumes of the media must be identical, except for the scale factor. Miller and Miller (1956) introduced dimensionless capillary pressure and conductivity, defined as

$$p_o = \frac{\lambda}{\sigma} p \qquad (2.34)$$

$$K_o = \frac{\mu}{\lambda^2 \rho g} K \tag{2.35}$$

where λ is a local characteristic length of the medium. Equation (2.35) differs slightly from the original in that ρg is not incorporated into K, whose units here are consistent with the current soil physics and groundwater literature. We are also following the usual practice of expressing the soil moisture pressure in terms of an equivalent water depth, so we shall employ

$$\psi_o = \frac{\lambda\gamma}{\sigma} \psi \tag{2.36}$$

instead of (2.34). We recognize in (2.35) the combination $\mu K/\rho g$, which is the intrinsic permeability of the medium (Bear, 1979, p. 67). In analogy, $\gamma\psi/\sigma$ may be considered the intrinsic matric potential (Eagleson, 1978). Thus,

$$k = K_o \lambda^2 \tag{2.37}$$

$$\psi' = \psi_o \lambda^{-1} \tag{2.38}$$

in which k is the intrinsic permeability and ψ' is the intrinsic matric potential. If we define α as the ratio of the local value of λ to its average over the family of similar soils, $\overline{\lambda}$,

$$\alpha = \lambda/\bar{\lambda} \tag{2.39}$$

we then obtain the relations

$$\psi(s) = \alpha^{-1}\,\bar{\psi}(s) \tag{2.40}$$

$$K(s) = \alpha^{2}\,\bar{K}(s) \tag{2.41}$$

where

$$\bar{\psi}(s) \equiv \frac{\sigma}{\gamma\bar{\lambda}}\,\psi_o(s) \tag{2.42}$$

$$\bar{K}(s) = \frac{\rho g\bar{\lambda}^2}{\mu}\,K_o(s) \tag{2.43}$$

are the moisture characteristics associated with $\bar{\lambda}$; they are not the average values of ψ or K. This representation and its consequences for soil moisture dynamics have been verified experimentally (Miller and Miller, 1955; Klute and Wilkinson, 1958; Wilkinson and Klute, 1959).

Recent analyses of field data have shown that much of the variability in soil characteristics can be accounted for by the scaling factor, α (Warrick et al., 1977; Keisling et al., 1977; Sharma et al., 1980). Scaling theory has thus become a powerful tool in the analysis of the field variability of soils and in the modeling of spatially variable hydrologic response.

Experimental evidence supports the use of the log-normal distribution to model the variability of α at field scale (Sharma et al., 1980). The probability density function of α can then be written

$$f_\alpha(\alpha) = (\sqrt{2\pi}\,\sigma_n\,\alpha)^{-1} \exp[-(\ln \alpha - \mu_n)^2/2\sigma_n^2] \qquad (2.44)$$

in which μ_n is the mean and σ_n the standard deviation of the logarithm of α. The mean value, μ_α, and standard deviation, σ_α, of α itself are given by

$$\mu_\alpha = \exp(\sigma_n^2/2 + \mu_n) \qquad (2.45)$$

$$\sigma_\alpha = \mu_\alpha(\exp \sigma_n^2 - 1)^{\frac{1}{2}} \qquad (2.46)$$

Defining the reference curves $\psi_o(s)$ and $K_o(s)$ as those associated with the mean value of α (i.e., setting μ_α equal to unity), and introducing the symbol CV to denote the coefficient of variation of α, we may use (2.45) and (2.46) to obtain

$$\sigma_n^2 = \ln(1 + CV^2) \qquad (2.47)$$

$$\mu_n = -\sigma_n^2/2 \qquad (2.48)$$

which define the probability density function of α in terms of a single parameter.

Calculated values of CV for small scale (several

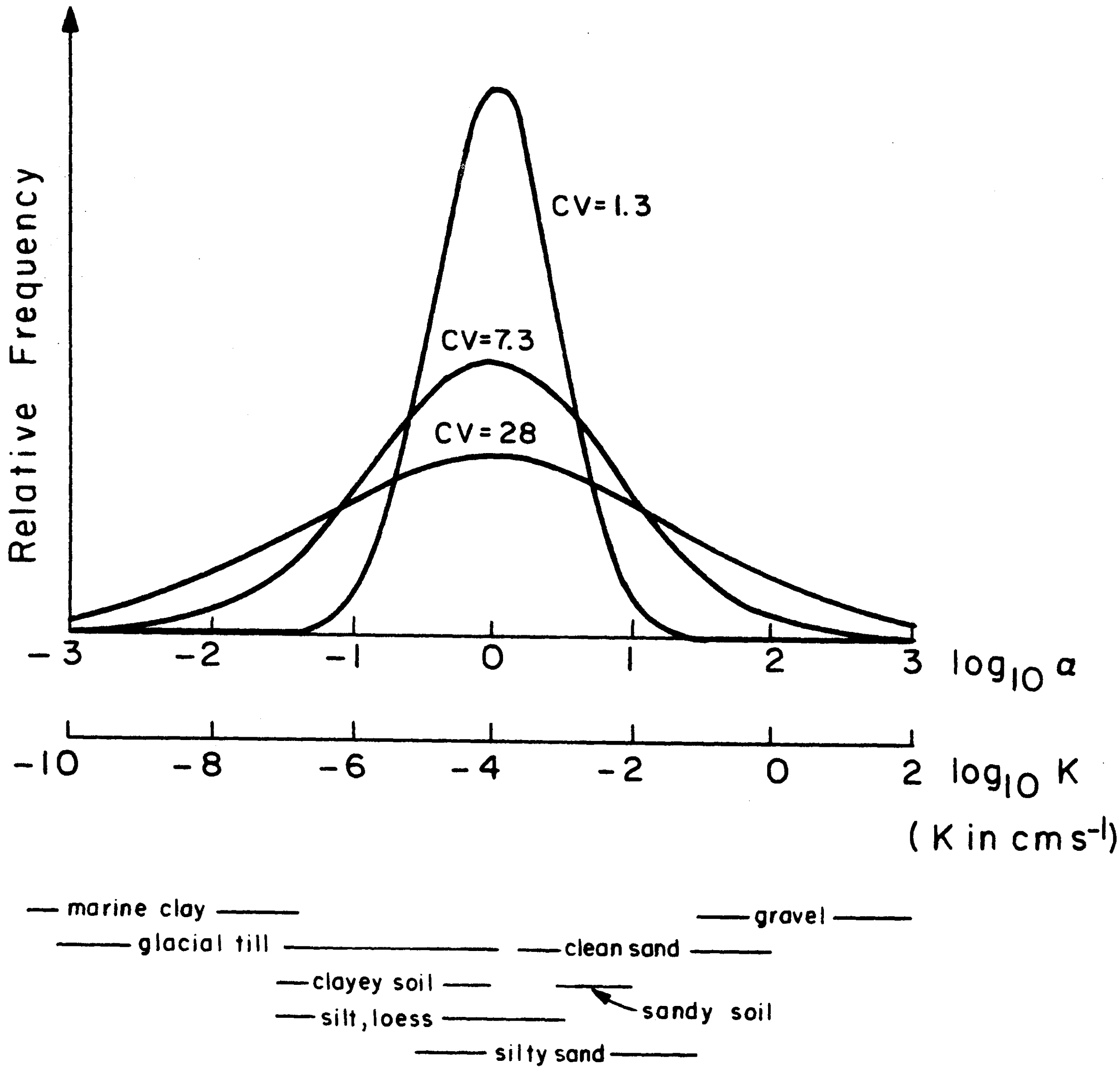

Figure 2.6

THE PROBABILITY DENSITY FUNCTION OF $\log_{10}\alpha$, WHERE α IS THE SCALING PARAMETER, SHOWING RELATION TO HYDRAULIC CONDUCTIVITY FOR $\overline{K}(1) = 10^{-4}$ cm s^{-1}. HYDRAULIC CONDUCTIVITY RANGES AFTER FREEZE AND CHERRY (1979) AND HILLEL (1980).

hectares) field data range up to a maximum of less than 2 (Keisling et al., 1977). For areas of many square kilometers and up, the pertinent data are not yet available. Either an increase of CV or a breakdown of soil similarity might be found at very large scales where regional variations in soil genesis come into play. The normal probability density function of $\ln(\alpha)$, corresponding to (2.44), is plotted in Figure 2.6 for large variability of α. We see that a value of CV=1.3, typical of values already observed, corresponds to the full range of variability of broad textural classes of soils. If a range of different, but geometrically similar, soil types is present in an area, values of CV significantly greater than this would be found. Keeping the assumption of log-normality, it appears that an upper limit of about CV=10 would be found, since this approaches the global limit of soil variability.

Soil similarity implies constancy of the soil parameters c and n. Although these parameters do vary, we shall work only with soil variability in the framework of similarity. This approach is supported by the analyses of field data cited earlier, which found that similarity theory sould account for much of the hydrologic variability even in dissimilar soils.

2.3.3 Initial Moisture Content

The moisture content of the soil exhibits random variations in space that can be represented well by the normal probability density function (Bell et al., 1980). Values of the standard deviation of the saturation ratio can be estimated from the gravimetric data of Bell et al. (1980), which yield a range from about 0.02 to 0.1.

Small-scale soil moisture variations may result from variations in soil type. This can occur in two ways. First, soil type controls infiltration, evaporation, drainage, and, consequently, changes in moisture storage. Second, considering a field in which the parallel soil columns are in equilibrium with each other, ψ is relatively constant. Equation (2.40) then implies variability of s_o resulting from variability of α, since the function $\overline{\psi}$ (s) is unique for the entire family of similar soils.

In some cases, it appears that near-surface moisture variations are strongly correlated with local topography (Zaslavsky and Sinai, 1981).

A bivariate normal distribution, accounting for the correlation between $\ln(\alpha)$ and s_o, would appear to be a realistic model of the spatial variability of those parameters. In the current analysis, whose goal is to isolate the most important parameters, we shall ignore the correlation of $\ln(\alpha)$ and s_o. Should the variability of both prove to be critical, then further analysis would be justified. The probability density function of s_o may now be written as

$$f_{S_o}(s_o) = (\sqrt{2\pi}\,\sigma_s)^{-1} \exp[-(s_o - \mu_s)^2/2\sigma_s^2] \qquad (2.49)$$

where μ_s and σ_s are the mean and variance of the soil moisture saturation.

2.3.4 Depth to Water Table

In the present analysis, we shall model Z_w as the water table depth, ignoring the possibility of relatively impervious layers. Our results can be expected to apply qualitatively also to the latter case, however.

The water table depth may be viewed as the difference of two random fields - the land surface elevation and the water table elevation (Freeze, 1980). Here we shall apply a simpler deterministic model. A one-dimensional Dupuit model of groundwater flow toward a stream in a topographic low yields

$$b_1 = B_1\left[1 - \left(\frac{L-x}{L}\right)^2\right] \tag{2.50}$$

where b_1 is the difference between the elevation of the water table and the elevation of the discharge area, x is the distance from the stream, and L is the distance from the stream to the groundwater divide. The parameter B_1 gives the maximum height of the water table. Its value is

$$B_1 = \frac{NL^2}{2T} \tag{2.51}$$

where N is the uniform rate of recharge from the unsaturated zone and T is the transmissivity of the saturated zone.

The water table profile is often observed to be geometrically similar in cross section to the land surface, with the local irregularities of the land surface filtered out. As an approximation to the land surface profile, we shall write

$$b_2 = B_2\left[1 - \left(\frac{L-x}{L}\right)^2\right] \qquad (2.52)$$

where b_2 is the land surface elevation and B_2 is its maximum value. Then the normalized water table depth, u_2, is given by

$$u_2 = \frac{Z_w}{B} = \frac{b_2-b_1}{B} = 1 - \left(\frac{L-x}{L}\right)^2 \qquad (2.53)$$

where

$$B = B_2 - B_1 \qquad (2.54)$$

is the maximum water table depth. Given that x is uniformly distributed between 0 and L, we may derive the corresponding deterministic frequency distribution for u_2. The result is

$$F_2(u_2) = \{\text{Proportion of area with } U_2 \le u_2\}$$

$$= \frac{x(u_2)}{L} = 1 - (1 - u_2)^{\frac{1}{2}} \qquad 0 < u_2 < 1 \qquad (2.55)$$

2.4 Areal Average Infiltration

At this point, we summarize in dimensionless form the stochastic-dynamic infiltration model of the preceeding sections. Defining I as the ratio of the local infiltration depth to areal average rainfall, i.e.,

$$I = F_i(t_r)/\bar{h} \tag{2.56}$$

we have

$$I = \begin{cases} \min\{D(1-s_o)\,u_2,\ u_1\} & 1 \le \tau_o \\ \min\{D(1-s_o)\,u_2,\ \tau_o u_1 + S\alpha^{\frac{1}{2}}\phi_2(s_o) & \\ \cdot[(1-\tau')^{\frac{1}{2}} - (\tau_o-\tau')^{\frac{1}{2}}] + A(1+s_o^c)\,\alpha^2(1-\tau_o)\} & \tau < 1 \end{cases} \tag{2.57}$$

in which

$$\tau_o = \begin{cases} \dfrac{[S\phi_2(s_o)]^2\alpha}{2u_1[u_1 - A(1+s_o^c)^2]}\left\{1 + \dfrac{A(1+s_o^c)\alpha^2}{2[u_1 - A(1+s_o^c)^2]}\right\} & A\alpha^2 < u_1 \\ \infty & u_1 \le A\alpha^2 \end{cases} \tag{2.58}$$

and

$$\tau' = \tau_o - \frac{[S\phi_2(s_o)]^2\alpha}{4[u_1 - A(1+s_o^c)\alpha^2]^2} \tag{2.59}$$

In these equations, D, S, and A are constant dimensionless parameters. They are given by

$$D = \text{dimensionless soil storage capacity} = \frac{Bn}{\bar{h}} \tag{2.60}$$

$$S = \text{dimensionless sorptivity} = 2\left[\frac{5n\ \bar{K}(1)\ \bar{\psi}(1)\ t_r}{3\pi m\bar{h}^2}\right]^{1/2}\phi_1(d) \tag{2.61}$$

$$A = \text{dimensionless hydraulic conductivity} = \frac{\bar{K}(1)\ t_r}{2\bar{h}} \tag{2.62}$$

and therefore depend jointly upon soil and storm characteristics. The random variables are u_1, u_2, s_o, and α. Their (assumed independent) distributions are defined as follows:

$$F_1(u_1) = 1-\left(\frac{r_o}{R}\right)^2\left[\ln\frac{h_o}{\bar{h}u_1}\right]^2 \quad ; \frac{h_o}{\bar{h}}e^{-R/r_o} < u_1 < \frac{h_o}{\bar{h}} \tag{2.63}$$

$$F_2(u_2) = 1-(1-u_2)^{\frac{1}{2}} \qquad 0 < u_2 < 1 \tag{2.64}$$

$$s_o \sim N(\mu_s,\ \sigma_s^2) \tag{2.65}$$

$$\ln\alpha \sim N(0,\ \ln(1+CV^2)) \tag{2.66}$$

These distributions introduce the following parameters into the problem:

r_o/R = relative storm radius

μ_s = mean value of s_o

σ_s = variance of s_o

CV = coefficient of variation of α

Including the soil parameter c, there are therefore eight independent parameters.

The areal average value of I, which we shall term the infiltration efficiency and denote by $\bar{I}$, is found by integrating over the probability density functions of the random variables,

$$\bar{I}(D,S,A,c,\frac{r_o}{R},\mu_s,\sigma_s,CV) = \int\int\int\int I(u_1,u_2,s_o,\alpha;D,S,A,c)$$
$$f_1(u_1;\frac{r_o}{R})\, f_2(u_2)\, f_{S_o}(s_o\,;\mu_s,\sigma_s) f_\alpha(\alpha;CV) du_1\, du_2\, ds_o\, d\alpha \quad (2.67)$$

where

$$f_1(u_1;\frac{r_o}{R}) = \frac{dF_1}{du_1} \quad (2.68)$$

$$f_2(u_2) = \frac{dF_2}{du_2} \quad (2.69)$$

with F_1 and F_2 given by (2.33) and (2.55), respectively.

The results of numerical integration of (2.67) are presented in this section. The computer program is listed in Appendix A. Parameters for the various sensitivity runs are given by the key in Table 2.1. Note that the solution is independent of c for s_o equal to zero, according to (2.57) through (2.59).

2.4.1 Infiltration with Homogeneous Soil Type, Initial Saturation, and Rainfall

We first examine the behavior of the infiltration

Figure No.	A	S	D	CV	r_o/R	μ_s	σ_s
2.7	v.	v.	∞	0	100	0	0
2.8	0	v.	∞	0	100	v.	0
2.9	v.	0	∞	0	100	v.	0
2.10	0	v.	v.	0	100	0	0
2.11	v.	0	v.	0	100	0	0
2.12	0	v.	1	0	100	v.	0
2.13	0	v.	∞	0	100	0.7	v.
2.14	0	v.	1	0	100	0.7	v.
2.15	0	v.	∞	0	v.	0	0
2.16	v.	0	∞	0	v.	0	0
2.17	v.	0	∞	v.	100	0	0
2.18	0	v.	∞	v.	100	0	0

Table 2.1

MODEL PARAMETERS USED IN THE SENSITIVITY ANALYSIS

TO GENERATE FIGURES 2.7 THROUGH 2.18

v. - variable

model in the absence of spatial variability of soil type, moisture content, and precipitation, i.e., CV=0, σ_s=0, and r_o/R large. Variability of water table depth as required by (2.55) is retained in the examples that use a finite value of D. We first consider infinite D, then finite.

Figure 2.7 illustrates the dependence upon A and S of the infiltration efficiency of an initially dry, homogeneous soil (s_o=0) with a deep water table (D= ∞). When either parameter is much larger than the other, infiltration is insensitive to the smaller parameter. The upper left hand corner of Figure 2.7 represents the sorptivity-controlled response, while the lower right hand corner corresponds to conductivity control. For either extreme, $\bar{I}$ is a monotonically increasing function of the controlling variable up to the point where $\bar{I}$ reaches and remains at unity. This discontinuity is a threshold nonlinearity; no runoff occurs if A is greater than unity or if S is greater than about eight.

We should keep in mind that A and S contain storm parameters, so the dominance of sorptivity or conductivity for a given area is storm-dependent. Referring to Figure 2.7, we see that sorptivity dominates when A/S is less than about 0.03. Conductivity is the controlling factor for A/S greater than about 0.3. In between, both effects contribute significantly. From (2.61) and (2.62), the critical ratio may be computed to be

$$\frac{A}{S} = \left[\frac{3\pi m\bar{K}(1)}{5n\bar{\psi}(1)}\right]\phi_1(d)\ t_r^{\frac{1}{2}} \qquad (2.70)$$

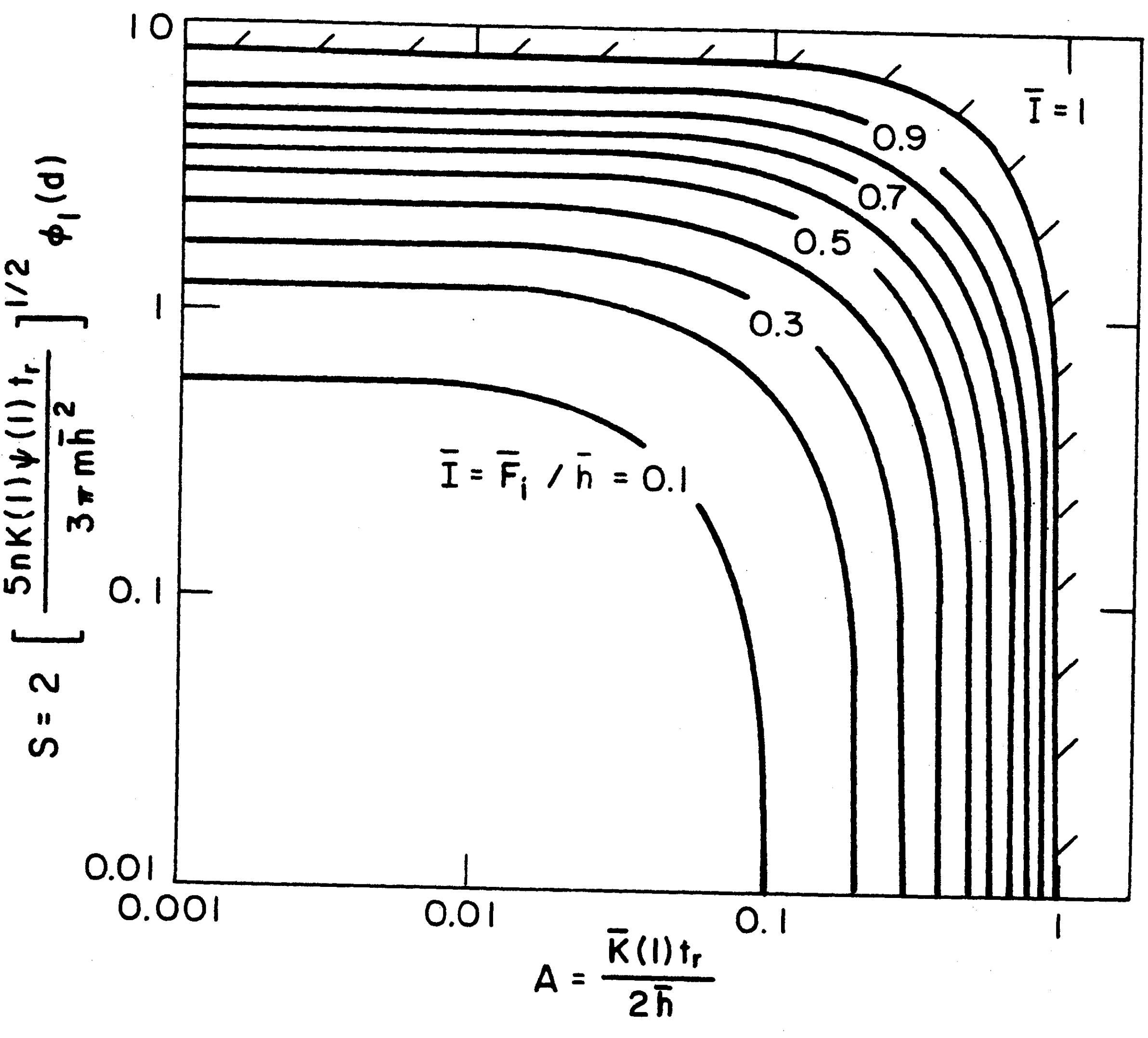

Figure 2.7

CONTOUR PLOT OF INFILTRATION EFFICIENCY, $\bar{I}$, AS A FUNCTION OF DIMENSIONLESS HYDRAULIC CONDUCTIVITY AND SORPTIVITY. PLOT IS FOR ZERO INITIAL SATURATION, DEEP WATER TABLE, AND NO SPATIAL VARIABILITY.

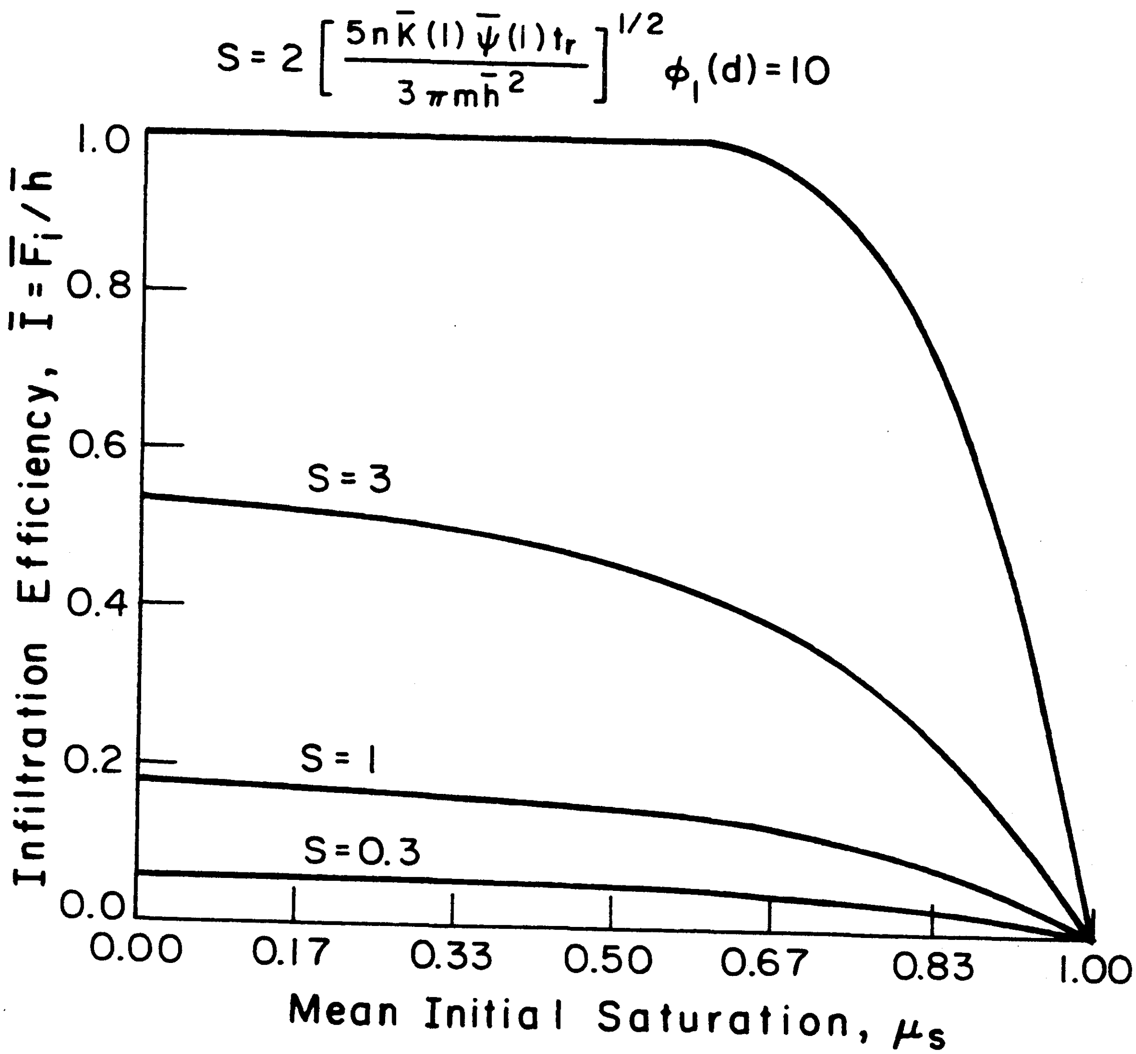

Figure 2.8

INFILTRATION EFFICIENCY AS A FUNCTION OF μ_s, FOR A SORPTIVITY-CONTROLLED SYSTEM. DEEP WATER TABLE, NO SPATIAL VARIABILITY.

This gives us a simple criterion for determining the relative importance of conductivity and sorptivity, for a given area, as a function of the storm duration, and independent of the average storm depth. The numerical limits suggested above, of course, apply only to the case of no spatial variability, since they are taken from Figure 2.7. Similar limits on A/S could be obtained for other situations in the same manner, however, and translated to storm durations by means of (2.70).

The influence of μ_s, the mean initial soil moisture saturation, on infiltration with a deep water table is shown in Figure 2.8 for varying S, and A equal to zero. For the three lower curves, the reduction of infiltration efficiency due to non-zero initial saturation corresponds roughly to the decrease in $\phi_2(s_o)$ with increasing s_o exhibited in Figure 2.1. For fixed μ_s, the infiltration is proportional to S. For large S, the infiltration efficiency is limited by its maximum value of unity and is independent of μ_s except for large μ_s. In general, there is little sensitivity to μ_s except when the soil is initially near saturation.

The behavior of the conductivity-dominated system as a function of μ_s is shown in Figure 2.9 with the soil parameter c equal to 4. The sensitivity to μ_s, which enters through the s_o dependence of A_o given in (2.3), is somewhat smaller than in the sorptivity-controlled case. In our analysis of infiltration with spatially variable initial soil moisture in Section 2.4.2, we shall concentrate on the latter system.

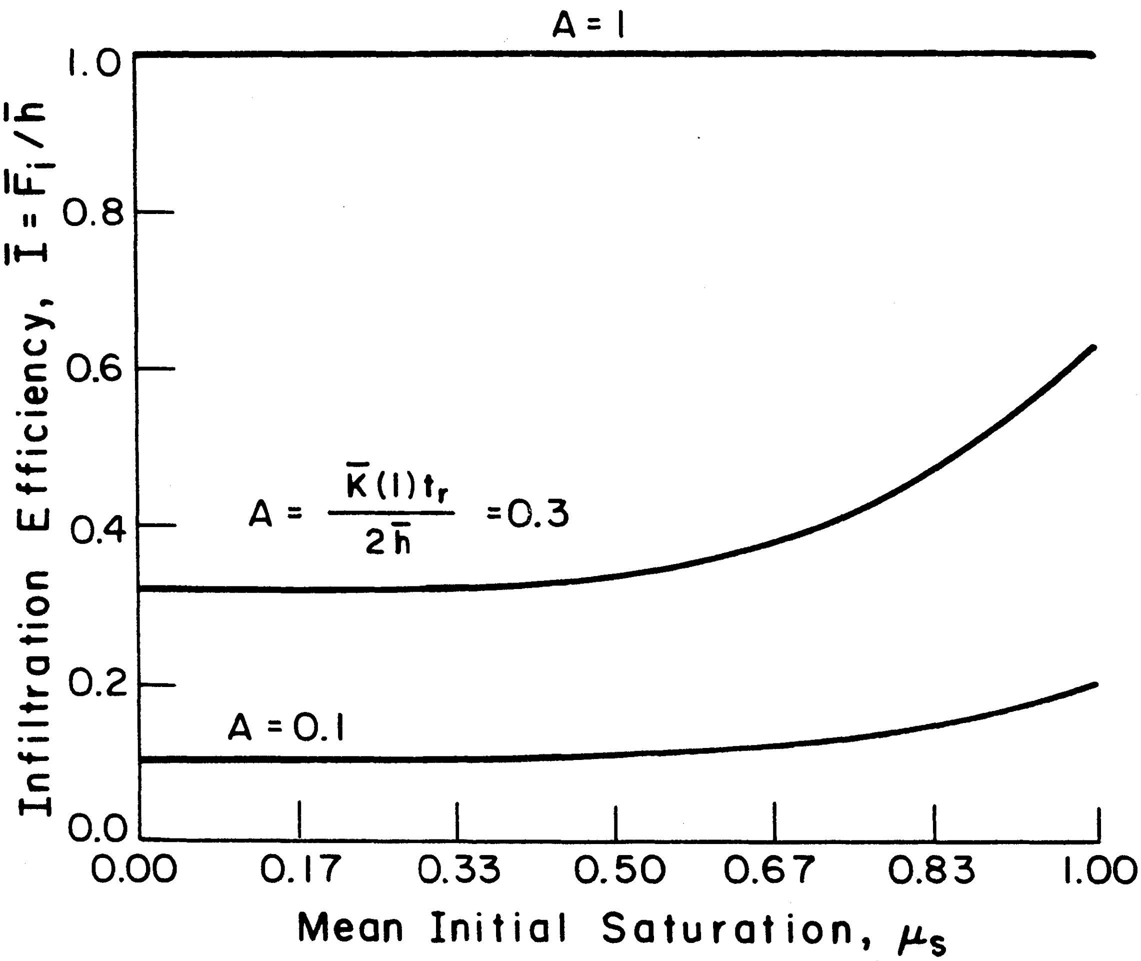

Figure 2.9

INFILTRATION EFFICIENCY AS A FUNCTION OF μ_s FOR A CONDUCTIVITY-CONTROLLED SYSTEM. DEEP WATER TABLE, NO SPATIAL VARIABILITY.

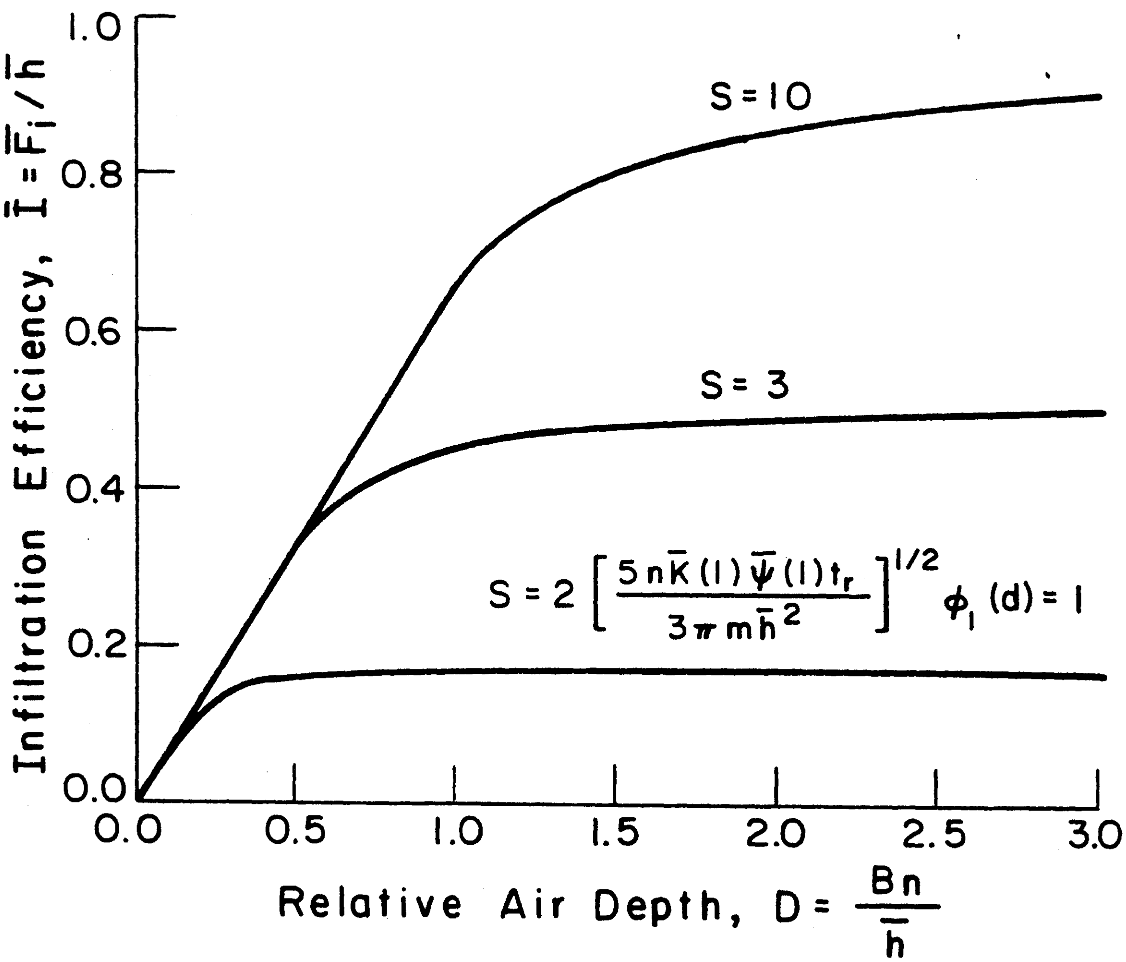

Figure 2.10

INFILTRATION EFFICIENCY AS A FUNCTION OF THE DIMENSIONLESS SOIL STORAGE CAPACITY FOR A SORPTIVITY-CONTROLLED SYSTEM. DEEP WATER TABLE; HOMOGENEOUS SOIL, INITIAL SATURATION, AND RAINFALL.

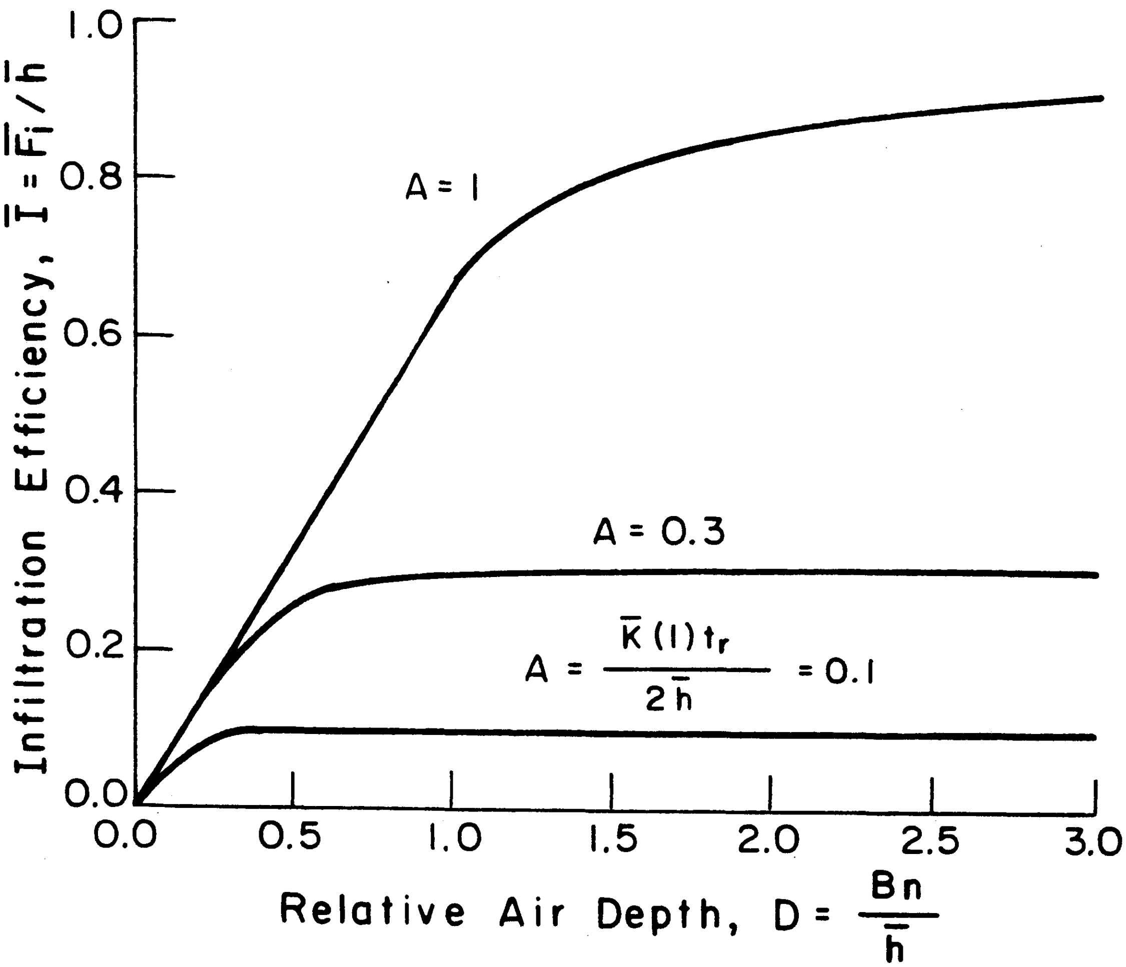

Figure 2.11

INFILTRATION EFFICIENCY AS A FUNCTION OF D FOR A CONDUCTIVITY-CONTROLLED SYSTEM. DEEP WATER TABLE; HOMOGENEOUS SOIL, INITIAL SATURATION, AND RAINFALL.

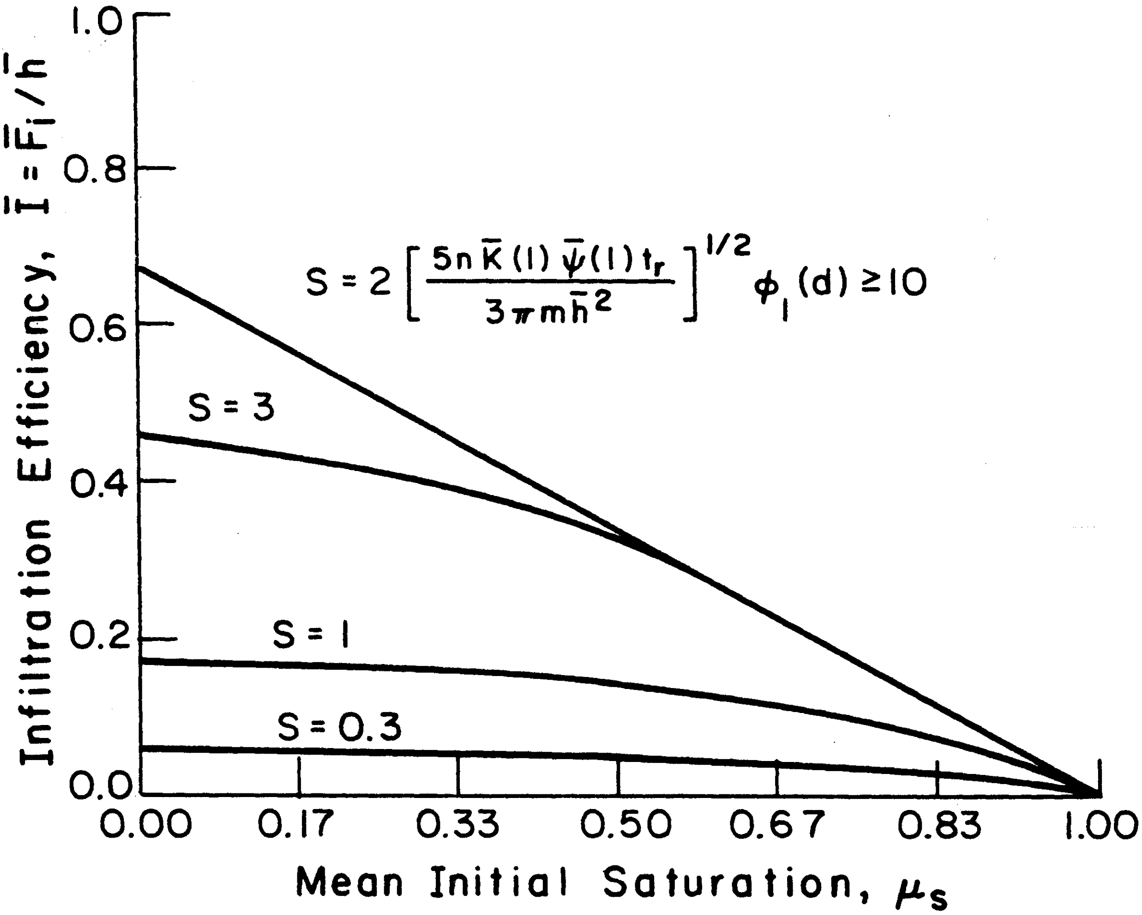

Figure 2.12

INFILTRATION EFFICIENCY AS A FUNCTION OF μ_s FOR A SORPTIVITY-CONTROLLED SYSTEM. D = 1, HOMOGENEOUS SOIL, INITIAL SATURATION, AND RAINFALL.

A sufficiently small value of D, which measures the available storage capacity, will decrease the average infiltration due to the shortage of vacant pore space able to receive water. Figures 2.10 and 2.11 illustrate this behavior for sorptivity-dominated and conductivity-dominated systems, respectively. Concentrating on Figure 2.10 and a single value of S, we see that the infiltration efficiency, $\bar{I}$, is proportional to the storage depth available when D is small. At this point, infiltration is everywhere limited absolutely by Z_w. As D becomes larger, the storage limit is active only in the portion of the area where the water table is relatively shallow, so the growth of $\bar{I}$ with D is sub-linear. This is because the sorptivity becomes a limiting factor over an increasingly large part of the area. For large D, the deep water table solution is approached asymptotically. Similar behavior for the conductivity-controlled system can be seen in Figure 2.11.

Since the available storage space is directly related to s_o, we expect a significant sensitivity of $\bar{I}$ to s_o when the water table is shallow. This is demonstrated in Figure 2.12 for the larger values of sorptivity or initial saturation. (The value of D is unity.) The uppermost straight line segment represents complete control of infiltration by the available storage capacity. The nearly horizontal curves at small S and μ_s show the relative insensitivity of infiltration to the initial moisture content, through $\phi_2(s_o)$, that was observed for small μ_s in Figure 2.8.

2.4.2 Infiltration with Spatially Variable Soil Moisture

Figure 2.8 showed the sensitivity of $\bar{I}$ to μ_s when σ_s was zero. It thus represents also the sensitivity to s_o itself. We are interested in knowing the sensitivity of infiltration to σ_s. If the relation between $\bar{I}$ and s_o were perfectly linear, then there would be no sensitivity at all to σ_s, since the expected value of a linear function is obtained by evaluating that function at the mean value of the argument. Over ranges of s_o corresponding to any fixed value of μ_s and reasonable values of σ_s(Section 6.3.3.3), the relationship is approximately linear. The most significant curvature in Figure 2.8 appears around μ_s=0.7. We have thus calculated infiltration as a function of σ_s for μ_s=0.7. The results are displayed in Figure 2.13, which suggests that soil moisture variations are unimportant for the prediction of infiltration, since the average response is almost independent of σ_s. An areal mean value of s_o is therefore sufficient for prediction of the hydrologic response to rainfall.

The corresponding calculations for a shallow water table are plotted in Figure 2.14. The insensitivity to σ_s is not surprising in view of the weakness of the nonlinearities displayed in Figure 2.11.

2.4.3 Infiltration with Spatially Variable Storm Depth

For r_o/R much larger than unity, the storm is large

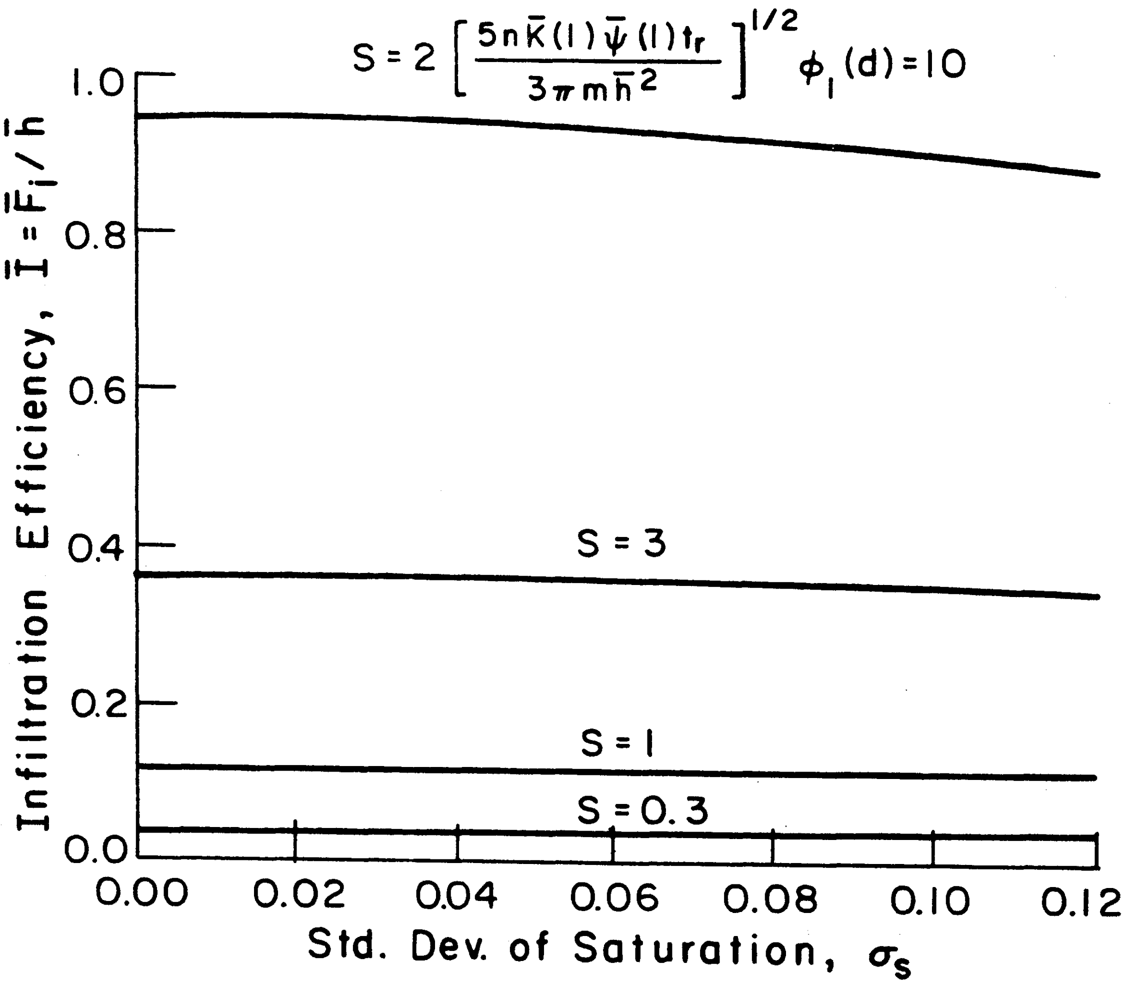

Figure 2.13

INFILTRATION EFFICIENCY AS A FUNCTION OF σ_s, FOR A SORPTIVITY-CONTROLLED SYSTEM. DEEP WATER TABLE, $\mu_s = 0.7$, AND HOMOGENEOUS SOIL AND PRECIPITATION.

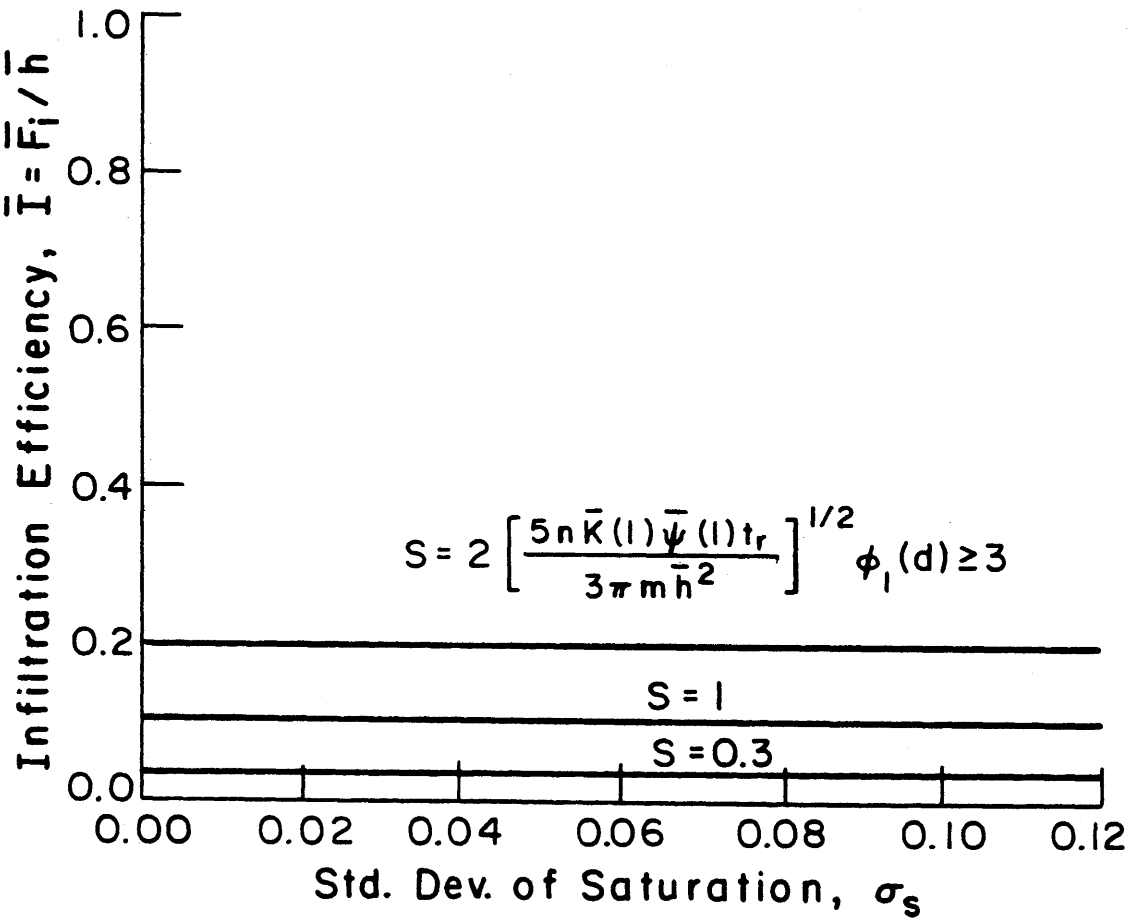

Figure 2.14

INFILTRATION EFFICIENCY AS A FUNCTION OF σ_s FOR A SORPTIVITY-CONTROLLED SYSTEM. $D = 1$, $\mu_s = 0.7$, AND HOMOGENEOUS SOIL AND PRECIPITATION.

relative to the modelled area, and h is almost constant. A value of r_o/R much less than unity implies great variability of rainfall, with most of the precipitation concentrated over a small area. The importance of this parameter in determining infiltration is shown clearly in Figures 2.15 and 2.16. The individual curves in Figure 2.15 show the decrease of infiltration that results from increasing variability of storm depth, i.e., decreasing relative storm radius, r_o/R. From (2.26), we have

$$\frac{\bar{R}_s}{\bar{h}} = 1 - \bar{I} \tag{2.71}$$

i.e., a decrease in the normalized average infiltration is balanced by an increase of the normalized average surface runoff. The quantity $\bar{R}_s/h$ is given by the vertical distance from the curves up to the unit ordinate. Figures 2.15 and 2.16 thus show the dramatic increase of surface runoff that results from increasing variability of storm depth, the average depth (or total volume) of rain being held constant.

Current large-scale hydrology parameterizations in use in atmospheric general circulation models specify the division of rainfall into infiltration and surface runoff by considering only the total volume, or average depth, of precipitation over the entire grid square. This is equivalent to using the large-r_o/R asymptotes of Figures 2.15 and 2.16 regardless of the storm type. Depending on the particular value of r_o/R for which a given parameterization has been cali-

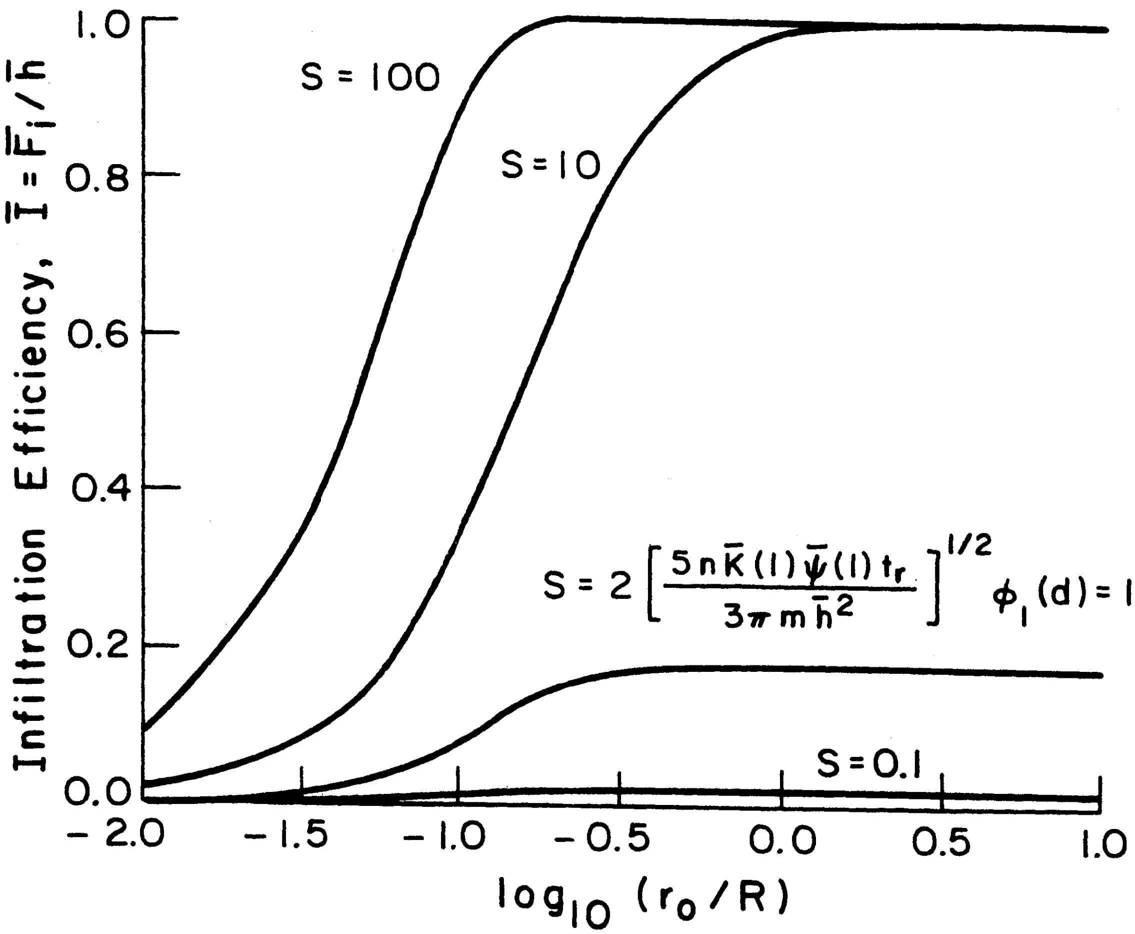

Figure 2.15

INFILTRATION EFFICIENCY AS A FUNCTION OF $\log_{10}(r_o/R)$ FOR A SORPTIVITY-CONTROLLED SYSTEM. DEEP WATER TABLE, $\mu_s = 0$, AND HOMOGENEOUS SOIL AND INITIAL SATURATION.

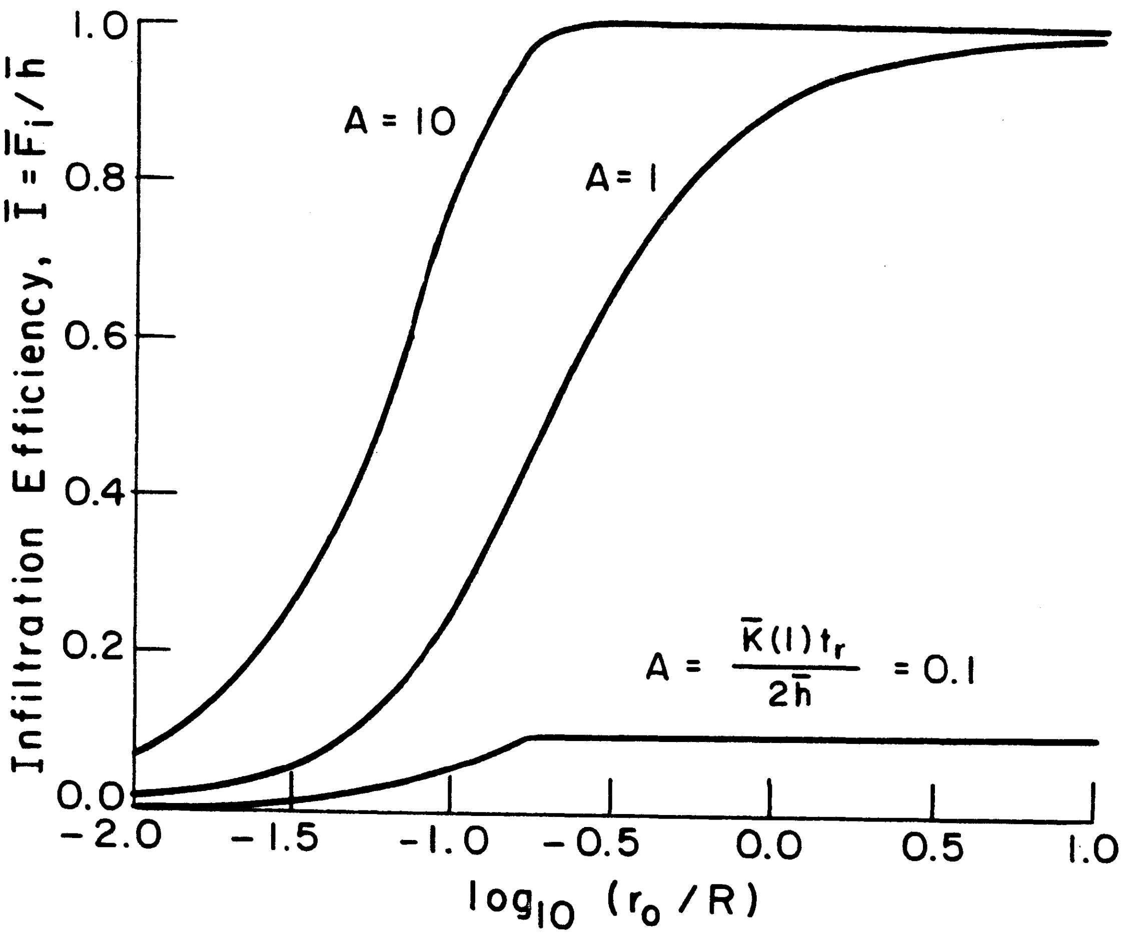

Figure 2.16

INFILTRATION EFFICIENCY AS A FUNCTION OF $\log_{10}(r_o/R)$ FOR A CONDUCTIVITY-CONTROLLED SYSTEM. DEEP WATER TABLE, $\mu_s = 0$, AND HOMOGENEOUS SOIL AND INITIAL SATURATION.

brated, these figures tell us that such a scheme will underestimate runoff from localized convective activity and/or overestimate runoff from regional cyclonic storms. The errors involved can apparently be very large.

Another interesting feature of the response to highly variable precipitation is the much wider range of A and S over which both infiltration and runoff are significantly different from zero. Perhaps this explains the often noted failure of lumped parameter (i.e., one-dimensional) rainfall-runoff models to yield surface runoff comparable to observations.

2.4.4 Infiltration into a Heterogeneous Soil

Figure 2.17 shows the strong sensitivity of the infiltration efficiency to the coefficient of variation of the soil scaling parameter when infiltration is gravity-dominated. As was seen for precipitation, the effect of spatial variability of soil properties is usually to decrease significantly the proportion of precipitation that enters soil storage. For A greater than or equal to unity, the average value of α is too large to cause surface runoff (hydraulic conductivity grows with α). Since increasing variability of α means a growing tail in the probability density function of α at small α, the infiltration efficiency decreases with growing CV. A similar argument explains the relatively insignificant reversal of this behavior for small A.

The same behavior, qualitatively speaking, is visi-

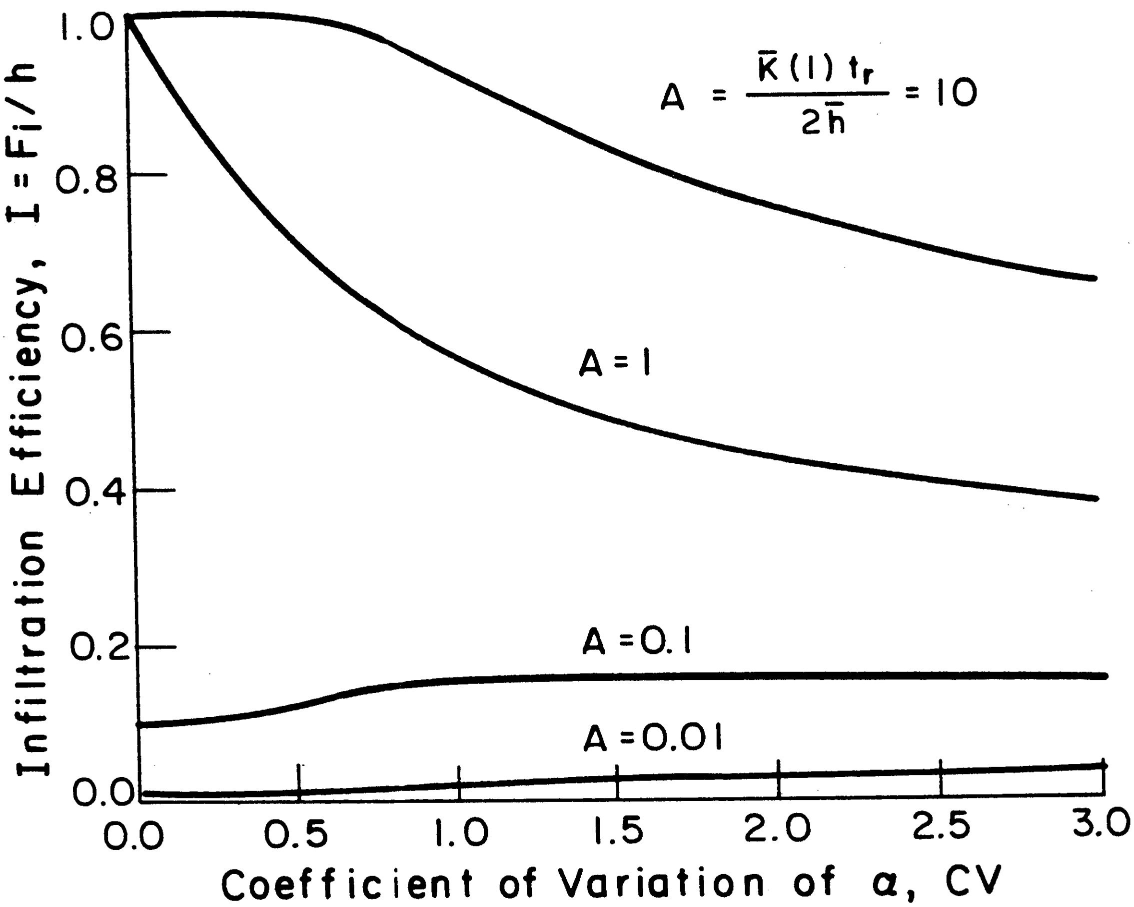

Figure 2.17

INFILTRATION EFFICIENCY AS A FUNCTION OF CV_α FOR A CONDUCTIVITY-CONTROLLED SYSTEM. DEEP WATER TABLE, $\mu_s = 0$, HOMOGENEOUS RAINFALL AND INITIAL SATURATION.

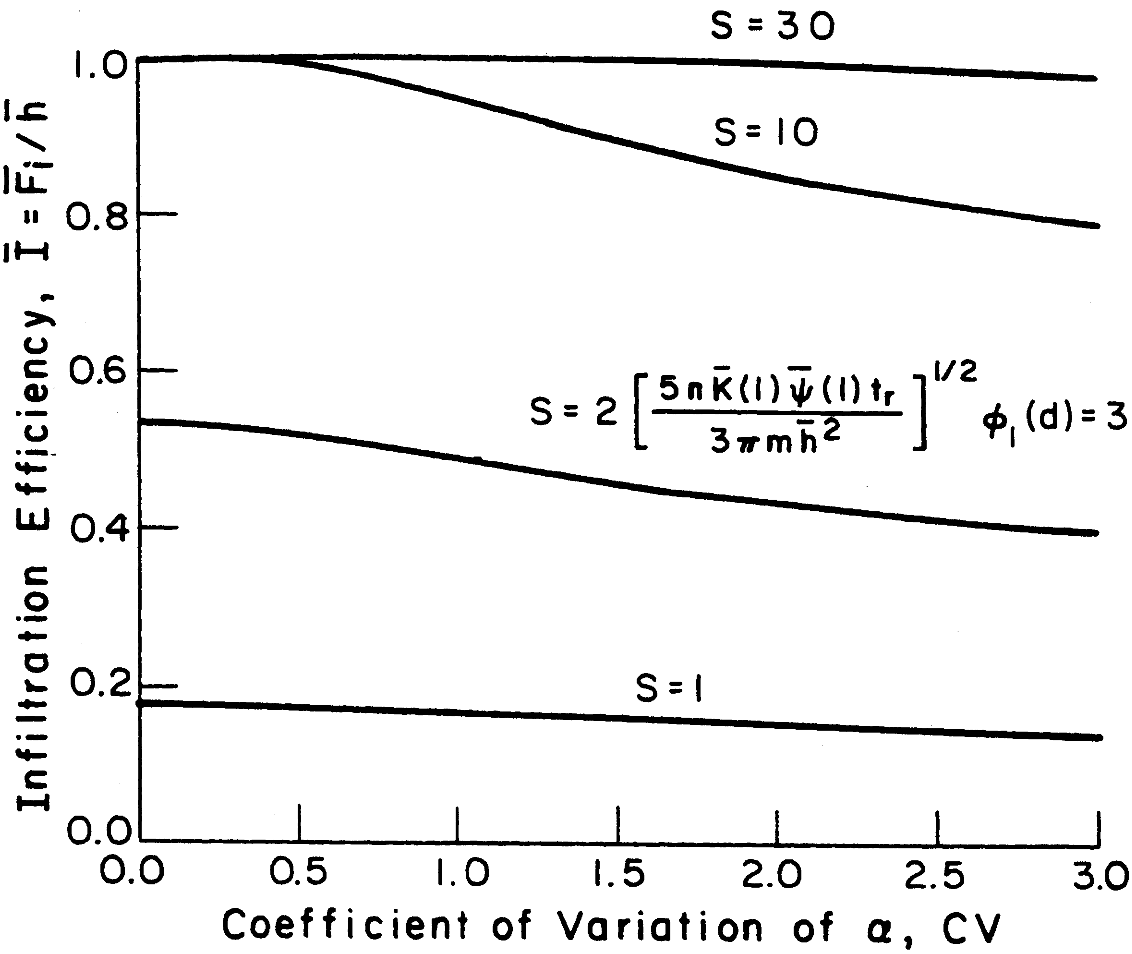

Figure 2.18

INFILTRATION EFFICIENCY AS A FUNCTION OF CV_α FOR A SORPTIVITY-CONTROLLED SYSTEM. DEEP WATER TABLE, $\mu_s = 0$, AND HOMOGENEOUS RAINFALL AND INITIAL SATURATION.

ble in Figure 2.18, which applies to the sorption-dominated infiltration process. The magnitude of this effect is considerably smaller, however. The quantitative difference in the effect of CV between Figures 2.17 and 2.18 results from the different exponents of α in the sorptivity and conductivity terms.

Recall that the average value of α has been defined as unity. If the "average" of a family of similar soils is defined as the member of that family with α equal to unity, then the response of that average soil is given by the intersections of the curves in Figures 2.17 and 2.18 with the y-axis. To average is thus to assign a value of CV=0 for the purpose of modelling. If the actual soil system in the area of interest has a CV of, say, two, then the response of this hypothetical average soil is clearly dissimilar to the average response of the area for some values of A and S. In Figure 2.17, with CV=2 and A=10, the "average" soil yields no runoff, while the actual runoff is 25 percent of the rainfall.

Notice also that the ranges of A and (to a certain extent) S over which runoff can occur grow with CV. This behavior is similar to that observed earlier for spatially variable rainfall.

2.5 Discussion

It is well known that physically-based models of homogeneous, or point, infiltration have threshold nonlinearities of the type shown in Figure 2.7. Furthermore, such a model is very sensitive to the parameters, in this case A and S, with only a narrow range of values allowing significant runoff and infiltration from the same event. Results presented in the previous section demonstrate that the inherent spatial variability of soil and storm properties is fundamental in shaping the infiltration function for an inhomogeneous basin. Figures 2.15 and 2.16 show how the sensitivity of infiltration to A and S decreases as the variability of storm depth increases. The similar result for soil variability can be seen in Figure 2.17.

Another particular feature of the inhomogeneous surface response is that increasing spatial variability, with mean parameters held constant, almost invariably results in decreased infiltration and increased surface runoff, as was seen in Figures 2.15 through 2.18. Estimates of surface runoff made using mean values of soil characteristics and storm depth will usually be biased significantly downwards.

The results of the previous section suggest that the spatial distribution of precipitation plays a major role in determining the average areal hydrologic response to a storm. This is especially true for large areas such as a GCM grid square, within which precipitation may be highly variable, and within which that variability is dependent upon storm type.

The role of soil variability appears no less critical for storms that generate gravity-dominated infiltration. The soil is simpler to treat, however, in that it is a static factor - CV does not vary from storm to storm.

The sensitivity of infiltration to the mean moisure saturation, shown in Figures 2.8, 2.9 and 2.12, is important only when the soil is near saturation or when the water table is shallow. Even then, the spatial variability of initial saturation can be ignored, according to our model, as demonstrated in Figures 2.13 and 2.14. Furthermore, Figures 2.8 and 2.9 suggest that the time variations of the areal average saturation are themselves only of secondary importance, supporting the use of a space-time mean value for modelling purposes when the system is not initially near saturation and does not initially have a shallow water table. The commonly observed sensitivity of infiltration to antecedent moisture conditions suggests that these conditions often fail to be met.

Chapter 3

SPATIAL VARIABILITY OF EVAPOTRANSPIRATION

3.1 Introduction

The rate of evaporation or transpiration varies over the land surface due to variations in net radiation, moisture availability, vegetation, and soil type. Atmospheric advection and diffusion are also factors. We begin our discussion of the spatial variability of evapotranspiration with a look at the Penman-Monteith equation and its assumptions. This provides some background for the remainder of the chapter.

A widely used conceptual model for the evaporation process is (Monteith, 1980)

$$LE = \frac{\rho c_p}{\gamma r_v} (e_o - e_z) \tag{3.1}$$

in which L is the latent heat of vaporization of water, E is the evaporation rate, ρ and c_p are density and specific heat of air, γ is the psychrometric constant, e_o is the vapor pressure at the evaporation source and e_z is the vapor pressure at height z. The resistance to vapor transfer, r_v, is often considered to be a sum of plant (or canopy) and aerodynamic resistances in series (Monteith, 1980),

$$r_v = r_c + r_a \tag{3.2}$$

so that the evaporation is considered to occur inside a leaf, the additional resistance being imposed by the plant stomata and cuticle. In the absence of canopy resistance (i.e., for externally wet vegetation or for a bare, wet soil surface), r_c is equal to zero.

In the cases covered above, e_o is normally considered to take its saturation value, i.e.,

$$e_o = e_s(T_o) \tag{3.3}$$

where T_o is the temperature of the evaporating surface. However, if surface soil moisture becomes low in the bare soil situation, then the vapor pressure is reduced by a factor that depends on the surface soil moisture potential so that (Edlefsen and Anderson, 1943)

$$e_o = e_s(T_o)\exp(\psi g/R_v T) \tag{3.4}$$

where ψ is the soil moisture potential (negative), g is the acceleration of gravity, and R_v is the gas constant for water vapor. Although an identical relation holds inside the leaves of a vegetal canopy, the magnitude of the leaf potential is relatively small and (3.4) should then reduce to (3.3).

When (3.3) holds, it can be linearized and combined with both (3.1) and an expression for sensible heat flux,

$$H = \frac{\rho c_p}{r_h} (T_o - T_z) \tag{3.5}$$

in the surface heat balance equation,

$$Rn - G = H + LE \tag{3.6}$$

to yield Monteith's modification of the Penman equation,

$$LE = \frac{\Delta(Rn - G) + \frac{\rho c_p}{r_h}[e_s(T_z) - e_z]}{\Delta + \gamma(r_v/r_h)} \tag{3.7}$$

In (3.5) through (3.7), H is the sensible heat flux upward from the surface, T_z is the temperature at height z, and r_h is the atmospheric resistance to heat diffusion, usually equated to r_a; Rn is net radiation, G is the heat flux into the soil, and Δ is the slope of the saturation vapor pressure curve, assumed constant.

A critical assumption in the derivation of (3.7) is that e_o and T_o pertain to the same surface, i.e., that the virtual sources of vapor and heat are identical, and that saturation conditions hold at this surface. The latter condition can be relaxed for dry, bare soil by introducing (3.4) instead of (3.3) to relate e_o and T_o, but then further assumptions have to be made about the feedback of E on ψ. This model thus has limited usefulness for a bare soil after the surface dries. At that time, evaporation goes from atmosphere control to soil control.

A relatively dry vegetated surface will actively strive to reduce evaporation by increasing its r_c as the soil moisture becomes low (Monteith, 1980). Inasmuch as the increasing canopy resistance is a response to reduced soil moisture potential, this can also be considered a transfer of control from atmosphere to soil. Again, the modelling problem requires knowledge of the feedback of E on ψ, because of the dependence of r_c on ψ. The dry, vegetated surface, like the dry, bare soil surface, is thus not easily analyzed using the atmosphere-based Penman-Monteith approach.

Equation (3.7) is a diagnostic relation giving evaporation as a function of measured meteorologic variables in the turbulent planetary boundary layer. It fails to account for the feedback effect of evaporation on these variables. More globally-oriented analyses of evaporation based on the theory of atmospheric diffusion and advection have dealt with this problem. The most general surface boundary condition for moisture considered in such an analysis (McNaughton, 1976a,b) uses the above-mentioned concept of saturated vapor pressure inside a leaf or canopy of specified constant resistance, and is thus applicable to many vegetated or bare soil surfaces with sufficient soil moisture. The bare soil situation is obtained by allowing r_c to go to zero.

In this chapter, we shall examine the problem of areal average evaporation when the soil is sufficiently wet for (3.3) to be used. Although this includes virtually all vegetated surfaces, our results will be most applicable to situations in which soil moisture is well above the point at which the plants become severely stressed. Under stress, the canopy resistances become increasingly sensitive to soil moisture, a feedback mechanism that we shall not address.

3.2 Mathematical Formulation

One approach to the analysis of evaporation is through turbulent transport theory. The lower layer of the atmosphere is treated as a turbulent fluid and the conservation equation for a given constituent is a partial differential equation. Thus, for water vapor,

$$\frac{\partial e}{\partial t} + \underset{\sim}{u} \cdot \nabla e = \nabla \cdot (\underset{\approx}{K} \nabla e) \tag{3.8}$$

in which e is the water vapor pressure, $\underset{\sim}{u}$ is the three-dimensional wind field, and $\underset{\approx}{K}$ is the turbulent diffusivity tensor. If we assume the existence of a unidirectional wind field (i.e., neglect the Ekman spiral), we may align the x coordinate in the direction of the wind. Then, invoking the boundary layer approximation that longitudinal dispersion is unimportant, (3.8) may be written

$$\frac{\partial e}{\partial t} + u \frac{\partial e}{\partial x} = \frac{\partial}{\partial y} (K_y \frac{\partial e}{\partial y}) + \frac{\partial}{\partial z} (K_z \frac{\partial e}{\partial z}) \tag{3.9}$$

The steady state version is

$$u \frac{\partial e}{\partial x} = \frac{\partial}{\partial y} (K_y \frac{\partial e}{\partial y}) + \frac{\partial}{\partial z} (K_z \frac{\partial e}{\partial z}) \tag{3.10}$$

which says that the increase in advected moisture along the wind is equal to the vertical and lateral diffusive convergence of moisture.

Most important evaporation problems can be characterized by one of the following three surface boundary conditions:

1. Specified vapor pressure.

$$e\Big|_{z=0} = F(x, y) \tag{3.11}$$

For instance, this would be applied to a wet surface, for which

$$F(x, y) = e_s(T\Big|_{z=0}) \tag{3.12}$$

where $e_s(T|_{z=0})$ is the saturation vapor pressure and $T|_{z=0}$ is the surface temperature.

2. Specified vapor flux.

$$-K_z \frac{\partial e}{\partial z}\Big|_{z=0} = q(x, y) \tag{3.13}$$

where q(x,y) is the surface flux of vapor. This would be the case when evaporation is known a priori, independently of atmospheric conditions. For us, it is not an interesting problem, since we hope to determine q(x,y) itself. When we know q(x,y) a priori, there is no need to solve the atmospheric diffusion problem.

3. Saturation vapor pressure and a resistant canopy. The vapor pressure is considered fixed at saturation inside the leaves of a vegetal canopy. The flux of vapor through the leaf is resisted by the leaf stomata. Equating the vertical vapor flux at the bottom of the atmosphere to the flux through the canopy, we obtain

$$-K_z \left.\frac{\partial e}{\partial z}\right|_{z=0} = \frac{1}{r_c}\left[e_s\left(T\big|_{z=0}\right) - e\big|_{z=0}\right] \tag{3.14}$$

in which r_c is the canopy resistance. Mathematically, this is a mixed-type boundary condition, involving both e and its derivative normal to the boundary. In general, the canopy resistance varies dynamically in space and time as different plant species respond to such environmental factors as soil moisture and solar radiation. In the present analysis, we shall treat r_c as an independently specified parameter field.

As r_c goes to zero, (3.14) reduces to the combination of (3.11) and (3.12). We shall thus use (3.14) in the following discussion of the first and third case.

Equation (3.14) requires knowledge of the surface temperature. Since temperature is so strongly influenced by evaporation, a useful analysis must incorporate its determination as part of the solution. We thus introduce a second diffusion equation,

$$u \frac{\partial \theta}{\partial x} = \frac{\partial}{\partial y} (K_y \frac{\partial \theta}{\partial y}) + \frac{\partial}{\partial z} (K_z \frac{\partial \theta}{\partial z}) \tag{3.15}$$

where we have assumed similarity of diffusion for moisture and heat. This equation is written in terms of θ, the potential temperature, which accounts for the adiabatic changes in temperature of air subjected to varying pressures. It is given by

$$\theta = T(\frac{p_o}{p})^{R_a/c_p} \tag{3.16}$$

where T is the actual temperature, p is pressure, p_o is surface pressure, R_a is the gas constant for air and c_p is the specific heat of air. At the surface, θ and T are identical.

The second surface boundary condition is the requirement of energy balance at the surface. It is

$$Rn - G = H + LE \tag{3.17}$$

in which Rn is the net radiation, G is heat conduction into the ground, L is the latent heat of vaporization of water, and

E and H are the surface moisture and heat fluxes, given by

$$LE = - \frac{\rho c_p}{\gamma} K_z \left.\frac{\partial e}{\partial z}\right|_{z=0} \tag{3.18}$$

and

$$H = -\rho c_p K_z \left.\frac{\partial \theta}{\partial z}\right|_{z=0} \tag{3.19}$$

Depending upon the situation, Rn and G may be significantly influenced by the surface temperature. To first order, that dependence may be expressed as

$$Rn - G = R + S(\theta\big|_{z=0} - \theta_m) \tag{3.20}$$

where θ_m is a typical temperature, around which Rn-G is linearized, and R and S are constants. Similarly, $e_s(T)$ in (3.14) is linearized as

$$e_s(T\big|_{z=0}) = e_s(\theta\big|_{z=0}) = e_m + \Delta(\theta\big|_{z=0} - \theta_m) \tag{3.21}$$

where

$$e_m \equiv e_s(\theta_m) \tag{3.22}$$

and

$$\Delta \equiv \left.\frac{de_s}{dT}\right|_{T=\theta_m} \tag{3.23}$$

Using (3.18) through (3.21), the surface boundary conditions (3.14) and (3.17) can be re-written as

$$-K_z \frac{\partial e}{\partial z}\bigg|_{z=0} = \frac{1}{r_c}\left| e_m - \Delta\theta_m - e\big|_{z=0} + \Delta\theta\big|_{z=0} \right| \tag{3.24}$$

and

$$R + S(\theta\big|_{z=0} - \theta_m) - \rho c_p K_z \frac{\partial \theta}{\partial z}\bigg|_{z=0} - \frac{\rho c_p}{\gamma} K_z \frac{\partial e}{\partial z}\bigg|_{z=0} \tag{3.25}$$

A complete mathematical statement of the steady evaporation and heat balance problem for a surface on which the canopy resistance model is valid consists of the conservation equations (3.10) and (3.15), the boundary conditions (3.24) and (3.25), and the specification of upwind or "initial" conditions,

$$e\big|_{x=0} = e_a(y, z) \tag{3.26}$$

$$\theta\big|_{x=0} = \theta_a(y, z) \tag{3.27}$$

In addition, the vertical profiles of u, K_y, and K_z, and the surface variation of r_c, R and S must be given.

3.3 Crosswind Variability

The distributions of e and θ may depend on y, the crosswind coordinate, due to y-dependence of the upwind conditions or of the surface parameters r_c, R, or S. Since we are interested in areal average evaporation rates, we are willing to tolerate the loss of information induced by integrating our problem across the wind. Equation (3.10), integrated with respect to y, becomes

$$u \frac{\partial \bar{e}}{\partial x} = \frac{\partial}{\partial z} (K_z \frac{\partial \bar{e}}{\partial z}) + \frac{K_y}{y_2 - y_1} \frac{\partial e}{\partial y}\Bigg|_{y_1}^{y_2} \qquad (3.28)$$

in which

$$\bar{e} = \frac{1}{y_2 - y_1} \int_{y_1}^{y_2} e \, dy \qquad (3.29)$$

and y_1 and y_2 are the limits of the integration. If the lateral variations of the upwind conditions and the surface parameters are periodic, a symmetry argument can be invoked to justify dropping the lateral flux terms in (3.28) by choosing $(y_2 - y_1)$ large relative to the period,

$$u \frac{\partial \bar{e}}{\partial x} = \frac{\partial}{\partial z} (K_z \frac{\partial \bar{e}}{\partial z}) \qquad (3.30)$$

A similar integration converts the boundary condition (3.24) to

$$-K_z \frac{\partial \bar{e}}{\partial z}\Bigg|_{z=0} = \frac{1}{\bar{r}_c}(e_m - \Delta\theta_m) - \frac{1}{y_2 - y_1} \int_{y_1}^{y_2} \frac{1}{r_c} (e\Big|_{z=0} - \Delta\theta\Big|_{z=0}) dy \qquad (3.31)$$

where

$$\frac{1}{\bar{r}_c} \equiv \frac{1}{y_2-y_1} \int_{y_1}^{y_2} \frac{dy}{r_c} \qquad (3.32)$$

The final integral in (3.31) cannot be directly expressed as a linear combination of $\bar{e}$ and $\bar{\theta}$ or their derivatives. In order to proceed along this line of analysis, we shall assume that r_c is independent of y; the more general case will be treated in Section 3.5 using a simpler model. Equation (3.31) becomes

$$-K_z \left.\frac{\partial \bar{e}}{\partial z}\right|_{z=0} = \frac{1}{r_c}\left| e_m - \Delta\theta_m - \bar{e}\right|_{z=0} + \left.\Delta\bar{\theta}\right|_{z=0}\Big| \qquad (3.33)$$

The same approach, applied to the heat equation and to (3.25) yields

$$u \frac{\partial \bar{\theta}}{\partial x} = \frac{\partial}{\partial z} \left(K_z \frac{\partial \bar{\theta}}{\partial z}\right) \qquad (3.34)$$

and

$$\bar{R} + S(\left.\bar{\theta}\right|_{z=0} - \theta_m) = -\rho c_p K_z \left.\frac{\partial \bar{\theta}}{\partial z}\right|_{z=0} - \frac{\rho c_p}{\gamma} K_z \left.\frac{\partial \bar{e}}{\partial z}\right|_{z=0} \qquad (3.35)$$

where

$$\bar{R} = \frac{1}{y_2-y_1} \int_{y_1}^{y_2} R \, dy \qquad (3.36)$$

and, as with r_c, S is not a function of y. Upwind conditions

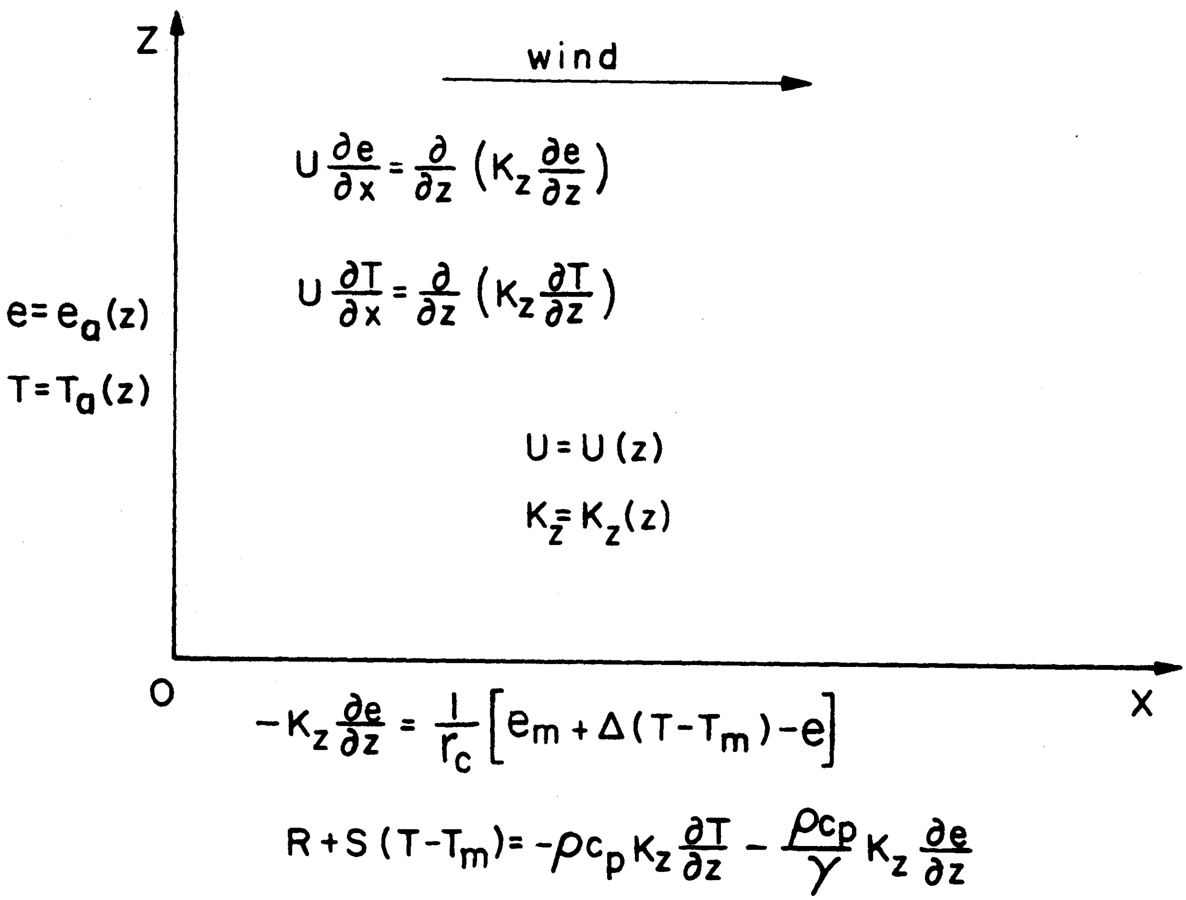

Figure 3.1

DIFFERENTIAL EQUATIONS AND BOUNDARY CONDITIONS FOR TWO-DIMENSIONAL, STEADY-STATE, TURBULENT DIFFUSION AND ADVECTION OF VAPOR AND HEAT IN THE ATMOSPHERE.

are

$$\bar{e}\Big|_{x=0} = \bar{e}_a(z) \tag{3.37}$$

$$\bar{\theta}\Big|_{x=0} = \bar{\theta}_a(z) \tag{3.38}$$

where $\bar{e}_a$ and $\bar{\theta}_a$ are lateral averages.

In summary, we have removed the y-coordinate from our original system of equations by restricting the canopy resistance and the temperature derivative of available energy to vary only in the direction of the wind. The two-dimensional formulation that has been obtained is the starting point for most partial differential equation analyses of advection effects on evaporation. It is illustrated in Figure 3.1. In the following sections, the overbars will be dropped.

3.4 Equilibrium Evaporation

Our goal is to determine areal average values of E, as given by (3.18), as a function of the distributions of r_c, R, and S, and the upwind conditions. A convenient approach to the problem of a surface discontinuity of one of these parameters relies on the concept of equilibrium humidity and temperature profiles (Laikhtman, 1964; Yeh and Brutsaert, 1971). It is hypothesized that the upwind conditions (3.37) and (3.38) satisfy the upwind surface boundary conditions and that they satisıy the conservation equations in such a way that the vertical flux divergences are zero. This assumption makes the problem analytically tractable. McNaughton (1976a) challenges this assumption and demonstrates that, strictly speaking, such equilibrium profiles never occur. Non-zero evaporation results in a continuous accumulation of water in the air. His further analysis of this problem is illuminating, so we shall consider it here.

It is possible to introduce two linear combinations of e and θ, each of which then satisfies the same diffusion equation. More significantly, if the combinations are properly chosen, the surface boundary conditions may be expressed independently in terms of the new variables, i.e., the two quantities are not coupled. McNaughton (1976a), who takes S as zero, shows that these new variables are

$$\psi_1 = \gamma\theta + e \tag{3.39}$$

and

$$\psi_2 = -\Delta\theta + e \tag{3.40}$$

Then the surface boundary conditions can be put in the form

$$-\rho c_p \, K_z \left.\frac{\partial\psi_1}{\partial z}\right|_{z=0} = \gamma R \tag{3.41}$$

and

$$-\rho c_p \, K_z \left.\frac{\partial\psi_2}{\partial z}\right|_{z=0} = -\Delta R + \frac{\Delta+\gamma}{\Delta} \frac{\rho c_p}{r_c} \left(e_{sm} - \Delta\theta_m - \left.\psi_2\right|_{z=0}\right) \tag{3.42}$$

Defining

$$\Psi_i \equiv -\rho c_p K_z \frac{\partial \psi_i}{\partial z} \tag{3.43}$$

for both i, we have also

$$H = (\Delta+\gamma)^{-1} \left(\Psi_1\Big|_{z=0} - \Psi_2\Big|_{z=0}\right) \tag{3.44}$$

and

$$LE = \gamma^{-1}(\Delta+\gamma)^{-1}\left(\Delta \Psi_1\Big|_{z=0} + \gamma \Psi_2\Big|_{z=0}\right) \tag{3.45}$$

Thus, evaporation can be computed when the surface values of Ψ_1 and Ψ_2 are known. From (3.41) and (3.43), we know $\Psi_1\big|_{z=0}$ a priori, without solving the new diffusion equation. It is

$$\Psi_1\Big|_{z=0} = \gamma R \tag{3.46}$$

and therefore

$$LE = \frac{\Delta}{\Delta+\gamma} R + \frac{1}{\Delta+\gamma} \Psi_2\Big|_{z=0} \tag{3.47}$$

McNaughton (1976a) shows that, if K_z increases sublinearly or not at all for large z (a situation which holds generally in the free atmosphere), then Ψ_2 must approach zero for large x over a homogeneous surface. Assuming that such an equilibrium has been reached upwind of a surface discontinuity at x=0, the upwind condition on ψ_2 may be written, using (3.42), as

$$\psi_2\Big|_{x=0} \equiv \psi_o = e_{sm} - \Delta\theta_m - \frac{\Delta}{\Delta+\gamma}\,\frac{r_c'}{\rho c_p}\,R' \qquad (3.48)$$

in which r_c' and R' are associated with the upwind surface.

The problem of approach to equilibrium with a new surface then reduces to the solution of the conservation equation

$$u\,\frac{\partial\psi_2}{\partial x} = \frac{\partial}{\partial z}\left(K_z\,\frac{\partial\psi_2}{\partial z}\right) \qquad (3.49)$$

subject to (3.42) and (3.48). The solution yields $\Psi_2\Big|_{z=0}$ as a function of x. The distance in x required for this flux to decay to a small proportion of its initial value just downwind of the discontinuity is a characteristic length defining the horizontal range over which advection is important. We shall now estimate the order of magnitude of this distance. Several models will be considered, as no single one can give a definitive answer.

McNaughton (1976b) solves (3.42), (3.48), and (3.49) for u and K_z given by the power law expressions

$$u = a\,u_*(z/z_o)^m \qquad (3.50)$$

$$K_z = bu_* z_o (z/z_o)^{1-m} \tag{3.51}$$

in which u_* is the friction velocity, z_o is the surface roughness, and a, b, and m are constants having reasonable values as follows:

$$m = 1/7$$

$$a = 6.2$$

$$b = 1.1$$

His solution, expressed as

$$\Phi(x) \equiv (\Psi_2\big|_{z=0})/(\Psi_2\big|_{\substack{z=0\\x=0^+}}) \tag{3.52}$$

is reproduced in Figure 3.2 for m equal to 1/6 and 1/8. As he notes, (3.50) and (3.51) are valid only in the lowest 100 meters of the atmosphere. We may convert this height to a fetch by means of an approximate boundary layer growth model (Equation 3.111). For a surface roughness of one meter, the corresponding fetch is about 300 meters. For a surface roughness of one centimeter, it is one kilometer. Choosing typical values (Table 3.1) of the parameters $\gamma r_c u_*/(\Delta+\gamma)=10$ and $z_o=0.1$ m, Φ goes to about 0.4 for a fetch of 500 meters, the approximate limit of validity of the solution imposed by the use of (3.50) and (3.51). Farther downwind, the model predicts Φ as large as 0.2 for a distance of ten thousand kilometers. In order to look at the large-fetch behavior, we shall use two other mod-

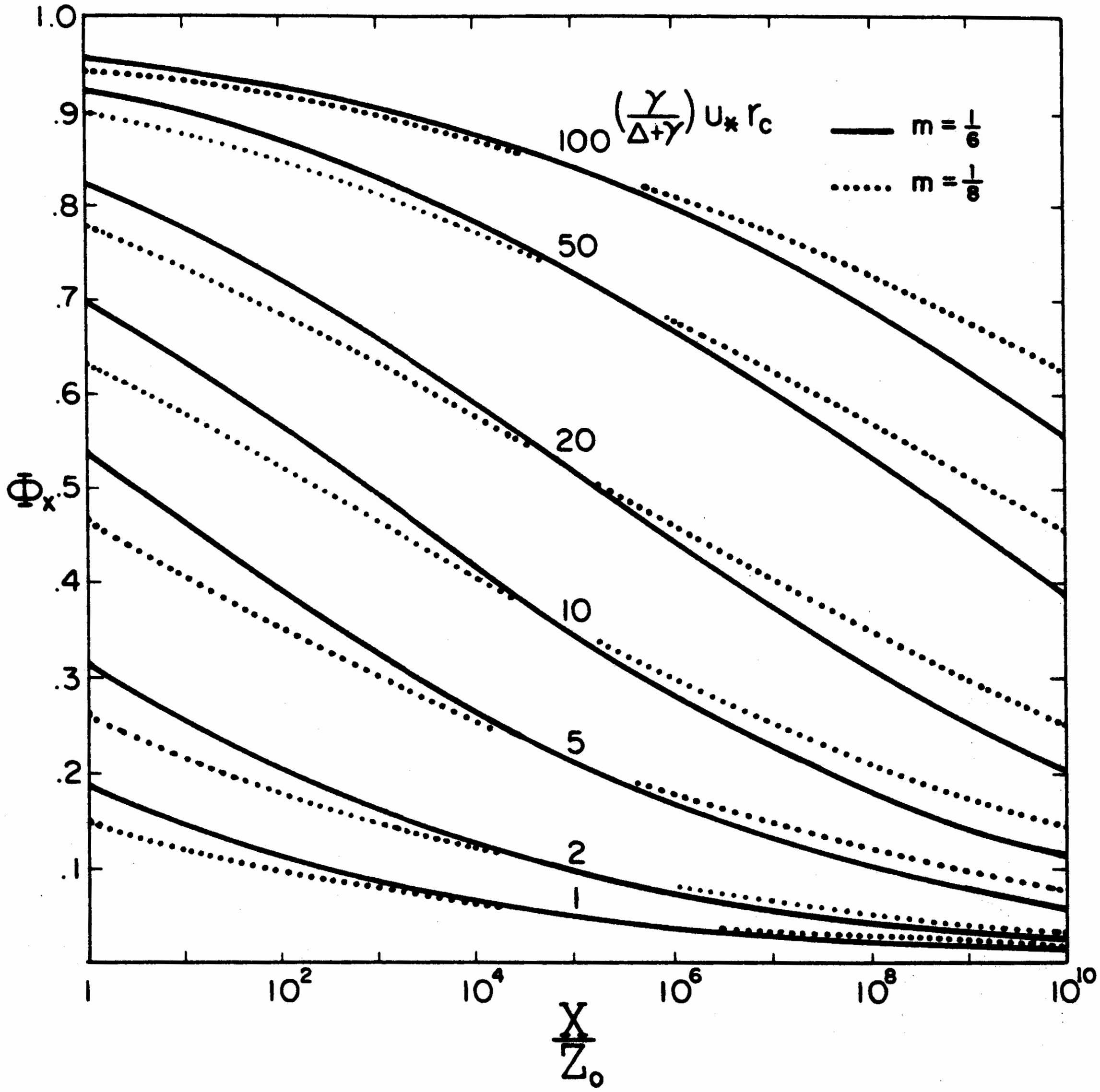

Figure 3.2

DECAY OF Φ DOWNWIND OF A SURFACE DISCONTINUITY FOR POWER LAW DIFFUSIVITY AND WINDSPEED. FROM MacNAUGHTON (1976).

els.

McNaughton (1976b) proposed a second model, in which a fully mixed layer existed beneath an inversion layer at height h. It predicted that Φ would decay exponentially in x with a distance constant of $\gamma r_c uh/(\Delta+\gamma)$, where u is a constant velocity. For h equal to one kilometer and $\gamma r_c u/(\Delta+\gamma)$ equal to 10, McNaughton obtains a distance constant of 10 kilometers. A more typical value of the latter parameter equal to 100 would yield a distance constant of 100 kilometers. This model is quite limited due to its assumption of instantaneous vertical mixing and an inversion barrier. In general, we would expect it to underestimate the equilibrium distance.

Since neither of McNaughton's models is directly applicable to the problem of evaporation into a free atmosphere at large fetch, we propose a third model. At a height d in the planetary boundary layer above which u and K_z do not vary strongly with altitude (say d=50 m), u and K_z in (3.49) are taken to be constants, U and K_o. Although these quantities do vary, we shall select typical values in order to obtain an order-of-magnitude estimate of the equilibrium evaporation distance. We may take U as the geostrophic wind. K_o is evaluated in Section 3.5.3.

The inhomogeneous surface layer is represented as a resistance to vertical diffusion, and its storage capacity is neglected. This view is consistent with the expected behavior at large fetch. The flux through this layer is given by

$$\Psi_2 = -\frac{\rho c_p}{r_a}\left(\psi_2\big|_{z=d} - \psi_2\big|_{z=0}\right) \tag{3.53}$$

in which r_a is the aerodynamic resistance to flow through the layer, and d is its thickness. Elimination of $\psi_2|_{z=0}$ between (3.42) and (3.53) yields

$$-\left(\frac{\Delta}{\Delta+\gamma} + \frac{r_a}{r_c}\right) K_o \frac{\partial\psi_2}{\partial z}\bigg|_{z=d} + \frac{1}{r_c}\psi_2\big|_{z=d} =$$

$$\frac{1}{r_c}(e_{sm} - \Delta\theta_m) - \frac{\Delta R}{(\Delta+\gamma)\rho c_p} \tag{3.54}$$

The "initial" condition is given by (3.48). This is a standard heat diffusion problem for a semi-infinite domain with a mixed-type boundary condition. The solution, obtained by using a Fourier transform, is

$$\psi_2 = \psi_o + \psi_{oo}\left\{\operatorname{erfc}\left[\frac{z-d}{2}\sqrt{\frac{U}{K_o x}}\right]\right.$$

$$\left. -\exp\left[\omega(z-d) + \frac{K_o\omega^2 x}{U}\right]\operatorname{erfc}\left[\omega\sqrt{\frac{K_o x}{U}} + \frac{z-d}{2}\sqrt{\frac{U}{K_o x}}\right]\right\} \tag{3.55}$$

in which ψ_o is given by (3.48), and the other parameters are

$$\psi_{oo} = \frac{\Delta}{(\Delta+\gamma)\ \rho c_p}(r_c' R' - r_c R) \tag{3.56}$$

$$\omega = \left[\left(\frac{\Delta}{\Delta\ \gamma} r_c + r_a\right) K_o\right]^{-1} \tag{3.57}$$

The value of Φ is given by (3.52), (3.43), and (3.55) as

$$\Phi(x) = \exp\left(\frac{\omega^2 K_o x}{U}\right) \operatorname{erfc}\left(\omega \sqrt{\frac{K_o x}{U}}\right) \tag{3.58}$$

which is plotted in Figure 3.3. We can define a decay constant

$$X = \frac{U}{\omega^2 K_o} \tag{3.59}$$

for this function. Typical values of the relevant parameters, listed in Table 3.1, yield a value of about two thousand kilometers for X.

This analysis, as well as our interpretation of McNaughton's (1976b) work, support the conclusion that an equilibrium evaporation rate, as defined by McNaughton (i.e., $\Psi_2\big|_{z=0}$ goes to zero), is unlikely to occur over the earth's land surface wnen the availability of water is characterized by a non-zero canopy resistance. This conclusion is consistent with a number of studies that have found that the first term on the right hand side of (3.47) underestimates actual evapotranspiration from extensive surfaces (Brutsaert and Stricker, 1979).

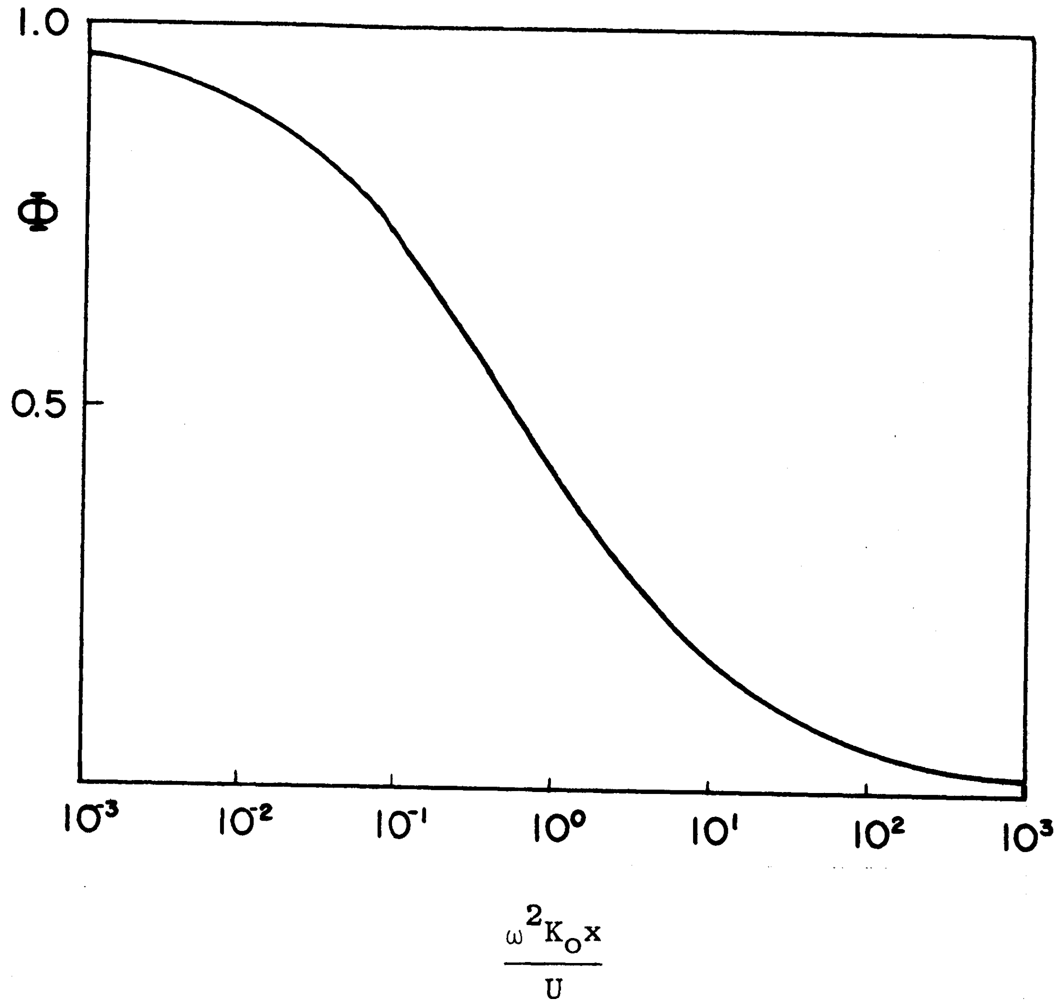

Figure 3.3

DECAY OF Φ DOWNWIND OF A SURFACE DISCONTINUITY ACCORDING TO (3.58).

SYMBOL	DESCRIPTION	TYPICAL VALUE(S)
U	geostropic wind	$10\ m\ s^{-1}$ (Holton, 1979, p. 36)
k	von Karman constant	0.4
u_*	friction velocity	$\sim U/30$ (Jensen, 1978)
h_o	parameter in (3.95)	50 m (Section 3.5.3)
K_o	asymptotic value of K_z in (3.95)	$5\ m^2\ s^{-1}$ (using (3.103))
Δ/γ	Δ: slope of saturation vapor pressure curve	2 at 19°C
	γ: psychrometric constant	(Eagleson, 1970, p. 228)
z_o	surface roughness height	
	short grass	.01 m (Eagleson, 1970, p. 230)
	brush, tall crops	.1 m (Eagleson, 1970, p. 230)
	forest	1 m (Eagleson, 1970, p. 230)
$r_a(z_o, h_o)$	aerodynamic resistance between surface and height h_o in (3.53)	
	$z_o = .01$ m	$240\ sm^{-1}$ (Using (3.99))
	$z_o = .1$ m	$130\ sm^{-1}$ (Using (3.99))
	$z_o = 1$m	$50\ sm^{-1}$ (Using (3.99))
f	Coriolis parameter	$10^{-4}\ s^{-1}$
De	depth of Ekman layer	10^3 m

Table 3.1

NOMINAL ATMOSPHERIC AND SURFACE PARAMETERS USED IN THIS CHAPTER

(continued on next page)

SYMBOL	DESCRIPTION	TYPICAL VALUE(S)	
r_c	canopy resistance		
	wet vegetation or surface	0	
	crops, short grass	*30-70 s m^{-1}	Oke (1978) and Eagleson (1970)
	forests	*100-150 s m^{-1}	
	any dry surface	∞	

*These represent minimum values, thus implying sufficient soil moisture availability.

Table 3.1
(cont.d)

NOMINAL ATMOSPHERIC AND SURFACE PARAMETERS USED IN THIS CHAPTER

3.5 A Conceptual Model of Evaporation from a Surface of Varying Roughness, Canopy Resistance, and Available Energy

3.5.1 Introduction

The results of the previous section imply that the internal boundary layers associated with changes of surface properties or states ordinarily do not grow so large as to permit us to neglect advection. Over a homogeneous surface, evaporation and sensible heat flux will vary slowly. Variations are so slow, in fact, that they may often be negligible. Referring to Figure 3.3, for X=100 km, we see that Φ does not vary by more than 10 percent of its value at x=100 km over a range of 130 km. i.e., from x=50 km to x=180 km. A useful rule of thumb is that the distance over which evaporation can be considered constant is of the order of the fetch of the region downwind of the discontinuity.

Consider now the simple case of evaporation from a surface whose available energy alternates periodically with fetch in the direction of the wind, all other factors being constant. The high energy surfaces will be associated with higher evaporation rates than will the low energy surfaces. Internal moisture boundary layers associated with the different surfaces will grow with fetch. At a sufficient height, the individual internal boundary layers merge and the moisture profile becomes almost independent of fetch, in the sense of the situation discussed in the paragraph above. This situation is depicted in Figure 3.4, which shows a locally constant vapor pressure profile, and hence vapor flux, for large z The logarithmic profile changes slope for small z, implying a variable surface flux. The dashed line in the upper graph gives the evaporation rate corresponding to the large-z, constant-flux profile, while the solid line shows actual evaporation. By continuity, the dashed line thus gives the average height of the solid lines. The depth of influence of a new surface grows with fetch, as indicated by the traces of the growing boundary layers in the x-z plane of Figure 3.4.

The sensible heat flux and temperature profiles would exhibit variability similar to those discussed above for vapor. Whereas the evaporation rate is continuous in x due to the presence of a constant canopy resistance and a continuous e field, the available radiation discontinuities will be reflected in the surface heat fluxes.

In natural situations, there would also be variations of surface roughness and canopy resistance, probably correlated with the variations of energy availability, since all of these are due mainly to differences in the vegetal canopy.

In this section, we shall present a very simple conceptual model of evaporation from such heterogeneous surfaces. Although several limiting assumptions are made, the results should nevertheless reflect reality qualitatively. We shall sacrifice precision and generality in the interest of simplicity and physical insight for a specific set of assumptions.

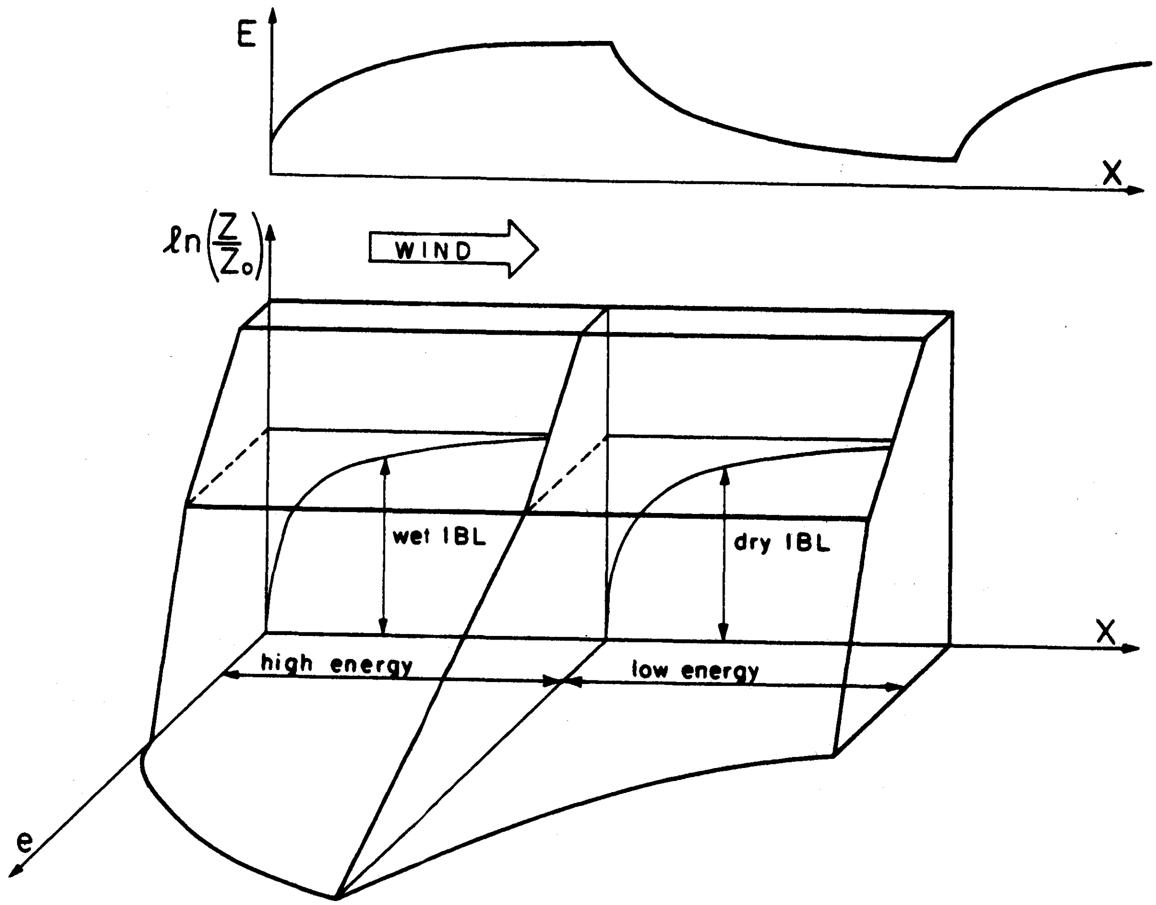

Figure 3.4

THE DEVELOPMENT OF INTERNAL BOUNDARY LAYERS AND THE ASSOCIATED EVAPORATION RATES OVER A REGULAR, INHOMOGENEOUS SURFACE. INHOMOGENEITY IS WITH RESPECT TO AVAILABLE ENERGY ONLY.

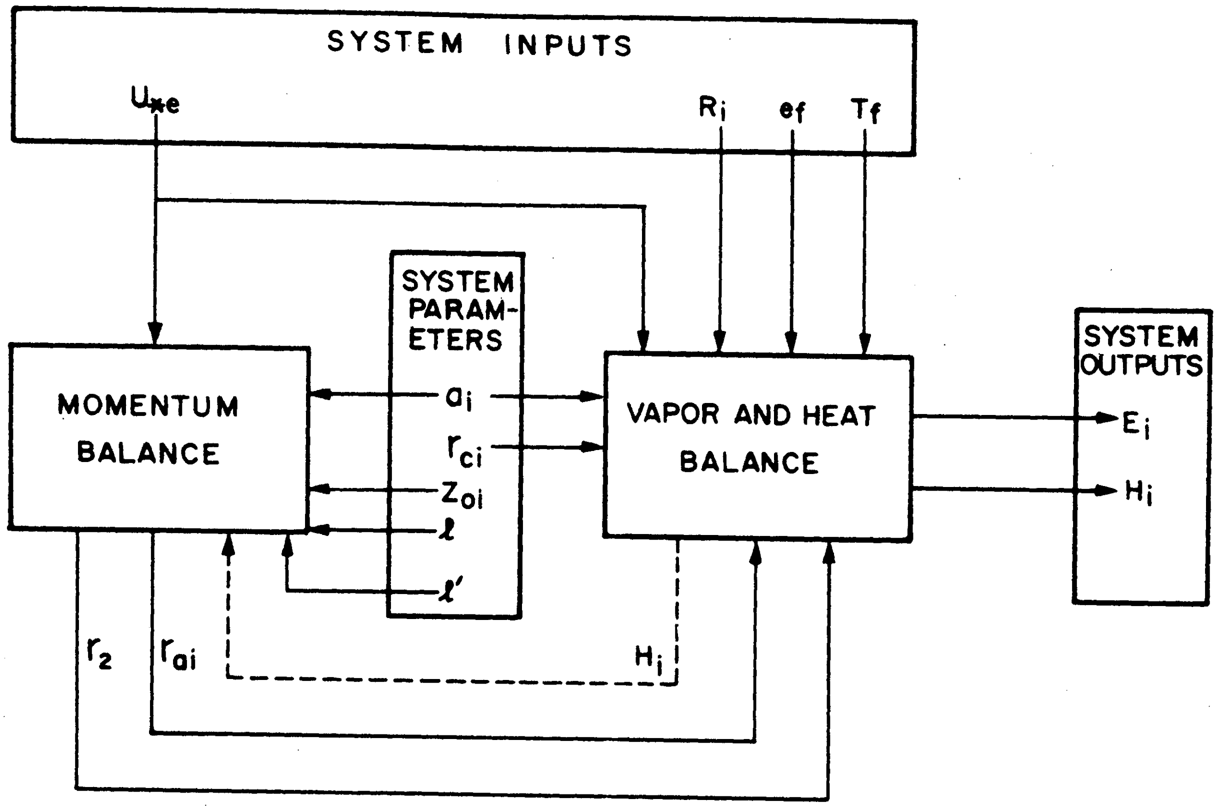

Figure 3.5

SYSTEM DIAGRAM OF THE COMBINED VAPOR, HEAT, AND MOMENTUM BALANCE OF THE PROPOSED MODEL. DASHED LINE INDICATES THE FEEDBACK OF HEAT FLUXES ON THE LEVEL OF TURBULENCE, NEGLECTED IN THIS STUDY.

The problem under consideration is the computation of the areal average evapotranspiration rate and its distribution, given an inhomogeneous area of length l' in the direction of the wind. The inhomogeneous area is a mosaic of homogeneous patches. Within a patch the available radiation, the canopy resistance, and the surface roughness are constant. Patches with the same values of this parameter set belong to the same patch type. Between patch types any or all of these quantities may differ. The number of patch types is given by N, and the actual number of patches may be considerably larger. Relative proportions of area covered by each patch type are specified. The scale of the inhomogeneity is defined by l, the characteristic patch size.

Also specified are upwind or free-stream conditions on vapor pressure and potential temperature, and the effective friction velocity.

The overall behavior of the atmosphere and the land surface is represented in Figure 3.5 as a system composed of two components - the momentum balance and the combined vapor and heat balance. The system is characterized by a set of parameters describing the heterogeneous land surface and is forced by inputs from the free atmosphere. The distributions of evaporation and sensible heat flux from the surface are the system outputs. The momentum balance (Figure 3.5) determines the resistances to turbulent diffusion of vapor and heat. We ignore the influence of heat fluxes on the state of turbulence and hence on the momentum balance (dashed line in Figure 3.5).

The boundary layer is neutrally stable. The feedback of the system outputs, the E_i's and H_i's, on free stream conditions (e_f and T_f) is not considered. Its importance is minimized by choosing the free stream height to be approximately at the top of the layer of influence of the modelled area. Thus, the height at which e_f and T_f are defined increases with the maximum fetch of the land surface under consideration.

The momentum, heat, and vapor balances are based on resistance networks whose common structure is defined by the surface heterogeneities. The inhomogeneous surface is composed of homogeneous patches of average length l, the patch size. Associated with each patch is what we shall loosely term an internal boundary layer - its area of influence - of average depth h (Figure 3.5), characterized by a resistance to turbulent diffusion. At and above the height h, we assume that there are no areal variations in the windspeed, temperature or vapor profiles. The system of parallel resistances is then in series with a single resistance between heights h and h', the free stream height. In analogy to h, h' is defined as the top of the layer of influence of the entire modelled area, the set of surface patches (Figure 3.6). The heights h and h' are on the order of the depth to which an internal boundary layer would grow at fetches l and l', the lengths of the homogeneous patches and of the entire area, respectively. In this conceptual model, we shall define them as such identically (Figure 3.6). The growth of an internal boundary layer is governed at short fetch by the surface roughness and at larger

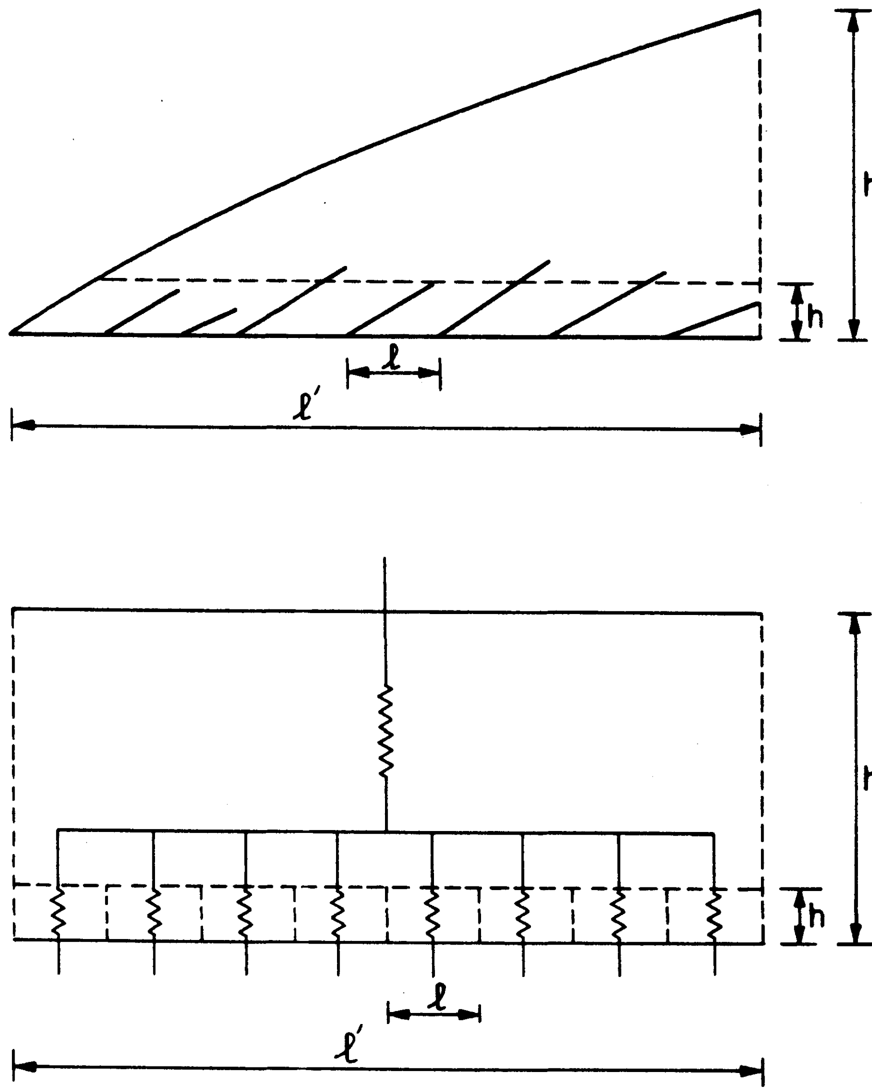

Figure 3.6

THE GROWTH OF THE DEPTH OF INFLUENCE OF THE PATCHES AND THE ENTIRE AREA WILL FETCH. THE DISTANCES ℓ AND h ARE AVERAGES. TOP: ACTUAL SITUATION. BOTTOM: CONSTANT-FETCH, CONSTANT-DEPTH IDEALIZATION FOR THE RESISTANCE NETWORK.

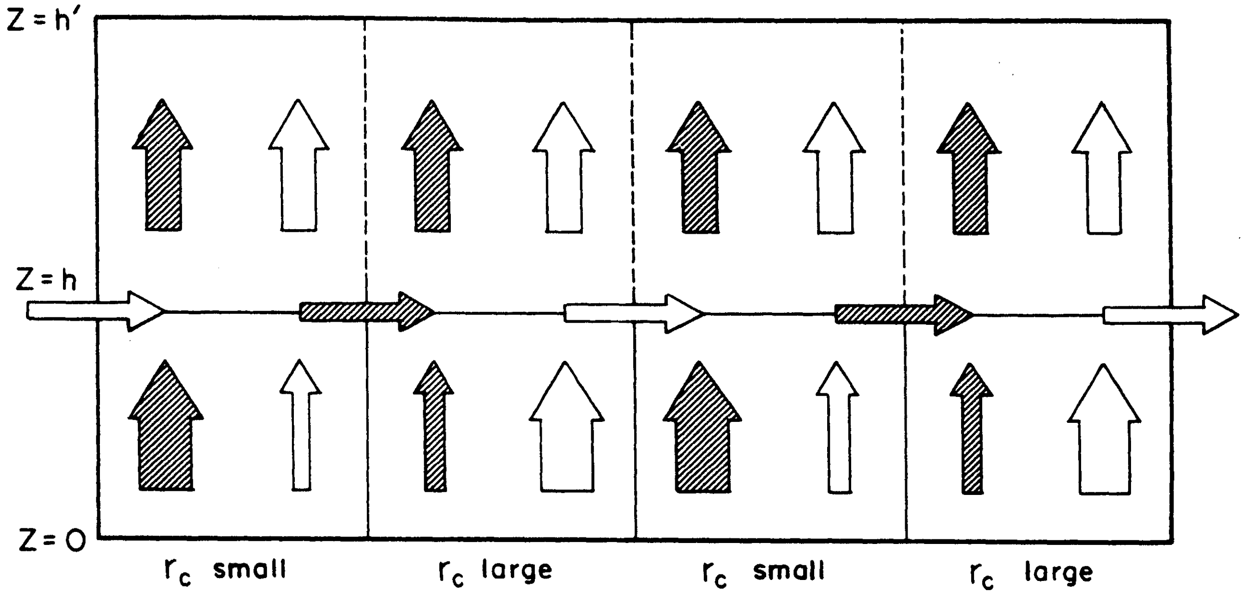

Figure 3.7

FLOWS OF VAPOR (CROSS-HATCHED ARROWS) AND HEAT (WHITE ARROWS) IMPLIED BY THE MODEL STRUCTURE. CONSTANT-IN-HEIGHT FLUXES, EXCEPT FOR DISCONTINUITIES AT HEIGHT h, IMPLY NET ADVECTIVE DIVERGENCES OF THE TRANSPORTED QUANTITIES.

fetch by the intensity of turbulence at higher levels.

The momentum, heat, and vapor balances are modelled by assuming that there are constant vertical fluxes through each internal boundary layer and through the homogeneous upper layer. We shall thus not include explicitly the local advective enhancement of evaporation that results from the passage of hot, dry air (from above a dry patch) over a wet patch. There is, nevertheless, a concentrated advective flux divergence at height h implicit in the model formulation. Weighted average evaporation per unit area from all the surface patches is equal to the constant vertical vapor flux per unit area in the upper layer. Since the flux rates through various internal boundary layers differ, this results in vertical flux discontinuities at the height h. These discontinuities imply a net advective divergence of vapor (and of heat) between patches (Figure 3.7). This effect is active also in the momentum balance when surface roughness is variable. Although the advective divergence is lumped at the top of the surface layers, rather than being distributed through the entire depth, its influence is nevertheless qualitatively correct. In order to include advective divergence over the entire depth h explicitly, it would be necessary to define in detail the geometric connections among the various patch types. The resulting set of equations cannot be so easily analyzed as the formulation proposed here.

An outline of the solution procedure follows:

1. The turbulent diffusion equations for vapor and heat are written in terms of bulk diffusion resistances. These equations, combined with the appropriate surface boundary conditions of energy conservation and canopy resistance, yield an explicit expression for the evaporation rate from each patch type. It is of the form

$$\frac{\Delta+\gamma}{\Delta}\,\frac{LE_i}{\overline{R}} = f_1\left[\frac{L\overline{E}}{\overline{R}},\ q,\ u_{*e}r_2;\ (a_i,\ \frac{R_i}{\overline{R}},\ u_{*e}r_{ai},\ u_{*e}r_{ci})_{i=1,N}\right] \qquad (3.60)$$

where the subscript i denotes the i'th patch type and the overbar means an areal average. The parameter q defines the importance of regional advection, u_{*e} is the friction velocity associated with the areal average momentum flux, r_{ai} is the aerodynamic resistance between the surface and height h, r_{ci} is the canopy resistance, and r_2 is the resistance between heights h and h'. The areal average evaporation is derived from the same model as

$$\frac{\Delta+\gamma}{\Delta}\,\frac{L\overline{E}}{\overline{R}} = f_2\left[q,\ u_{*e}r_2;\ (a_i,\ \frac{R_i}{\overline{R}},\ u_{*e}r_{ai},\ u_{*e}r_{ci})_{i=1,N}\right] \qquad (3.61)$$

2. The vertical turbulent diffusivity is assumed to have the form

$$K_z = K_o\left(\frac{z}{z+h_o}\right) \qquad (3.62)$$

where h_o is a constant. By identifying the aerodynamic resistance as the height integral of the reciprocal of K_z, we derive the expressions

$$u_{*i} r_{ai} = f_3(h,\ z_{oi}) \tag{3.63}$$

$$u_{*e} r_2 = f_4(h,\ h') \tag{3.64}$$

where u_{*i} is the friction velocity and z_{oi} the surface roughness of the i'th patch type. The requirement of continuity of the wind field at height h gives a relation describing the momentum flux discontinuity there,

$$\frac{u_{*i}}{u_{*e}} = f_5(h,\ z_{oe},\ z_{oi}) \tag{3.65}$$

where z_{oe} is an effective surface roughness. We then have

$$u_{*e} r_{ai} = f_6(h,\ z_{oe},\ z_{oi}) \tag{3.66}$$

The solution now rests on the definition of h, h', and z_{oe}.

3. The requirement that areal average momentum flux be continuous at height h gives us an equation of the form

$$f_7[h,\ z_{oe},\ (z_{oi})_{i=1,N}] = 0 \tag{3.67}$$

A proposed boundary layer growth model yields

$$h = f_8(z_{oe},\ \ell) \tag{3.68}$$

and

$$h' = f_8(z_{oe}, \ell') \tag{3.69}$$

Equations (3.67) and (3.68) give z_{oe} and h as functions of the z_{oi}'s and l, and then (3.69) yields the value of h' in terms of l'. We can then compute $u_{*e}r_{ai}$ and $u_{*e}r_2$ and evaluate the evaporation rates in terms of the problem parameters.

$$\frac{\Delta+\gamma}{\Delta}\frac{LE_i}{\overline{R}} = f_9\left[\frac{L\overline{E}}{\overline{R}}, q, \ell, \ell'; \left(a_i, \frac{R_i}{\overline{R}}, u_{*e}r_{ci}, z_{oi}\right)_{i=1,N}\right] \tag{3.70}$$

$$\frac{\Delta+\gamma}{\Delta}\frac{L\overline{E}}{\overline{R}} = f_{10}\left[q, \ell, \ell'; \left(a_i, \frac{R_i}{\overline{R}}, u_{*e}r_{ci}, z_{oi}\right)_{i=1,N}\right] \tag{3.71}$$

The major assumptions in the analysis are listed below:

GENERAL

1. Steady state conditions apply.

2. The canopy resistance model is applicable and r_c can be specified exogenously.

3. Turbulent transport of vapor, heat, and momentum are similar so that the same diffusivities apply, and the virtual source/sink for each entity is at the same height, the surface roughness height. These assumptions are for convenience and are not essential.

4. The advective divergences are lumped at a single

height, h.

5. There is no radiative flux divergence at any height.

6. The constant-thickness conceptual model of the internal boundary layer is valid.

MOMENTUM BALANCE

1. The momentum flux divergence associated with the Coriolis force is unimportant.

2. Atmospheric boundary layer is neutrally stable, independent of heat fluxes.

3. A specific functional form for K_z is assumed.

4. Internal boundary layer depth is governed by surface roughness up to a certain fetch, after which further growth is controlled by conditions in the free atmosphere.

3.5.2 Vapor and Heat Balance of an Inhomogeneous Surface

In this section, we describe the simple resistance diffusion model as it is applied to the coupled vapor and heat balances. It will allow us to account for surface variations of surface roughness, canopy resistance, and available radiation. We shall temporarily treat the resistances as given. They will later be derived from the momentum balance

The proposed model is depicted schematically in Figure 3.8. There are N distinct surface types, each characterized by a unique set of values of available energy, canopy resistance and surface roughness. The subscript i is used to denote the i'th surface, e.g., R_i, r_{ai}, z_{oi}. The variables are defined as follows:

θ_{oi} potential temperature of patch type i

r_{ai} aerodynamic resistance between surface and height h for patch type i

H_i surface heat flux per unit area of surface i

θ_h potential temperature at height h

r_2 aerodynamic resistance between heights h and h'

$\overline{H}$ areal average sensible heat flux rate

θ_f potential temperature at height h', in the free stream

e_{oi} saturation vapor pressure at temperature T_{oi}

r_{ci} canopy resistance of surface type i

e_i effective surface vapor pressure at surface type i

E_i evaporation rate per unit area of surface type i

e_h vapor pressure at height h

$\overline{E}$ areal average evaporation rate

e_f vapor pressure at height h'

a_i proportion of area represented by type i surface

z_{oi} surface roughness of type i surface

R_i $(Rn-G)_i$, available energy of type i surface

In Figure (3.8), sensible heat diffuses from the different surfaces, through the corresponding internal boundary layers, to a height h, at which there is no lateral variation of potential temperature. From this height, heat diffuses up to h', a height at which the potential temperature, θ_f, is independent of the surface evaporation. The resistances to heat diffusion are assumed to be equal to those for

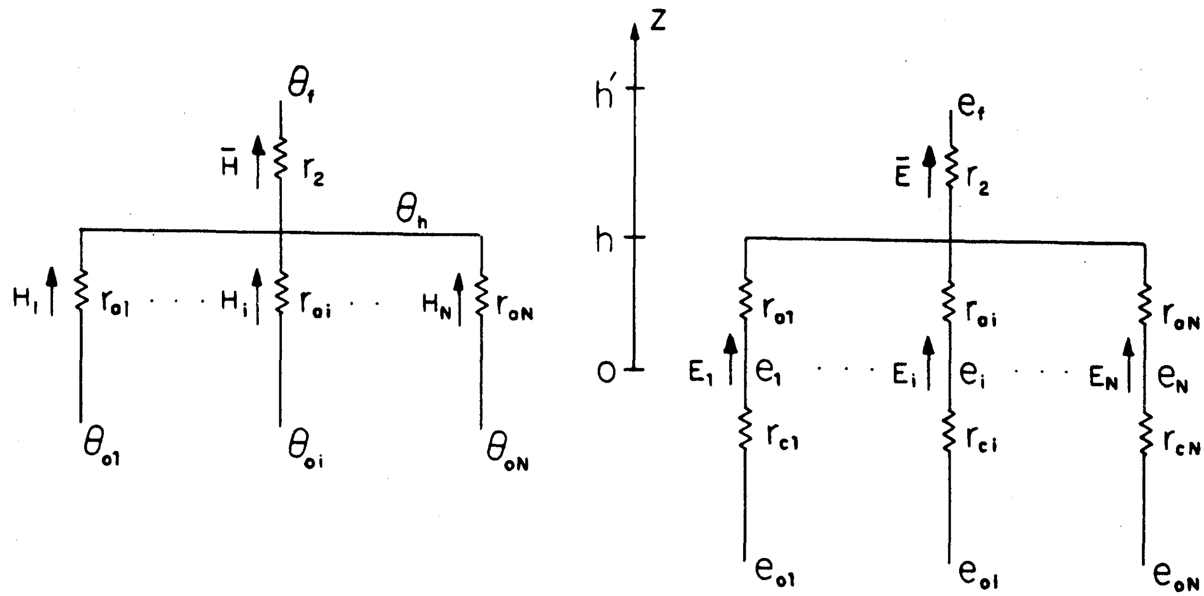

Figure 3.8

RESISTANCE NETWORKS FOR EVAPORATION AND SENSIBLE HEAT DIFFUSION FROM A HETEROGENEOUS SURFACE.

momentum. These aerodynamic resistances will be expressed in terms of surface roughness and characteristic lengths of the inhomogeneous surface.

A similar resistance network for vapor is also pictured in Figure 3.8. At each surface, a canopy resistance to vapor diffusion is added, in analogy to Monteith's modification of the Penman equation.

On the basis of Figure 3.8, we write the following equations:

$$H_i = \frac{\rho c_p}{r_{ai}} (\theta_{oi} - \theta_h) \qquad i = 1, \ldots, N \tag{3.72}$$

$$\overline{H} = \sum_{i=1}^{N} a_i H_i \tag{3.73}$$

$$\overline{H} = \frac{\rho c_p}{r_2} (\theta_h - \theta_f) \tag{3.74}$$

$$LE_i = \frac{\rho c_p}{\gamma r_{ci}} (e_{oi} - e_i) \qquad i = 1, \ldots, N \tag{3.75}$$

$$LE_i = \frac{\rho c_p}{\gamma r_{ai}} (e_i - e_h) \qquad i = 1, \ldots, N \tag{3.76}$$

$$L\overline{E} = \sum_{i=1}^{N} a_i LE_i \tag{3.77}$$

$$L\overline{E} = \frac{\rho c_p}{\gamma r_2} (e_h - e_f) \tag{3.78}$$

In addition, we approximate the relation between e_o and θ_o at the surface as a linear one,

$$e_{oi} = e_m + \Delta(\theta_{oi} - \theta_m) \qquad i = 1, \ldots, N \tag{3.79}$$

The surface heat balance is

$$R_i = H_i + LE_i \qquad i = 1, \ldots, N \tag{3.80}$$

We have above 5N+4 equations - (3.72) through (3.80) - in 5N+4 unknowns - θ_{oi}, H_i, e_{oi}, e_i, E_i; θ_h, $\overline{H}$, e_h, $\overline{E}$.

Elimination of e_i between (3.75) and (3.76) yields

$$LE_i = \frac{\rho c_p}{\gamma(r_{ai}+r_{ci})}(e_{oi} - e_h) \qquad i = 1, \ldots, N \tag{3.81}$$

Substitution of (3.79) for e_{oi}, using (3.72) and (3.80) to evaluate T_{oi}, yields

$$LE_i = \frac{\Delta R_i + \frac{\rho c_p}{r_{ai}}(e_{sh} - e_h)}{\Delta + \gamma(1 + r_{ci}/r_{ai})} \qquad i = 1, \ldots, N \tag{3.82}$$

in which

$$e_{sh} \equiv e_m + \Delta(\theta - \theta_m) \tag{3.83}$$

Equation (3.82) is essentially the Penman-Monteith equation for patch type i, expressing evaporation as a function of e and θ at height h. In the current problem, these values are unknowns.

Equations (3.73), (3.74), (3.77), (3.78), (3.80), (3.82), and (3.83) can be combined to obtain an expression for the areal average evaporation rate. It is

$$L\overline{E} = \frac{\sum_{i=1}^{N} a_i \left\{ \dfrac{R_i + \dfrac{\rho c_p}{r_{ai}} (e_{sf} - e_f) + \Delta \overline{R} \dfrac{r_2}{r_{ai}}}{\Delta + \gamma(1 + r_{ci}/r_{ai})} \right\}}{1 + \sum_{i=1}^{N} a_i \left\{ \dfrac{(\Delta+\gamma) r_2/r_{ai}}{\Delta + \gamma(1 + r_{ci}/r_{ai})} \right\}} \tag{3.84}$$

in which

$$e_{sf} \equiv e_m + \Delta(\theta_f - \theta_m) \tag{3.85}$$

This can be normalized by $\Delta\overline{R}/(\Delta+\gamma)$, which is the evaporative energy consumption rate when $e_f = e_{sf}$ and $r_{ci} = r_2 = 0$, and written as

$$\overline{E}' \equiv \frac{(\Delta+\gamma)\, L\overline{E}}{\Delta \overline{R}}$$

$$= \frac{\sum_{i=1}^{N} a_i \left\{ \dfrac{\dfrac{R_i}{\overline{R}} + \dfrac{q}{u_{*e} r_{ai}}}{1 + \dfrac{\gamma}{\Delta}(1 + r_{ci}/r_{ai})} \right\} + \sum_{i=1}^{N} a_i \left\{ \dfrac{r_2/r_{ai}}{1 + \dfrac{\gamma}{\Delta}(1 + r_{ci}/r_{ai})} \right\}}{\dfrac{\Delta}{\Delta+\gamma} \sum_{i=1}^{N} a_i \left\{ \dfrac{r_2/r_{ai}}{1 + \dfrac{\gamma}{\Delta}(1 + r_{ci}/r_{ai})} \right\}} \tag{3.86}$$

in which

$$q \equiv \rho c_p u_{*e} (e_{sf} - e_f)/\Delta \overline{R} \tag{3.87}$$

is a measure of the importance of advective enhancement of evaporation. Thus.

$$\overline{E}' = f[q,\ u_{*e}r_2;\ (a_i,\ \frac{R_i}{\overline{R}},\ u_{*e}r_{ai},\ u_{*e}r_{ci})_{i=1,\ N}] \tag{3.88}$$

Note that when r_2 is set to zero, the second terms in both the numerator and the denominator of (3.86) vanish, leaving a simple weighted-average of the individual Penman-Monteith expressions for the different surfaces.

In a similar manner, we define E_i' as

$$E_i' \equiv \frac{\Delta+\gamma}{\Delta} \frac{LE_i}{\overline{R}} \tag{3.89}$$

which can be written, using (3.74), (3.78), (3.82), and (3.83), as

$$E_i' = \frac{\frac{R_i}{\overline{R}} + \frac{q}{u_{*e}r_{ai}} + \frac{r_2}{r_{ai}}(1 - \overline{E}')}{1 + \frac{r_{ci}/r_{ai}}{1 + \Delta/\gamma}} \tag{3.90}$$

and which can thus also be expressed as a function of the arguments in (3.88).

In order to proceed with the analysis, we need a model for the aerodynamic resistances, r_{ai} and r_2. These will be derived next.

3.5.3 Aerodynamic Resistances - The Momentum Balance

The aerodynamic resistances are related to the turbulent diffusivity introduced earlier in this chapter. Equation (3.18), written as a boundary condition, is also true for all z when there is no vapor flux divergence in the vertical, so

$$LE = - \frac{\rho c_p}{\gamma} K_z \frac{\partial e}{\partial z} \tag{3.91}$$

Equation (3.91) can be integrated between any two heights to obtain

$$- \frac{\gamma LE}{\rho c_p} \int_{z_1}^{z_2} \frac{dz}{K_z} = e_2 - e_1 \tag{3.92}$$

In comparison with (3.76) or (3.78), we see

$$r_a(z_1, z_2) = \int_{z_1}^{z_2} \frac{dz}{K_z} \tag{3.93}$$

so the aerodynamic resistance between two heights is a function of the turbulent diffusivity profile between those levels.

Near the surface (up to tens of meters), the magnitude of K_z is linearly proportional to the height, while higher up it can be taken as a constant (Holton, 1979, p. 107). At a sufficient height above the Ekman layer, which is on the order of a kilometer deep, K_z goes to zero. Ignoring this large-z behavior, we shall hypothesize the following form for K_z:

$$K_z = K_o \frac{z}{z+h_o} \tag{3.94}$$

where h_o is the approximate height separating the linear-K_z and constant-K_z regimes, and K_o is the value above the surface layer. In order to estimate h_o, we can use the fact that the mixing length, λ, is proportional to K_z. Thus

$$\lambda = \lambda_o \frac{z}{z+h_o} \tag{3.95}$$

For small z,

$$\lambda = kz = 0.4z \tag{3.96}$$

where k is the von Karman constant. Then

$$h_o = 2.5\lambda_o \tag{3.97}$$

The value of λ_o may be estimated as (Holton, 1979, p. 107)

$$\lambda_o \sim \left(\frac{fDe^3}{2\pi^2 U}\right)^{1/2} \tag{3.98}$$

where De is the depth of the Ekman layer, f is the Coriolis parameter, and U is the geostrophic wind speed. Typical values of these parameters (Table 3.1) yield a value for λ_o of twenty meters. By (3.97), this gives h_o equal to fifty meters.

Substitution of (3.94) into (3.93) yields

$$r_a(z_1, z_2) = K_o^{-1}\left[(z_2 - z_1) + h_o \ln\left(\frac{z_2}{z_1}\right)\right] \tag{3.99}$$

With our assumption of a height-independent momentum flux (τ=constant). the wind profile can be calculated from

$$\tau = \rho u_*^2 = \rho K_z \frac{\partial u}{\partial z} \tag{3.100}$$

and (3.94) to be

$$u = \frac{u_*^2}{K_o}\left[(z - z_o) + h_o \ln\left(\frac{z}{z_o}\right)\right] \tag{3.101}$$

where the integration constant is determined by letting u go to zero at $z=z_o$. For small z, (3.101) is equivalent to the familiar logarithmic profile,

$$u = \frac{u_*}{k} \ln \frac{z}{z_o} \tag{3.102}$$

and we see that

$$K_o = k u_* h_o \tag{3.103}$$

and the resistance to transport is thus inversely proportional to the friction velocity, which in turn goes like the square root of the vertical momentum flux.

Since the momentum fluxes, like the vapor and heat fluxes, will vary laterally due to surface inhomogeneity, we shall have to extend our simple advection model to cover these momentum fluxes. In order to describe the momentum transport, we shall use the same conceptual model already described for evaporation. This model will thus ignore the vertical variations in momentum fluxes that are related to the Coriolis force and are important in the Ekman layer (from tens of meters above the ground to the top of the PBL). It seems that the error propagated out of the momentum analysis and into the analysis of moisture and heat should be small, since the transport parameters are not so strongly sensitive to the wind field.

With the assumption of a total momentum flux independent of height, and a conceptual mixing model like that proposed for moisture and heat, the problem may be schematized as in Figure 3.9. Associated with each surface type is a friction velocity, u_{*i}, that defines the local momentum flux.

$$u_{*i}^2 = u_h/r_{ai} \tag{3.104}$$

Equation (3.101), written for the height h above the i'th patch type, yields, using (3.103),

$$u_h = \frac{u_{*i}}{kh_o}\left(h + h_o \ln \frac{h}{z_{oi}}\right) \tag{3.105}$$

where we have recognized that z_{oi} is small compared to h. The

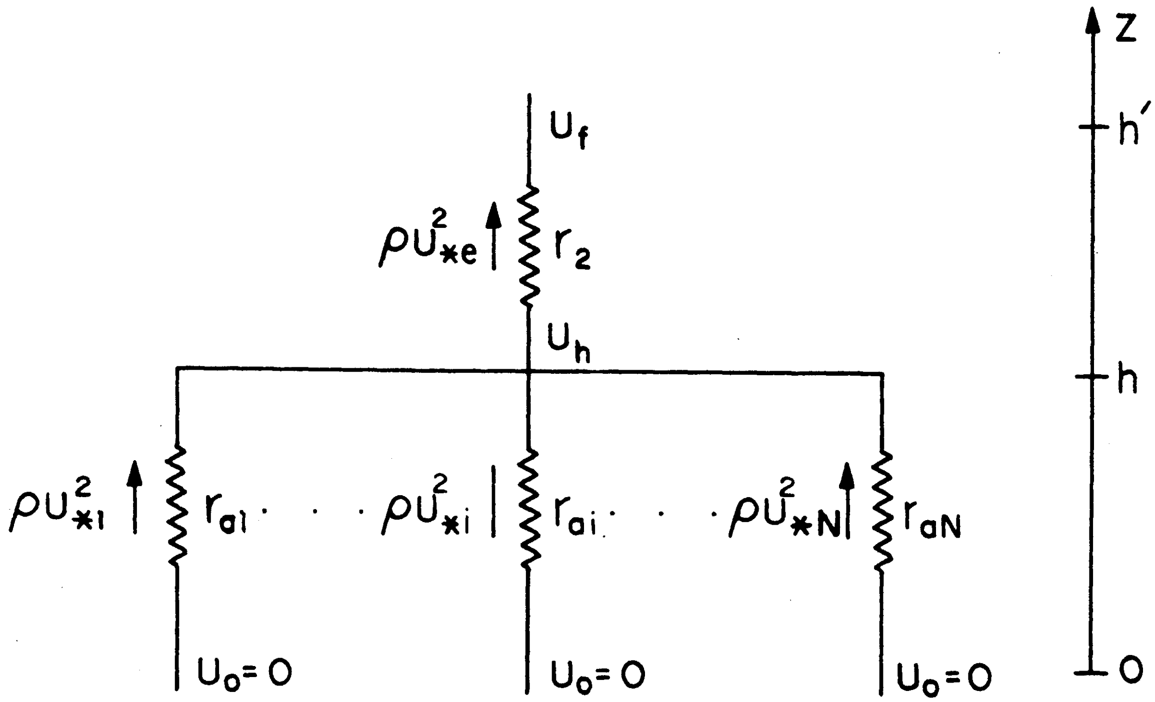

Figure 3.9

THE RESISTANCE NETWORK FOR MOMENTUM FLUXES.

resistance of the i'th internal boundary layer is given by (3.99), using (3.103), as

$$r_{ai} = (ku_{*i})^{-1}\left(\frac{h}{h_o} + \ell n \frac{h}{z_{oi}}\right) \tag{3.106}$$

where the virtual momentum sink is at height z_{oi}, the surface roughness height, and h is the top of the layer.

We assume that, above the height h, the wind profile (like the vapor and temperature profiles) is a unique function of z. Hypothesizing a form similar to (3.105) we have

$$u = \frac{u_{*e}}{k}\left(\frac{z}{h_o} + \ell n \frac{z}{z_{oe}}\right) \tag{3.107}$$

where u_{*e} is the effective friction velocity and z_{oe} is the effective surface roughness. Requiring continuity of the wind field at height h, we obtain, from (3.105) and (3.107)

$$\frac{u_{*i}}{u_{*e}} = \frac{h/h_o + \ell n(h/z_{oe})}{h/h_o + \ell n(h/z_{oi})} \tag{3.108}$$

The condition of momentum conservation at height h gives us a relation among the various friction velocities. Equating the vertical flux of momentum above the height h to the weighted average of the fluxes below that height, we obtain

$$u_{*e}^2 = \sum_{i=1}^{N} a_i u_{*i}^2 \tag{3.109}$$

Substituting (3.108) into (3.109), we finally arrive at

$$\left(\frac{h}{h_o} + \ell n \frac{h}{z_{oe}}\right)^{-2} = \sum_{i=1}^{N} a_i \left(\frac{h}{h_o} + \ell n \frac{h}{z_{oi}}\right)^{-2} \tag{3.110}$$

which can be solved for z_{oe} if the height h is either known or given as a function of z_{oe}.

In this conceptual model, recall that h is the height at which the internal boundary layers of the individual surface variations lose their identity and merge to produce a laterally homogeneous vertical profile. We have chosen here to identify h as a typical thickness of the internal boundary layers above the homogeneous surface patches. Specifically, it is the height to which the internal boundary layer of the average surface patch grows at the downwind end of the patch.

In the atmospheric surface (i.e., constant-stress) layer, a convenient formula for the growth of the internal boundary layer is (Jensen, 1978)

$$\frac{h}{z_o} = \left(\frac{\ell}{z_o}\right)^{4/5} \tag{3.111}$$

Here, l is the average patch length. Since we desire an approximate, unique value of h, we shall apply (3.111) using the effective surface roughness, z_{oe}.

Equation (3.111) is valid for l small enough that h is not greater than the order of h_o. In order to derive an alternative boundary layer growth law for large fetch, we consider the advection model of the free atmosphere, presented earlier, that results in (3.55). We define the thickness of the boundary layer as that height at which the effect of the upstream discontinuity is small compared to its effect at the surface. Algebraically,

$$\frac{\psi_2(\ell, h) - \psi_o}{\psi_2(\ell, 0) - \psi_o} = 0.1 \qquad (3.112)$$

where we have arbitrarily chosen a ten percent cutoff value to define the boundary layer. This criterion is used with (3.55) to solve for l as a function of x. The result is plotted in Figure 3.10 in terms of the dimensionless variables

$$\xi = \omega^2 K_o \ell / U \qquad (3.113)$$

$$\zeta = \omega(h - d) \qquad (3.114)$$

Solution for cutoff values of 0.5 and 0.01 are also plotted. To a good approximation we can take

$$\zeta = 2\xi^{1/2} \qquad (3.115)$$

or

$$h = h_o + 2(K_o \ell / U)^{1/2} \qquad (3.116)$$

where we have assumed that the d in (3.53) through (3.55) is the same as h_o. This describes the growth after the boundary

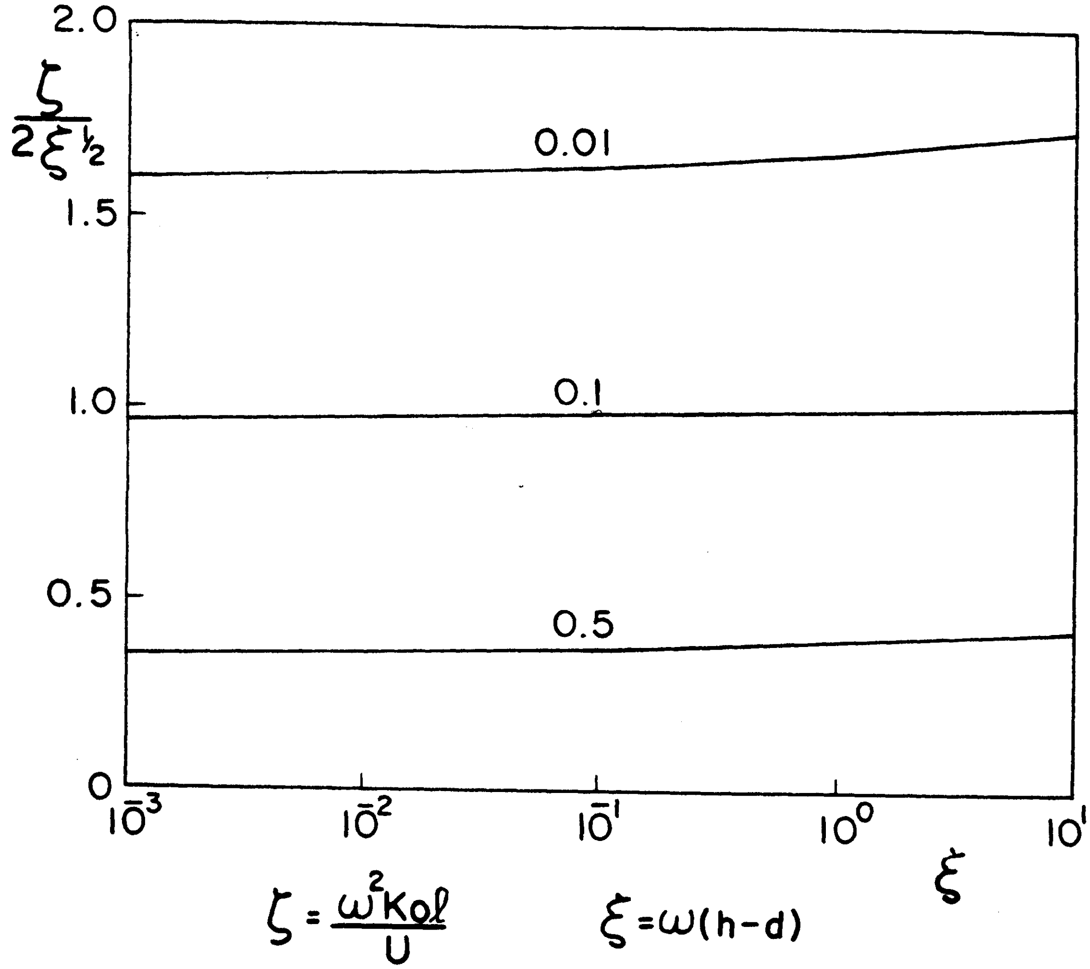

Figure 3.10

THE HEIGHT OF THE GROWING BOUNDARY LAYER GIVEN BY (3.112) (middle curve) AND BY TWO OTHER VALUES OF THE CUTOFF PARAMETER.

layer reaches height h_o. We shall assume that h grows according to (3.111) in the surface layer and then follows (3.116). Thus,

$$h = \begin{cases} z_{oe}^{1/5} \ \ell^{4/5} & \ell \leq h_o^{5/4} z_{oe}^{-1/4} \\ h_o + \left(\frac{K_o}{U}\right)^{1/2} (\ell - h_o^{5/4} \ z_{oe}^{-1/4})^{1/2} & \ell > h_o^{5/4} z_{oe}^{-1/4} \end{cases} \tag{3.117}$$

The value of h' is given by the same formula, with l' substituted for l.

Together, (3.110) and (3.117) yield an implicit equation for z_{oe} as a function of the z_{oi}'s and the a_i's, h_o, K_o, and l. With the effective roughness height determined, we can find h by (3.117). The resistances r_{ai} are then given by (3.106) and (3.108) as

$$r_{ai} = (ku_{*e})^{-1} \left(\frac{h}{h_o} + \ell n \ \frac{h}{z_{oi}}\right)^2 \left(\frac{h}{h_o} + \ell n \ \frac{h}{z_{oe}}\right)^{-1} \tag{3.118}$$

The resistance r_2 between heights h and h' is, using (3.99) and (3.103).

$$r_2 = (ku_{*e})^{-1} \left(\frac{h'-h}{h_o} + \ell n \ \frac{h'}{h}\right) \tag{3.119}$$

Finally, the effective resistance r_1 between the surface and height h is given by (3.109). We have thus defined the aerodynamic resistances in (3.84) as functions of the z_{oi}'s and a_i's, h_o, l, l', K_o, and u_{*e}.

As an example of the application of this conceptual resistance model, we consider a checkerboard pattern of squares having alternating values of surface roughness, i.e., the red squares have $z_o=z_{o1}$ while the black have $z_o=z_{oi}$. Then $N=2$ and $a_i=0.5$. The side of an individual square has length l, while the overall streamwise dimension of the area is l'. Taking l' as 100 km, we plot in Figure 3.11 the effective roughness as a function of l, calculated for $z_{o1}=10$ cm and $z_{o2}=$ 1 cm using (3.110) and (3.117). The effective surface roughness decreases first rapidly, then more gradually, with the logarithm of l.

Figure 3.12 shows the corresponding normalized aerodynamic resistances for this problem. Equations (3.118) and (3.119) give r_2 and the r_{ai}'s, and r_1 is defined by

$$\frac{1}{r_1} = \sum_{i=1}^{N} \frac{a_i}{r_{ai}} \tag{3.120}$$

With increasing l, the height h separating the surface from the homogeneous upper flow grows, so the r_{ai} and r_1 increase while r_2 decreases. The total resistance, r_1+r_2, remains approximately constant. While the r_{ai} and r_1 are independent of l', r_2 is not. The dependence of r_2 on l for a value of $l'=10^3$ m has also been plotted for comparison. The bumps in the curves around $l=300$ m are due to the change in the growth rate of h at about that fetch, as prescribed by (3.117).

One of the striking features of Figure 3.12 is the relatively constant difference between r_{a1} and r_{a2}. The result is that, for small l, r_{a1} is several times smaller than

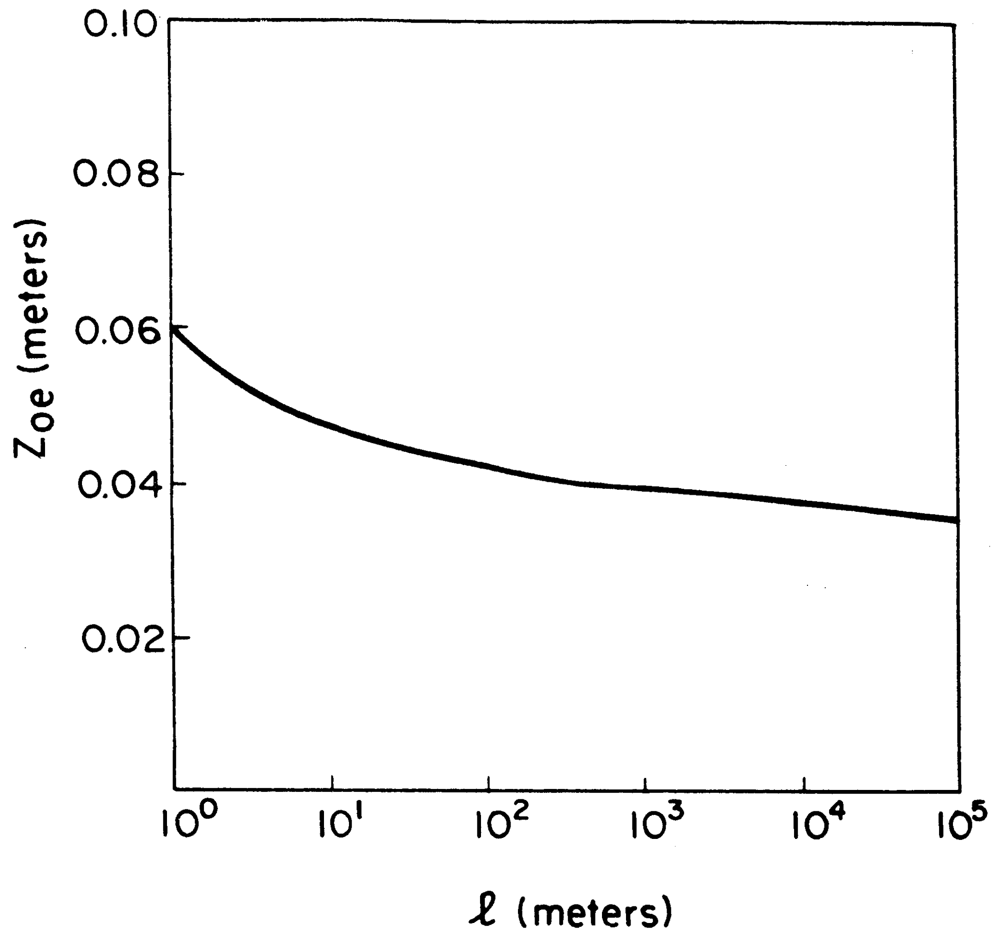

Figure 3.11

THE EFFECTIVE ROUGHNESS HEIGHT, z_{oe}, AS A FUNCTION OF ℓ, THE PATCH SIZE, WITH EQUAL PROPORTIONS OF THE AREA HAVING SURFACE ROUGHNESSES OF 0.1 m AND 0.01 m.

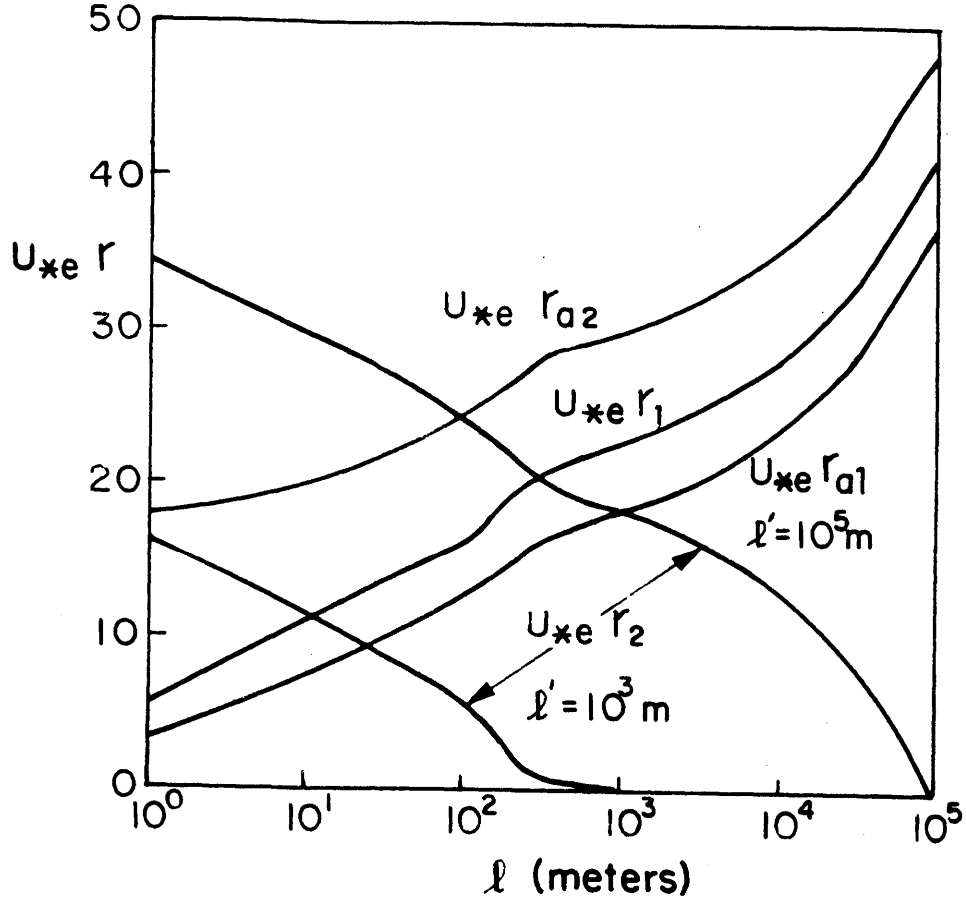

Figure 3.12

DIMENSIONLESS RESISTANCES AS A FUNCTION OF ℓ FOR THE EXAMPLE PARAMETERS.

r_{a2}, while the difference is less significant at larger l. According to (3.104), this means that the distribution of surface stress will be sensitive to l. As we shall see, the same effect is active in the evaporation process.

3.5.4 Model Results

Using (3.88), (3.110), (3.117), (3.118), and (3.119), we can write

$$\overline{E}' = f[q, \ell, \ell'; (a_i, \frac{R_i}{\overline{R}}, u_{*e} r_{ci}, z_{oi})_{i=1,N}] \qquad (3.121)$$

and E_i' is also determined by these same parameters.

In this section. we shall examine the behavior of E' and the individual E_i' for some simple situations in which N=2 and the two surface types have equal areal coverage, i.e., a_i=0.5. In a final example, we will consider the effect of varying the a_i's. We shall take l' to be 10 km. As in the example for aerodynamic resistances, we shall plot results as a function of l, the distance scale of the inhomogeneity. A summary of the parameters used to obtain these results is given in Table 3.2. A computer program used to calculate the resistances and evaporation rates is listed in an appendix.

We consider first the case of constant R_i and r_{ci}, with differing surface roughnesses. Patch type 1 is smoother than patch type 2. The middle curve in Figure 3.13 is obtained for zero vapor pressure deficit and canopy resistance. It can be shown that the existence of a zero vapor pressure

Figure No.	Z_{o1}	Z_{o2}	$R_1/\bar{R}$	$R_2/\bar{R}$	$u_{*e}r_{c1}$	$u_{*e}r_{c2}$	q	α_1	α_2
	0.1 m	1 m	1	1	0	0	0	0.5	0.5
3.13	0.1 m	1 m	1	1	30	30	0	0.5	0.5
	0.1 m	1 m	1	1	0	0	10	0.5	0.5
	0.1 m	0.1 m	1.1	0.9	0	0	0	0.5	0.5
3.14	0.1 m	0.1 m	1.1	0.9	30	30	0	0.5	0.5
	0.1 m	0.1 m	1.1	0.9	0	0	10	0.5	0.5
	0.1 m	0.1 m	1	1	0	300	0	0.5	0.5
3.15	0.1 m	0.1 m	1	1	30	300	0	0.5	0.5
	0.1 m	0.1 m	1	1	0	300	10	0.5	0.5
3.16	1 m	0.01 m	1.1	0.9	30	15	10	0.5	0.5
	1 m	0.01 m	1.1	0.9	30	∞	10	0.5	0.5
	1 m	0.01 m	1.1	0.9	30	∞	10	1	0
3.17	1 m	0.01 m	1.1	0.9	30	∞	10	0.5	0.5
	1 m	0.01 m	1.1	0.9	30	∞	10	0.1	0.9

Table 3.2

SUMMARY OF PARAMETERS USED IN THE SENSITIVITY ANALYSIS

OF THE EVAPORATION MODEL

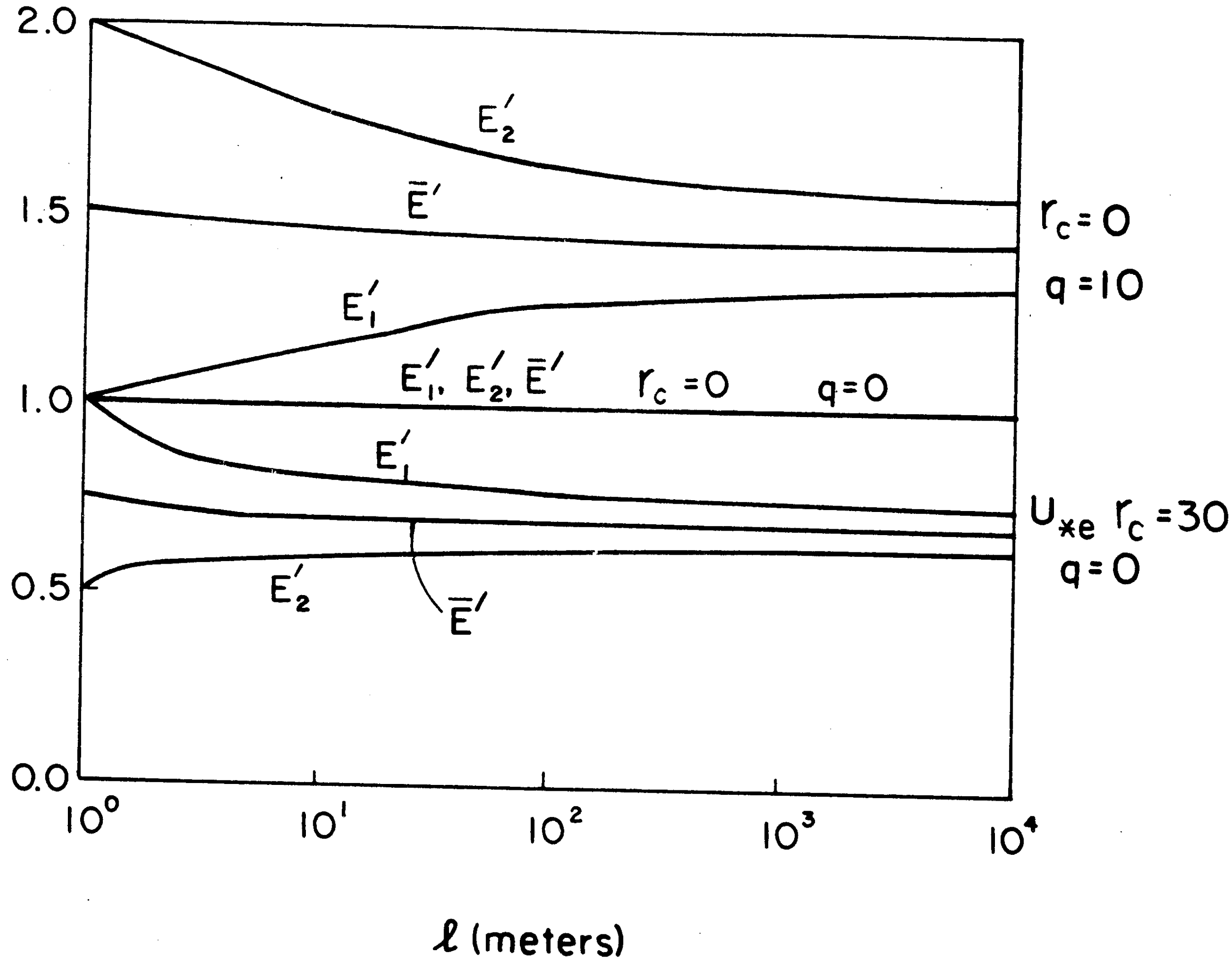

Figure 3.13

PATCH EVAPORATION (E_i') AND THE AREAL AVERAGE ($\bar{E}'$) AS FUNCTIONS OF ℓ FOR TWO PATCH TYPES THAT DIFFER ONLY IN SURFACE ROUGHNESS; $z_{o1} = 0.1$ m, $z_{o2} = 1$ m.

deficit at height h' and at the surface (the latter since $r_c=0$) forces the vapor pressure deficit to zero also in between. We can then see from (3.82) that, with $r_{ci}=0$ and $R_i=R$, the evaporation must be the same from both surfaces.

The lower set of curves in Figure 3.13 corresponds to the same problem with a normalized canopy resistance of 30. Given the increased resistance to vapor transport, the evaporation rates will be lower, in general, than in the first case. At the right ends of the curves, l goes to l', so r_2 goes to zero and the surfaces are independent. Variations in the height of a curve for smaller l thus reflect the interactions of individual surfaces. The insensitivity of E' to l is clear. The rougher surface has less evaporation than the other because its smaller value of r_a favors sensible heat transport over evaporation as a means of transferring the given amount of available energy away from the surface. This can be seen, for example, from the radiation term in (3.82). This effect is strongest at small l, where there is the greatest relative difference between r_{a1} and r_{a2}. (Recall the discussion of Figure 3.12.)

The upper curves in Figure 3.13 give the evaporation rates when there is significant advective enhancement of evaporation and the canopy resistance is zero. As in the previous case, the average evaporation is almost independent of l, though its distribution clearly is not. In this situation, the rough surface experiences greater evaporation than the smooth one, a reversal of the behavior for the radiation-dominated, canopy-controlled case discussed above. Evaporation is enhanced by the vertical diffusion of both vapor and heat, since the downward sensible heat flux (or reduction in upward sensible heat flux) that results from the advection term is complementary, rather than competitive, to evaporation. Here again, the difference in evaporation is greatest for small l since that is when the contrast in aerodynamic resistances is greatest.

Figure 3.14 contains three sets of curves analogous to those in Figure 3.13. Surface roughness and canopy resistance are considered constant, while the available radiation takes two values, ten percent above and below the mean. Such a variation could result from differing surface albedoes. For no canopy control (r_c=0) and no advective enhancement (q=0), the evaporation is independent of l and proportional to R_i. As before, this behavior can be understood in terms of (3.82).

In the lower set of curves, E' is reduced due to the action of canopy control. At the l=l' end of the curves, E_i' goes like R_i, as it should for independent surfaces without advective enhancement. Since $r_{a1}=r_{a2}=r_1$ and $r_{c1}=r_{c2}=r_c$, we can use (3.90) to write

$$E_1' - E_2' = \frac{R_1-R_2}{\bar{R}}\left[1 + \frac{r_c/r_1}{1+\Delta/\gamma}\right] \qquad (3.122)$$

which predicts the decreasing contrast in evaporation rates for small r_1 and thus for small l.

The upper three curves in Figure 3.14, representing

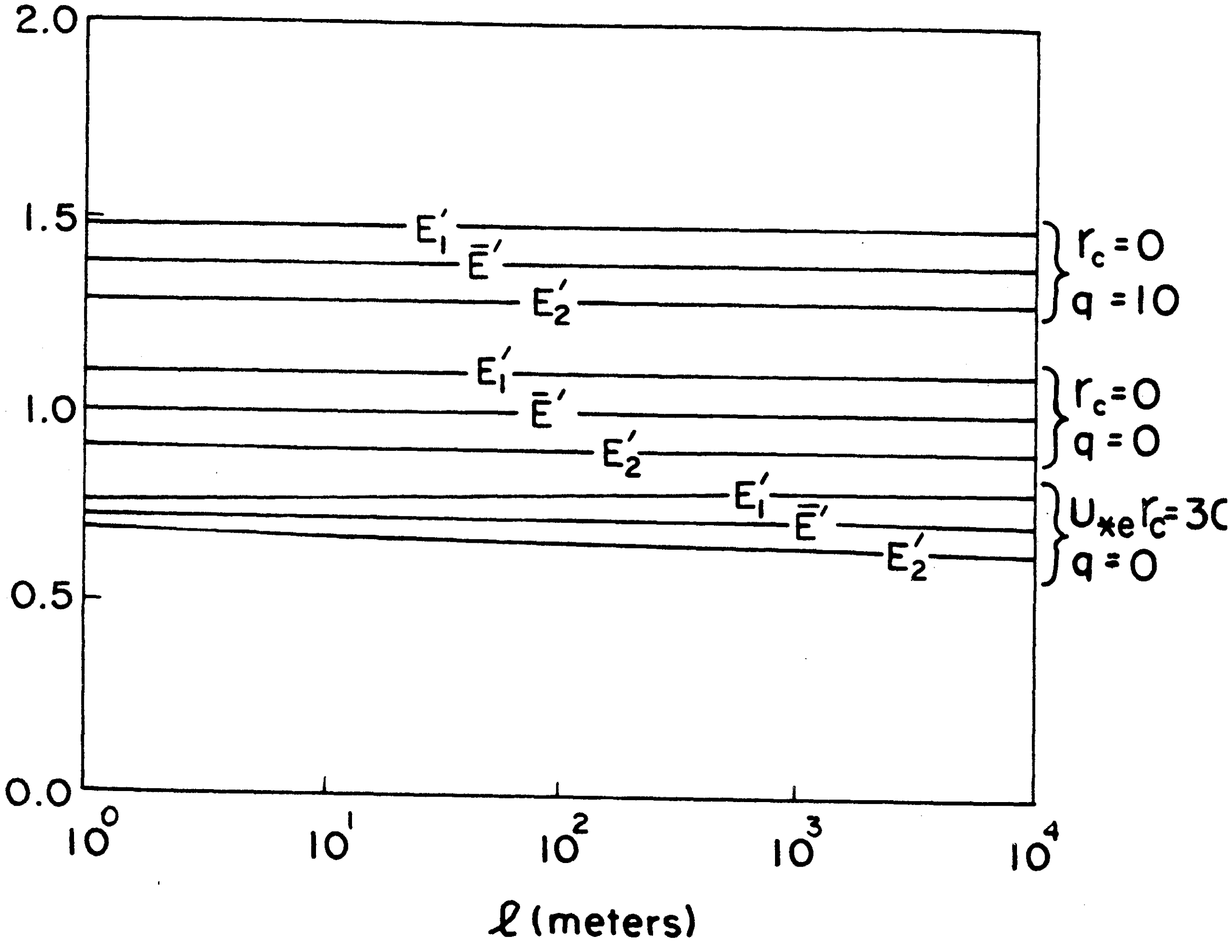

Figure 3.14

PATCH EVAPORATION (E_i') AND THE AREAL AVERAGE ($\bar{E}'$) AS FUNCTIONS OF PATCH SIZE. PATCHES DIFFER ONLY IN AVAILABLE ENERGY; $R_1/\bar{R} = 1.1$, $R_2/\bar{R} = 0.9$.

advectively-enhanced free evaporation, are the same as the middle set of curves with an added constant shift due to the advection term. The constant difference between E_1' and E_2', even with the advection term, is predicted by (3.122) with $r_c=0$.

In Figure 3.15 are plotted the evaporation results for a surface that has constant R and z_o, but two different values of canopy resistance. The dotted-dashed lines represent an advection-free system with $r_{c1}=0$ and $u_{*e}r_{c2}=300$. The latter is meant to represent a relatively dry surface, while the former corresponds to a wet surface. Consequently, evaporation from the first surface type greatly exceeds that from the second, while the mean is approximately one-half of the wet surface rate. Evaporation from the wet surface increases with the increasing interaction between patches that results from smaller l. Loosely speaking, small values of l allow a portion of the sensible heat, and hence the vapor pressure deficit, released from the dry surfaces to diffuse back down to the wet surfaces and thereby to increase evaporation. In the present example, the evaporation from the wet surface is 40 percent higher for l=10 m than for completely independent surfaces ($l=10^4$ m).

The other two sets of curves in Figure 3.15 exhibit the similar behavior of advectively-enhanced evaporation and evaporation with more canopy control.

In the foregoing analysis we have considered inhomogeneity with respect to only one of the three surface

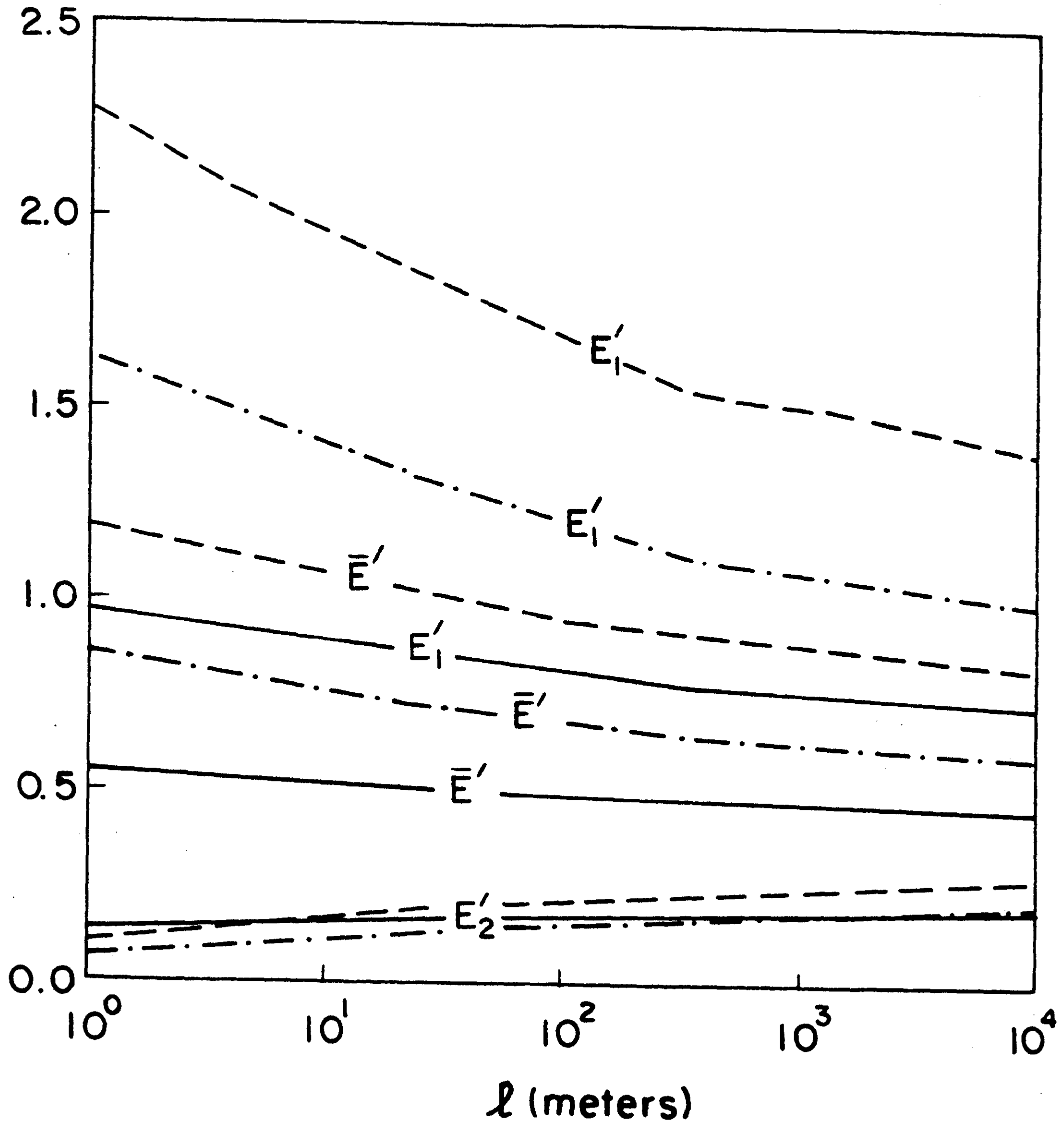

Figure 3.15

PATCH AND AREAL AVERAGE EVAPORATION AS FUNCTIONS OF PATCH SIZE FOR PATCHES THAT DIFFER ONLY IN CANOPY RESISTANCE.

	$u_{*e}r_{c1}$	$u_{*e}r_{c2}$	q
dotted-dashed lines	0	300	0
dashed lines	0	300	10
solid lines	30	300	10

parameters at a time. In reality, of course, variations of all three parameters will occur together. All three may be correlated due to their dependence on a common underlying factor. e.g., vegetation. Consider. for example, a savanna-like vegetal cover with two dominant types of vegetation - trees and grasses - that tend to be grouped in patches of size l. The trees will have a large surface roughness - perhaps 1 m - while a short grass could go down to 1 cm. The tree cover would tend to have a lower albedo and a lower temperature (thus less backwave radiation) than a relatively bare and dry grassy surface, so R_i/R might be 1.1 for the trees and 0.9 for the grass. Assuming sufficient soil moisture in the tree root zone, the moisture availability could be characterized using the canopy resistance model, with a normalized canopy resistance of 30 (Tables 3.1 and 3.2). When the grass has a sufficient supply of moisture at its disposal, it may have a normalized resistance of 15. The shallow grass root zone may dry out, at which point the canopy resistance model does not apply. Nevertheless, the condition of relative dryness, or negligible evaporation, can be imposed by setting the grass resistance to infinity.

A set of parameters similar to those outlined above would also apply to alternately fallow and irrigated, cropped fields in an agricultural setting.

The evaporation rates plotted in Figure 3.16 are based on the parameters suggested above. The full set of parameters is given in Table 3.2. Wet conditions are modelled

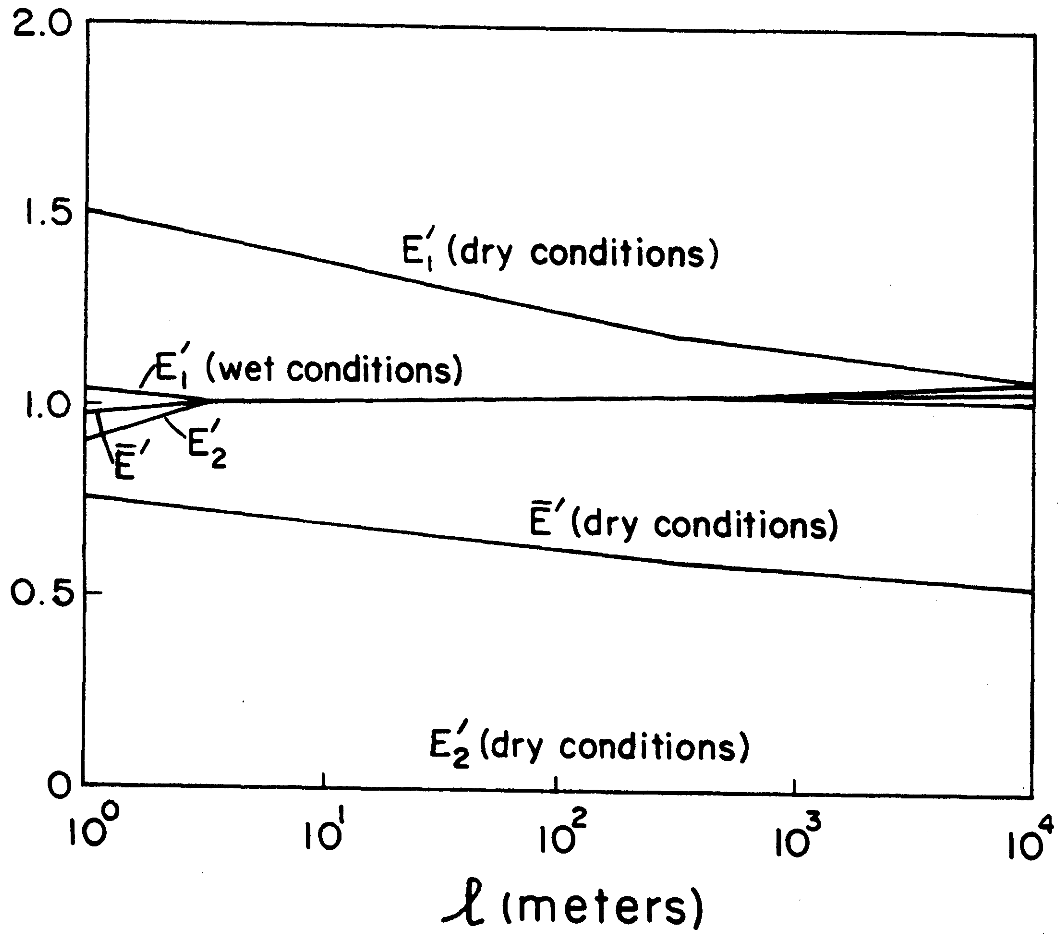

Figure 3.16

PATCH AND AREAL AVERAGE EVAPORATION AS A FUNCTION OF PATCH SIZE FOR TWO PATCH TYPES DIFFERING IN SURFACE ROUGHNESS, AVAILABLE ENERGY, AND CANOPY RESISTANCE (SEE TABLE 3.2). THE THREE CURVES NEAR UNITY ARE FOR WET CONDITIONS ($u_{*e}r_{c2} = 15$), WHILE THE OTHERS ARE FOR RELATIVELY DRY CONDITIONS ($u_{*e}r_{c2} = \infty$). IN BOTH CASES, $u_{*e}r_{c1} = 30$, $z_{o1} = 0.01$ m, $z_{o2} = 1$ m, $R_1/\bar{R} = 1.1$, $R_2/\bar{R} = 0.9$, $q = 10$.

using a normalized grass resistance of 15. Under these conditions, there is virtually no difference in the evaporation rates from the two different types of surfaces and no dependence of evaporation on l. With this arbitrarily selected problem, the excess radiation to the trees is balanced by the lower canopy resistance and higher aerodynamic resistance (due to lower roughness) of the grass to produce equal evaporation rates. The normalized evaporation rates happen to be near unity because of a chance balance of the vapor pressure deficit and the canopy resistance.

Relatively dry soil conditions are represented by the other curves in Figure 3.16 using an infinite grass canopy resistance. Evaporation from the grass is thus zero. Tree evaporation, and consequently the areal mean, increases with decreasing patch size in a manner similar to that already seen in Figure 3.15.

As a final application of the proposed model, we consider the effect of the a_i's, which define the relative frequencies of the surface types. We use the parameters of the last case, for dry soil, but consider two additional sets of a_i's. For equal cover of trees and grass (a_1=a_2=0.5; solid lines), the solution from Figure 3.16 has been replotted in Figure 3.17. For comparison we also plot the results for small tree cover (a_1=0.1, a_2=0.9; dashed lines) and for total tree cover (a_1=1.0, a_2=0.0; dotted-dashed lines). Upper lines represent tree evaporation, while lower lines give the areal average. Grass evaporation is zero. Note that decreasing

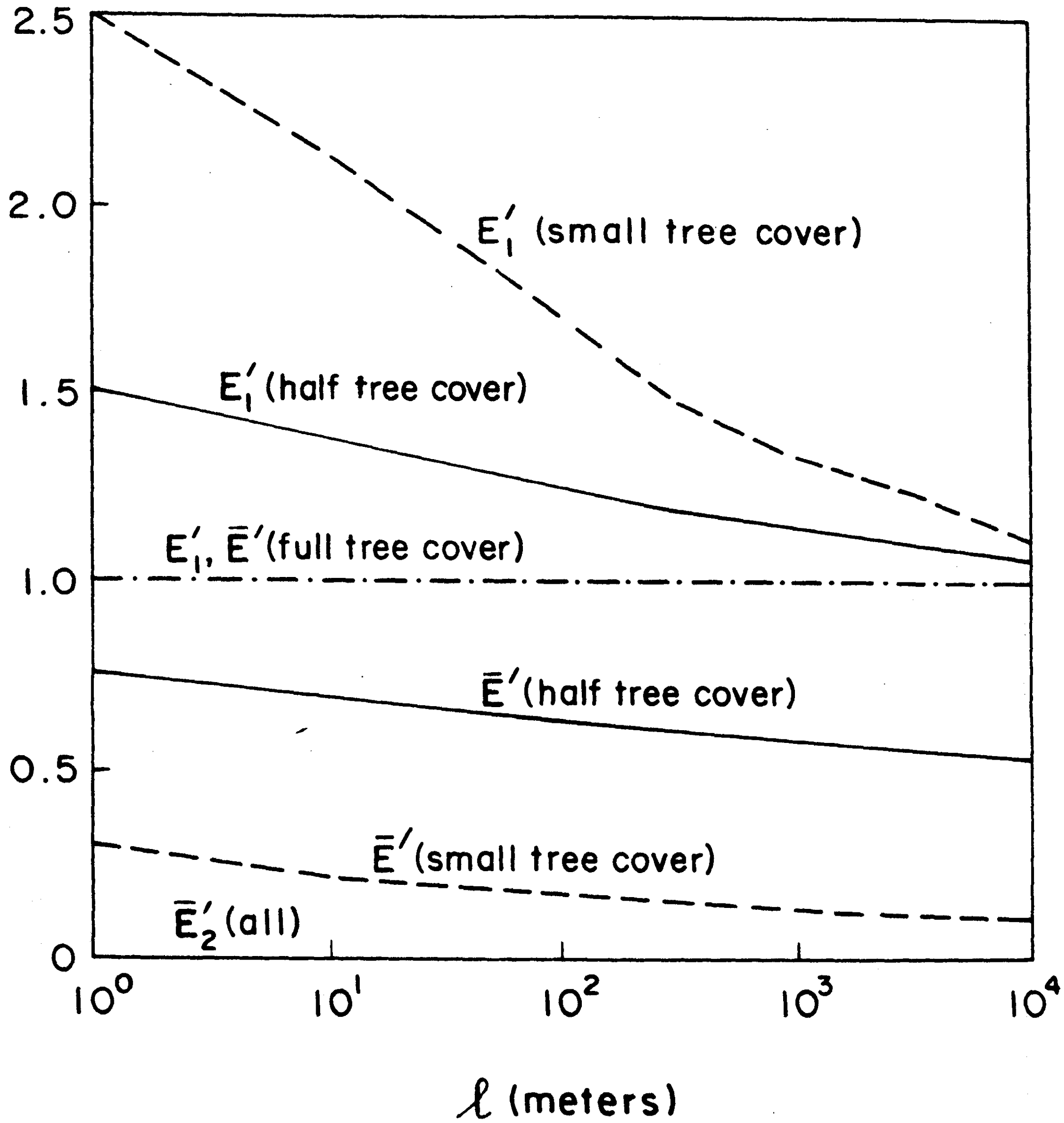

Figure 3.17

SAME AS THE DRY CONDITIONS OF FIGURE 3.16, WITH VARYING VALUES OF THE a_i's AS FOLLOWS:

	a_1	a_2
dotted-dashed lines	1.0	0
solid lines	0.5	0.5
dashed lines	0.1	0.9

areal coverage by the transpiring trees is accompanied by increased evaporation therefrom. The increase is not sufficient, however, to keep the areal average evaporation rate from decreasing almost in proportion to a_1.

3.6 Summary and Discussion

Spatial variability of evaporation and transpiration from the land surface is intimately connected to advection of water vapor in the atmosphere. We have explored this connection using a highly idealized conceptualization of advection, turbulent diffusion, and water availability at the land surface. The emphasis here has been on local variability due to patchiness of the surface, rather than on regional trends in average evapotranspiration that result from large-scale advection. The many gross assumptions regarding boundary layer growth, similarity of turbulent diffusivities and 'roughness' heights, geometry, atmospheric stability, etc., may all be expected to affect our findings, certainly quantitatively, less likely qualitatively. Our conceptualization should therefore be viewed as an analogue from which physical generalizations can be drawn, not as a tool for precise predictions of evapotranspiration.

We assume that spatial variability of the surface can be adequately characterized in terms of the relative proportions of area having given combinations of available energy, aerodynamic roughness, and canopy resistance, and in terms of the characteristic scale of that variability -- the patch size. The proposed mathematical model expresses mean areal average and patch average evapotranspiration as functions of these characteristics and of the atmospheric conditions outside the surface internal boundary layers.

Several examples illustrate the effects of land surface spatial variability on evapotranspiration. In general, advection above the patches leads to adjustments in otherwise independent evapotranspiration rates. In many, but not all, cases these adjustments are negligible. As one example. Figure 3.13 shows the barely perceptible influence of patch size (an indirect measure of advective connectivity of patches) on the areal average. Only in one case depicted there does advection have a significant effect on the areal distribution. Even these effects are virtually absent when the variability of the surface is mainly one of available energy (Figure 3.14).

Advective feedback appears to be most important when patches have greatly differing canopy resistance (Figure 3.15). In these cases the assumption of lateral independence leads to significant underestimation of the areal average evapotranspiration rate, due to the underestimation of the component from the less resistant ('wetter') canopies. Advection provides a route by which excess sensible heat generated from radiation at the drier surfaces can be transported to the wetter surfaces, where it fuels additional evaporation.

Since the most significant effect of advection observed in our analysis is with somewhat extreme values of the canopy resistance, it may well be that factors other than advection will always be in control. This is because a very large canopy resistance is indicative of a serious limitation of water supply at the land surface. In such a situation, it is likely that the soil has a fixed maximum rate at which it can supply water, regardless of atmospheric conditions. Then r_c, in effect, adjusts itself accordingly, and atmospheric conditions, advectively-modified or otherwise, can have no effect on the evapotranspiration rate.

The foregoing suggests that many problems in spatially-variable evapotranspiration could be analyzed more effectively by concentrating on the supply side -- soil moisture dynamics -- and less on the atmospheric demand side. Certainly this is the case for relatively scarce water at the land surface. An analysis of the sort presented for infiltration in Chapter 2 can be applied to study transient evaporation from a bare soil surface.

Chapter 4

SUMMARY AND CONCLUSIONS

4.1 Summary

We have employed simplified descriptions of moisture movement in soil and in the atmosphere in order to study some of the effects of spatial variability on infiltration and evapotranspiration.

In order to calculate areal average infiltration from an inhomogeneous surface, we treat the soil mass as a battery of independent, parallel soil columns, ignoring the possible effects of lateral interactions. Spatial variability of soil properties, storm depth, and initial saturation is considered.

The problem of advection in the atmosphere and its effect on spatially variable evapotranspiration under canopy control is addressed. The inhomogeneous land surface is characterized as a mosaic of patches within which the available energy, the canopy resistance, and the surface roughness are constant, but between which these quantities may vary. A simplified flux network model based on the concept of aerodynamic resistances is proposed. It allows the calculation of patch evaporation and areal average evaporation.

4.2 Conclusions

The spatial variability of land surface hydrology results in a dissimilarity between point and areal average response. For storm surface infiltration and for evapotranspiration, this scale effect is a result of the spatial variability of the physical parameters of the surface. For evapotranspiration it also reflects the interaction between different locations on the land surface that occurs due to atmospheric advection.

A few particular effects of spatial variability on the areal average division between infiltration and storm surface runoff have been noted (Chapter 2). The integration of infiltration over a finite area, in which forcing and parameters are variable, yields a mean infiltration that is much less sensitive to the mean forcing and soil parameters than is the point infiltration (Sections 2.4.3 and 2.4.4). Spatial variability of either rainfall or soil type ordinarily causes an increase in surface runoff over the value yielded by the mean rain (Section 2.4.3) or by the average soil characteristics (Section 2.4.4). In particular, it appears that information on the distribution of storm depth (perhaps parameterized by storm type) within the grid square of a general circulation model would be useful for improved representation of the land surface hydrology in climate simulations, provided an appropriate hydrologic parameterization accounting for spatial variability were employed.

Physically plausible effects of lateral advection and land surface variability on the areal mean evapotranspiration rate and its distribution under conditions of canopy control can be obtained using a relatively simple conceptual model (Section 3.5). According to this model, local advection affects the areal average evapotranspiration rate only slightly in most cases (Section 3.5.4). The most significant influence of advection occurs when the canopy resistance to transpiration is highly variable, with large values occurring over significant portions of the area (Section 3.5.4). Since a large canopy resistance is indicative of soil control of evaporation, this result suggests that soil moisture dynamics should be considered in future analyses of advection and its influence on evapotranspiration (Section 3.6).

4.3 Recommendations for Future Research

In this work we have only looked at two limited topics in spatial variability - laterally-independent infiltration and advection-affected, steady-state evapotranspiration under canopy control. Further work is required in observation and quantification of spatial variability, in analysis of specific problems such as those dealt with here, and in the integration of all of the results into a coherent accounting scheme for spatially variable areas.

Some specific research problems related to the present work can be identified:

1. The importance of lateral flows during infiltration must be assessed. Both surface and subsurface flows should be considered. These would be analyzed at the

hillslope scale, with due consideration of soil profile layering. The spatially and temporally variable "partial source area" deserves special attention.

2. Further modeling of evapotranspiration without consideration of local advective feedback appears justified, given the complexity of the spatial variability problem and the relative insensitivity of our findings to advection.

3. Regional advection effects, spatial variability of soil moisture supply, and vegetal control of r_c all deserve attention in the evapotranspiration problem.

REFERENCES

Atkinson, T. C., Techniques for measuring subsurface flow on hillslopes, in Hillslope Hydrology, ed. M. J. Kirkby, John Wiley & Sons, 1978.

Bear, J., Hydraulics of Groundwater, McGraw-Hill, New York, 1979.

Bell, K. R., B. J. Blanchard, T. J. Schmugge, and M. W. Witczak, Analysis of surface moisture variations within large-field sites, Water Resour. Res., 16(4), 796-810, 1980.

Boyer, M. C., A correlation of the characteristics of great storms, Trans. Amer. Geophys. Union, 38(2), 233-236, 1957.

Brutsaert, W. and H. Stricker, An advection-aridity approach to estimate actual regional evapotranspiration, Water Resour. Res., 15(2), 443-450, 1979.

Chorley, R. J., The Hillslope Hydrological Cycle, in Hillslope Hydrology, ed. M. J. Kirkby, 1-42, John Wiley & Sons, New York, 1978.

Eagleson, P. S., Dynamic Hydrology, McGraw-Hill, New York, 1970.

Eagleson, P. S., Climate, soil, and vegetation (7 parts), Water Resour. Res., 14(5), 705-776, 1978.

Edlefsen, N. A. and A. B. C. Anderson, Thermodynamics of soil moisture, Hilgardia, 15(2), 1943.

Freeze, R. A., A stochastic-conceptual analysis of rainfall-runoff processes on a hillslope, Water Resour. Res., 16(2) 391-408, 1980.

Freeze, R. A. and J. A. Cherry, Groundwater, Prentice-Hall, Englewood Cliffs, New Jersey, 1979.

Gupta, V. K. and E. C. Waymire, A stochastic kinematic study of subsynoptic space-time rainfall, Water Resour. Res., 15(3), 1979.

Hillel, D., Applications of Soil Physics, Academic Press, 1980.

Hillel, D. and G. M. Hornberger, Physical model of the hydrology of sloping heterogeneous fields, Soil Sci. Soc. Am. Proc., 43(3), 434-439, 1979.

Holton, J. R., An Introduction to Dynamic Meteorology, Academic Press, 1979.

Jensen, N. O., Change of surface roughness and the planetary boundary layer, Quart. J. R. Met. Soc., 104, 351-356, 1978.

Keisling, T. C., J. M. Davidson, D. L. Weeks, and R. D. Morrison, Precision with which selected soil parameters can be estimated, Soil Sci., 124(4), 241-248, 1977.

Klute, A. and G. E. Wilkinson, Some tests of the similar media concept of capillary flow, 1. Reduced capillary conductivity and moisture characteristic data, Soil Sci. Soc. Am. Proc., 22(4), 278-281, 1958.

Laikhtman, D. L., Physics of the Boundary Layer of the Atmosphere, translated from Russian by I. Shechtman, U. S. Department of Commerce, Office of Technical Services No. OTS 64-11016, 1964.

McNaughton, K. G., Evaporation and advection I: Evaporation from extensive homogeneous surfaces, Quart. J. R. Met. Soc., 102, 181-191, 1976a.

McNaughton, K. G., Evaporation and advection II: Evaporation downwind of a boundary separating regions having different surface resistances and available energies, Quart. J. R. Met. Soc., 102, 193-202, 1976b.

Miller, E. E. and R. D. Miller, Theory of capillary flow: I. Practical implications, Soil Sci. Soc. Am. Proc., 19(3) 267-271, 1955.

Miller, E. E. and R. D. Miller, Physical theory for capillary flow phenomena, J. Appl. Phys., 27(4), 324-332, 1956.

Milly, P. C. D. and P. S. Eagleson, Parameterization of moisture and heat fluxes across the land surface for use in atmospheric general circulation models, Technical Report 279, R. M. Parsons Laboratory, Department of Civil Engineering, MIT, Cambridge, Massachusetts, 1980.

Monteith, J. L., The development and extension of Penman's evaporation formula, in Applications of Soil Physics, by D. Hillel, Academic Press, 1980.

Nielsen, D. R., J. W. Biggar, and K. T. Erh, Spatial variability of field measured soil-water properties, Hilgardia, 42(7), 215-260, 1973.

Philip, J. R., The theory of infiltration: 1. The infiltration equation and its solution, Soil Sci., 83(5), 345-357, 1957.

Reeves, M. and E. E. Miller, Estimating infiltration for erratic rainfall, Water Resour. Res., 11(1), 102-110, 1975.

Sharma, M. S., G. A. Gander, and C. G. Hunt, Spatial variability of infiltration in a watershed, J. Hydrology, 45, 101-102, 1980.

Sharma, M. L. and R. J. Luxmoore, Soil spatial variability and its consequences on simulated water balance, Water Resour. Res., 15(6), 1567-1573, 1979.

Smith, R. E. and R. H. B. Hebbert, A Monte Carlo analysis of the hydrologic effects of spatial variability of infiltration, Water Resour. Res., 15(2), 419-429, 1979.

Smith, R. E. and D. A. Woolhiser, Overland flow on an infiltrating surface, Water Resour. Res., 7(4), 899-913, 1971a.

Smith, R. E. and D. A. Woolhiser, Mathematical simulation of infiltrating watersheds, Hydrology Paper No. 47, Colorado State University, Fort Collins, Colorado, 1971b.

Van Bavel, C. H. M., Potential evaporation: The combination concept and its experimental verification, Water Resour. Res., 2(3), 455-467, 1966.

Warrick, A. W., G. J. Mullen, and D. R. Nielsen, Scaling field-measured soil hydraulic properties using a similar media concept, Water Resour. Res., 13(2), 355-362, 1977.

Wilkinson, G. E. and A. Klute, Some tests of the similar media concept of capillary flow, 2. Flow systems data, Soil Sci. Soc. Am. Proc., 23(6), 434-437, 1959.

Yeh, G. -T. and W. Brutsaert, A solution for simultaneous turbulent heat and vapor transfer between a water surface and the atmosphere, Bound. Layer Met., 2, 64-82, 1971.

Zaslavsky, D. and G. Sinai, Surface hydrology: I - Explanation of Phenomena, J. Hyd. Div., ASCE, 107(HY1), 1-16, 1981.

Appendix A

COMPUTER PROGRAM USED TO CALCULATE AREAL AVERAGE INFILTRATION

```
C*****************************************************************************
C
C     ANALYSIS OF SENSITIVITY OF AREAL-AVERAGE INFILTRATION
C     TO SPATIAL VARIABILITY OF SOIL AND RAINFALL PARAMETERS.
C     USES CALCOMP SOFTWARE IF PLOTTING IS SELECTED.
C
C*****************************************************************************
      EXTERNAL AXIS2(DESCRIPTORS)
      EXTERNAL SYMBOL(DESCRIPTORS)
      CHARACTER*40 IX
      DIMENSION X(20),Y(20)
      DIMENSION ICHAR(10),IX(6),NIX(6),NSIG(6)
      DATA ICHAR /0,1,2,5,12,0,1,2,5,12/
      DATA IX /'MEAN MOISTURE SATURATION','STD. DEV. OF SATURATION',
     *    'COEFFICIENT OF VARIATION OF ALPHA','LOG10 OF NORMALIZED STORM
     * RADIUS','NORMALIZED AIR DEPTH','S'/
      DATA NIX/24,23,33,32,20,1/
      DATA NSIG/2,2,1,1,1,2/
      PRINT,'PLOTTED OUTPUT?  (1=YES 0=NO)'
      READ(5,) IPLOT
      IF(IPLOT.EQ.1) CALL SET_DIMENSION(13.)
C*****************************************************************************
C
C     INITIALIZE PARAMETERS WITH NOMINAL VALUES.
C     THE PARAMETERS D,S,A, AND CV ARE AS DEFINED IN PART B.
C     RZERO IS LITTLE-R-SUB-ZERO DIVIDED BY BIG-R, THE RELATIVE
C     STORM RADIUS. SMEAN IS MU-SUB-S AND SIGS IS SIGMA-SUB-S.
C
      D=1.E4
      S=0.
      A=0.
      RZERO=100.
      SMEAN=0.0
      SIGS=0.
      CV=0.
C*****************************************************************************
C
C     PRINT CURRENT PARAMETER VALUES AND CHANGE IF REQUESTED
C
   40 WRITE(6,1010) A,S,D
 1010 FORMAT(1X,'A = ',F10.4,5X,'S = ',F10.4,5X,'D = ',F10.4)
      PRINT,'WOULD YOU LIKE TO CHANGE ANY OF THESE VALUES?'
      PRINT,'     ( 1=YES  0=NO )'
      READ(5,) IKOD
      IF(IKOD.NE.1) GO TO 30
      PRINT,'ENTER A, S, D'
      READ(5,) A,S,D
      GO TO 40
   30 WRITE(6,1020) RZERO,SMEAN,SIGS,CV
 1020 FORMAT(1X,'RZERO =',F10.4,5X,'SMEAN =',F10.4,5X,'SIGS =',F10.4,
     *   5X,'CV = ',F10.4)
      PRINT,'WOULD YOU LIKE TO CHANGE ANY OF THESE VALUES?'
      READ(5,) IKOD
      IF(IKOD.NE.1) GO TO 60
      PRINT,'ENTER RZERO, SMEAN, SIGS, CV'
      READ(5,) RZERO,SMEAN,SIGS,CV
      GO TO 30
   60 CONTINUE
C*****************************************************************************
C
```

```
C     DEFINE PARAMETERS FOR SENSITIVITY ANALYSIS.
C     THE 'PRIMARY INDEPENDENT VARIABLE' WILL BE USED AS THE X-COORDINATE
C     IN THE SENSITIVITY PLOTS. THE 'SECOND INDEPENDENT VARIABLE' WILL BE
C     USED AS THE PARAMETER FOR DIFFERENT CURVES IN THE SENSITIVITY PLOTS.
C
      PRINT,'CHOOSE PRIMARY INDEPENDENT VARIABLE'
      PRINT,'    1 MEAN VALUE OF S'
      PRINT,'    2 STANDARD DEVIATION OF S'
      PRINT,'    3 CV OF ALPHA'
      PRINT,'    4 LOG10 OF NORMALIZED STORM RADIUS'
      PRINT,'    5 NORMALIZED AIR DEPTH'
      PRINT,'    6 DIMENSIONLESS SORPTIVITY'
      READ(5,) IP
      NP=13
      PRINT,'ENTER SMALLEST VALUE OF PRIMARY VARIABLE'
      READ(5,) FV
      PRINT,'ENTER THE INCREMENT'
      READ(5,) DV
      PRINT,'CHOOSE SECONDARY INDEPENDENT VARIABLE'
      PRINT,'    1 HYDRAULIC CONDUCTIVITY'
      PRINT,'    2 SORPTIVITY'
      PRINT,'    3 STORAGE DEPTH'
      READ(5,) IS
      PRINT,'ENTER THE NUMBER OF VALUES OF THE SECONDARY VARIABLE'
      READ(5,) NS
      PRINT,'ENTER THE SMALLEST EXPONENT OF SECONDARY VARIABLE'
      READ(5,) FE
      PRINT,'ENTER THE INCREMENT OF THE EXPONENT'
      READ(5,) DE
      C=1.0
      IF(IP.GT.2.AND.SMEAN.LT..0001.AND.SIGS.LT..0001) GO TO 66
      PRINT,'ENTER PORE DISCONNECTEDNESS INDEX, C'
      READ(5,) C
   66 CONTINUE
C*****************************************************************************
C
C     DEFINE PLOT SIZE PARAMETERS AND SET UP PLOT.
C
      IF(IPLOT.NE.1) GO TO 70
      X(NP+1)=FV
      X(NP+2)=DV*2.
      Y(NP+1)=0.
      Y(NP+2)=.2
      CALL PLOTS
      CALL PLOT(1.,4.5,-3)
      CALL AXIS2(0.,0.,IX(IP),NIX(IP),6.,0.,FV,DV*2.,NSIG(IP),0,1.,
     *  .15,.15)
      CALL AXIS2(0.,0.,'NORMALIZED INFILTRATION',23,5.,90.,0.,.2,1,0,1.,
     * .15,.15)
C*****************************************************************************
C
C     INFILTRATION CALCULATION LOOPS. OUTER LOOP GETS DATA FOR NS CURVES.
C     INNER LOOP GETS DATA FOR NP POINTS ON EACH CURVE.
C
   70 DO 10 I=1,NS
      IF(IS.EQ.1) A=10.**(FE+(I-1)*DE)
      IF(IS.EQ.2) S=10.**(FE+(I-1)*DE)
      IF(IS.EQ.3) D=10.**(FE+(I-1)*DE)
      DO 20 J=1,NP
      IF(IP.EQ.1) SMEAN=FV+(J-1)*DV
```

```
      IF(IP.EQ.1) X(J)=SMEAN
      IF(IP.EQ.2) SIGS=FV+(J-1)*DV
      IF(IP.EQ.2) X(J)=SIGS
      IF(IP.EQ.3) CV=FV+(J-1)*DV
      IF(IP.EQ.3) X(J)=CV
      IF(IP.EQ.4) RZERO=10.**(FV+(J-1)*DV)
      IF(IP.EQ.4) X(J)=FV+(J-1)*DV
      IF(IP.EQ.6) S=FV+(J-1)*DV
      IF(IP.EQ.6) X(J)=S
      IF(IP.EQ.5) D=FV+(J-1)*DV
      IF(IP.EQ.5) X(J)=D
C
C     SUBROUTINE INFILT RETURNS THE NORMALIZED AVERAGE INFILTRATION IN Y(J).
C
   20 CALL INFILT(A,S,D,RZERO,SMEAN,SIGS,CV,Y(J),C)
      IF(IPLOT.NE.1) GO TO 10
C
C     PLOT THE LINE.
C
      CALL MYLINE(X,Y,NP,1,0,1)
   10 CONTINUE
      IF(IPLOT.EQ.1) CALL PLOT(0.,0.,33)
      PRINT,'FINISHED?'
      READ(5,) IFIN
      IF(IFIN.NE.1) GO TO 40
      IF(IPLOT.NE.1) STOP
      CALL PLOTS
      CALL ENDPLT(10.,2.,999)
      STOP
      END
C***************************************************************************
C
      SUBROUTINE INFILT(A,S,D,RZERO,SMEAN,SIGS,CV,FIL,C)
C
C     CALCULATES THE AREAL AVERAGE NORMALIZED INFILTRATION DEPTH, 'FIL'.
C     THE ARRAYS ALPHA, SO, AND U2 CONTAIN EQUAL PROBABILITY VALUES OF THE
C     SOIL SCALING FACTOR, THE INITIAL SATURATION, AND THE NORMALIZED WATER
C     TABLE DEPTH. ARRAYS U1 AND F1 CONTAIN DISCRETE VALUES OF THE
C     NORMALIZED STORM DEPTH AND THE ASSOCIATED FINITE PROBABILITIES.
C     ARRAY PHI2 CONTAINS VALUES OF THE APPROXIMATING FUNCTION PHI-SUB-2
C     EVALUATED AT THE SO VALUES IN SO.
C
      DIMENSION ALPHA(100),SO(100),U1(100),U2(100),F1(100),PHI2(100)
C
C     CALCULATE THE AVERAGE STORM DEPTH, FAC.
C
      FAC=RZERO*RZERO
      IF(RZERO.LT..02) GO TO 33
      FAC=2.*RZERO*RZERO*(1.-EXP(-1./RZERO)*(1.+1./RZERO))
   33 CONTINUE
C
C     DISCRETIZE THE DISTRIBUTION OF U1 (NORMALIZED STORM DEPTH)
C     INTO EQUAL RADIUS INTERVALS. N1 IS THE NUMBER OF INTERVALS.
C
      N1=20
      IF(RZERO.GT.50.) N1=1.
      DO 10 N=1,N1
      ARG=(N-.5)/N1/RZERO
      IF (ARG.GT.30.) ARG=30.
      U1(N)=EXP(-ARG)/FAC
```

```
 10   F1(N)=(FLOAT(N)/FLOAT(N1))**2.
      DO 15 N=1,N1
      IF(N.EQ.N1) GO TO 15
      F1(N1+1-N)=F1(N1+1-N)-F1(N1-N)
 15   CONTINUE
C
C
C     COMPUTE PARAMETERS OF THE LOG-NORMAL DIST. OF ALPHA
C
      VARN=ALOG(1.+CV*CV)
      ALPHAMN=-0.5*VARN
      SIGN=SQRT(VARN)
C
C      DISCRETIZE ALPHA INTO EQUALLY LIKELY VALUES. NA IS THE NUMBER
C      OF ALPHA VALUES. MDNRIS IS THE INVERSE CDF OF THE STANDARD
C      NORMAL DEVIATE, AN IMSL SUBROUTINE.
C
      NA=20
      IF(CV.LT.1.-8) NA=1
      DO 20 N=1,NA
      P=(N-0.5)/NA
      CALL MDNRIS(P,ALPHA(N),IER)
 20   ALPHA(N)=EXP(ALPHAMN+SIGN*ALPHA(N))
C
C
C     NORMALIZE THE DISCRETIZED VALUES OF ALPHA TO INSURE UNIT MEAN.
C
      AM=0.
      DO 25 N=1,NA
 25   AM=AM+ALPHA(N)
      AM=AM/NA
      DO 26 N=1,NA
 26   ALPHA(N)=ALPHA(N)/AM
C
C      DISCRETIZE NORMALIZED STORAGE DEPTH. N2 IS THE NUMBER OF VALUES
C      OF U2.
C
      N2=20
      IF(D.GT.100.) N2=1
      DO 30 N=1,N2
      X=(N-.5)/N2
 30   U2(N)=X*(2.-X)
C
C
C     DISCRETIZE 'SO' IN EQUAL PROBABILITY INTERVALS. NS IS THE NUMBER
C     OF SO VALUES.
C
      NS=20
      IF(SIGS.LE.1.E-10) NS=1
      DO 40 N=1,NS
      P=(N-0.5)/NS
      CALL MDNRIS(P,SO(N),IER)
      SO(N)=SMEAN+SO(N)*SIGS
      IF(SO(N).LT.O.) SO(N)=0.
      IF(SO(N).GE.0.999) SO(N)=0.999
      G=SO(N)/(1.-SO(N))
 40   PHI2(N)=(1.-SO(N))**5.*(0.176+0.857*G+1.64*G*G+1.5*G*G*G
     *     +0.6*G*G*G*G)
C
C
```

```
C
C     CALCULATE AVERAGE INFILTRATION DEPTH, NORMALIZED BY AVERAGE STORM DEPTH.
C
      FIL=0.
      DO 100 I=1,NA
      TERM3P=A*ALPHA(I)*ALPHA(I)
      TERM2P=S*SQRT(ALPHA(I))
      DO 100 J=1,NS
      TERM2=TERM2P*PHI2(J)
      TERM2SQ=TERM2*TERM2
      TERM3=TERM3P*(1.+SO(J)**C)
      TERM1P=D*(1.-SO(J))
      DO 100 K=1,N2
      TERM1=TERM1P*U2(K)
      DO 100 L=1,N1
C
C     SUBPROGRAM FILT RETURNS THE VLAUE OF THE NORMALIZED INFILTRATION
C     DEPTH, GIVEN THE SPECIFIED PARAMETERS.
C
      FILTT=FILT(TERM1,TERM2,TERM2SQ,TERM3,U1(L),U2(K),SO(J),
     *   ALPHA(I))
 100  FIL=FIL+FILTT*F1(L)
      FIL=FIL/(NS*NA*N2)
      RETURN
      END
C***************************************************************************
C
      FUNCTION FILT(TERM1,TERM2,TERM2SQ,TERM3,U1,U2,SO,ALPHA)
      IF(TERM3.GE.U1) GO TO 10
      TZERO=0.5*TERM2SQ/(U1*(U1-TERM3))*(1.+0.5*TERM3/(U1-TERM3))
      GO TO 20
  10  TZERO=1.E+20
  20  IF(TZERO.LT.1.) GO TO 30
      FILT=AMIN1(U1,TERM1)
      RETURN
  30  TPRIME=TZERO-0.25*TERM2SQ/((U1-TERM3)*(U1-TERM3))
      FILT=TZERO*U1+TERM2*(SQRT(1.-TPRIME)-SQRT(TZERO-TPRIME))
     *     +TERM3*(1.-TZERO)
      FILT=AMIN1(FILT,TERM1)
      RETURN
      END
C***************************************************************************
C
      SUBROUTINE MYLINE(X,Y,NN,I1,I2,I3)
C
C   PLOTS A LINE.
C
      EXTERNAL SYMBOL (DESCRIPTORS)
      DIMENSION X(1),Y(1)
      XP=(X(1)-X(NN+1))/X(NN+2)
      YP=(Y(1)-Y(NN+1))/Y(NN+2)
      CALL PLOT(XP,YP,3)
      IF(I2.NE.0) CALL SYMBOL(XP,YP,.08,I3,0.,-1)
      KODE=2
      IF(I2.LT.0) KODE=3
      DO 10 I=2,NN
      XP=(X(I)-X(NN+1))/X(NN+2)
      YP=(Y(I)-Y(NN+1))/Y(NN+2)
      CALL PLOT(XP,YP,KODE)
      DIST=SQRT((XP-XPOLD)*(XP-XPOLD)+(YP-YPOLD)*(YP-YPOLD))
```

```
      IF(DIST.LT.O.2) GO TO 10
      IF(I2.NE.O) CALL SYMBOL(XP,YP,.08,I3,O.,-1)
      XPOLD=XP
      YPOLD=YP
   10 CONTINUE
      RETURN
      END
C***************************************************************************
C
      SUBROUTINE AXIS2( X , Y , BCD , NO , SIZE , THETA , YMIN , DY ,
     * ND , K , FM , H1 , H2 )

C
C   PLOTS AN AXIS.
C
C      MODIFICATION OF
C      CALCOMP ROUTINE -AXIS1-   MIT-SUPPLIED SUBROUTINE INCLUDED
C    FOR USE BY MIT USERS WITH 905 STANDARD CALCOMP PACKAGE
C     BECAUSE IT CONTAINS 3 ARGUMENTS MORE THAN STANDARD AXIS ROUTINE
C    AND THUS ALLOWS  MORE FLEXIBILITY IN DRAWING AXES.  E.G., IT
C     ALLOWS TIC MARKS TO BE SPACED BY USER.
C     JULY 1974
C     MODIFIED BY PAM NORTHRIDGE 12/10/74
C
C      ******************************************************************
C
      EXTERNAL SYMBOL (DESCRIPTORS)
      LOGICAL*1 LOG
      CHARACTER*25 BCD
C                          INITIALIZE
   86 TH=THETA*.1745329E-1
C     *CHANGE FROM NC TO NO IN IABS CALL
      NC=IABS(NO)
      KOD=1
      KODE=1
      IF (NO.LT.O) KOD=-1
      IF (THETA.GT.45.) KODE=-1.
   76 SW=O.
   84 SS=H2
   85 YB=SIN(TH)
      S=ABS(SIZE)
      XA = X - KOD * O.1 * YB
      XB=COS(TH)
      XC=X
      YA = Y - KOD * O.1 * XB
      YC=Y
      ST=X*XB+Y*YB
      HS=S/2.
      LOG=.FALSE.
      IF(SIZE.LT.O.)LOG=.TRUE.
      BASE=10.
      IF(K)60,61,60
   60 E=.36*H2/.14
      GO TO 63
   61 E=O.
   63 I3=3
C                          DRAW AXIS FROM LEFT TO RIGHT
C                                    MOVE TO TIP OF TIC MARK
C  16 CALL PLOT1(XA,YA,I3)
   16 CALL PLOT (XA,YA,I3)
```

```
C                                 MOVE TO BASE OF TIC MARK
C      CALL PLOT1(XC,YC,2)
       CALL PLOT (XC,YC,2)
       XC=XC+XB*FM
       YC=YC+YB*FM
       XA=XA+XB*FM
       YA=YA+YB*FM
C                                 MOVE TO BASE OF NEXT TIC MARK
C      CALL PLOT1(XC,YC,2)
       CALL PLOT (XC,YC,2)
   20 I3=2
C                                 END OF AXIS TEST
       IF((XC*XB+YC*YB)-S+.00001)16,80,80
C  80 CALL PLOT1(XA,YA,2)
   80 CALL PLOT (XA,YA,2)
C                    WRITE NUMBERS UNDER AXIS MOVING FROM RIGHT TO LEFT
       DIST=.05*FM+H1*0.5*(1.+KOD*KODE)
       XA=XA-KOD*DIST*YB
       YA=YA-KOD*DIST*XB
       XC=(XC-X)*XB
       YC=(YC-Y)*YB
C                         USE POSITION ON AXIS TO COMPUTE NUMBER TO BE
C                               WRITTEN.
       VALUE=((XC+YC)*(DY/FM)*10.**(-K))+(YMIN*10.**(-K))
 91       NQ=ND
       IF(.NOT.LOG)GO TO 92
       CALL NUMBR1(XA,YA,-.10,BASE,THETA,0)
       XEXP=999.
       YEXP=YA+.05
        IF(THETA.GT.45.)XEXP=XA-.05
        IF(THETA.GT.45.)YEXP=999.
       CALL NUMBR1(XEXP,YEXP,.07,VALUE,THETA,NQ)
       GO TO 93
C                WRITE NUMBER
   92  XA1=XA-XB*H1*(NQ+2)*0.5
       YA1=YA-YB*H1*(NQ+2)*0.5
       CALL NUMBR1(XA1,YA1,-H1,VALUE,THETA,NQ)
 93    TEST=XC+YC
C                         TEST IF TIME TO WRITE LABEL
       IF(TEST-HS-ST/2.)55,55,54
    54 XA=XA-XB*FM
       YA=YA-YB*FM
       XC=XC-FM*ABS(XB)
       YC=YC-FM*ABS(YB)
C                         DECREASE VALUE TO BE WRITTEN BY 1 UNIT
    81 VALUE=VALUE-DY*10.**(-K)
       TEST=XC+YC
C                         TEST IF PAST STARTING POINT OF AXIS
       IF(TEST   +.00005)30,91,91
    30 RETURN
C                         IS LABEL WRITTEN
    55 IF(SW)70,70,54
C                         WRITE LABEL
    70 SW=1.
       VAL=NC/2
       CP=HS-ST/2.-SS*VAL-E
       XD=X+XB*CP-KOD*(DIST+2.2*SS*FM)*YB
       YD=Y+YB*CP-KOD*(DIST+2.2*SS*FM)*XB
          NW=NC
       CALL SYMBOL(XD,YD,SS,BCD,THETA,NW)
```

```
C                       IS EXPONENT TO BE WRITTEN AFTER LABEL
      IF(K)53,54,53
C             WRITE 10 TO XX
   53 FNC=NC
      CP=H1*(FNC+1.)
      XD=XD+CP*XB
      YD=YD+CP*YB
      TEN=10.001
        CALL NUMBR1 (XD,YD,H1,TEN,THETA,0)
      HEXP=.7*H1
      XD=XD+2.*H1*XB-HEXP*YB
      YD=YD+2.*H1*YB+HEXP*XB
      CAY=K
      CALL NUMBR1(XD,YD,HEXP,CAY,THETA,0)
      GO TO 54
      END
```

Appendix B

COMPUTER PROGRAM USED TO CALCULATE AREAL AVERAGE EVAPOTRANSPIRATION

```
C***********************************************************************
C
C   Program to calculate patch and areal average evapotranspiration given
C   patch values of surface roughness (ZO), normalized available energy
C   (R), and canopy resistance (RC), as well as the proportions of area
C   covered by each patch type (ALPHA). Also input are the dimensionless
C   factor for regional advection (FAC, 'q' in the paper) and the overall
C   length of the modeled area (ELPP, 1' in the paper). Dimensions are
C   in meters.
C
C***********************************************************************
      DIMENSION RA(10),RC(10),R(10),E(10)
      COMMON ZO(10),ALPHA(10),HO,D,H,N
      GD=0.5
C***********************************************************************
C
C   Read the problem parameters. Currently programmed to read information
C   for two patch types only. N is the number of patch types.
      PRINT,'ENTER ALPHA(1), ALPHA(2)'
      READ(5,) ALPHA(1), ALPHA(2)
      PRINT,'ENTER RC(1), RC(2)'
      READ(5,) RC(1),RC(2)
      PRINT,'ENTER R(1), R(2)'
      READ(5,) R(1),R(2)
      PRINT,'ENTER ZO(1), ZO(2)'
      READ(5,) ZO1,ZO2
      PRINT,'ENTER FAC'
      READ(5,) FAC
      N=2
      PRINT,'ENTER L-PRIME IN METERS'
      READ(5,) ELPP
C   NI is the number of EL (1) values used.
      NI=ALOG10(ELPP)*2.+1.
C***********************************************************************
C
C   Loop to calculate evaporation for different values of the patch size.
C
      DO 100 I=1,NI
      ZO(1)=ZO1
      ZO(2)=ZO2
      HO=50.
      ELLOG=-.5+0.5*I
      EL=10.**ELLOG
C
C   Non-dimensionalize the parameters.
C
      DO 20 J=1,N
   20 ZO(J)=ZO(J)/EL
      HO=HO/EL
      ELP=ELPP/EL
      D=1./EL
C
C   Find the effective surface roughness, ZOE.
C
      CALL EFRUF(ZOE)
C
C   Find dimensionless aerodynamic resistances, RA, R1, and R2.
C
      CALL RESIST(ZOE,ELP,RA,R1,R2)
C
```

```
C   Calculate the mean (EVAP) and the patch (E) evaporation, normalized.
C
      S1=0.
      S2=0.
      DO 30 J=1,N
      A1=1./(1.+GD*(1.+RC(J)/RA(J)))
      S1=S1+ALPHA(J)*A1*(R(J)+FAC/RA(J))
   30 S2=S2+ALPHA(J)*A1*R2/RA(J)
      EVAP=(S1+S2)/(1./(1.+GD)+S2)
      DO 40 J=1,N
   40 E(J)=(R(J)+FAC/(RA(J))+(R2/RA(J))*(1.-EVAP))/
     *  (1.+RC(J)/(RA(J)*(1.+1./GD)))
      PRINT, 'L=',EL,'       EVAP=',EVAP
      PRINT, (E(J),J=1,N)
  100 CONTINUE
      STOP
      END
C*************************************************************************
C
      SUBROUTINE EFRUF(ZOE)
C
C   Calculate the effective surface roughness.
C
      EXTERNAL F
      COMMON ZO(10),ALPHA(10),HO,D,H,N
      ZMIN=1.E10
      ZMAX=0.
      DO 10 I=1,N
      ZMIN=AMIN1(ZMIN,ZO(I))
   10 ZMAX=AMAX1(ZMAX,ZO(I))
      MAXFN=100
C
C   ZBRENT is an IMSL subroutine to find the root of a user-supplied
C   function 'F' and return it in ZMAX. Initially, ZMIN and ZMAX are
C   user-supplied bounds on the root.
C
      CALL ZBRENT(F,1.E-6,20,ZMIN,ZMAX,MAXFN,IER)
      ZOE=ZMAX
      RETURN
      END
C*************************************************************************
C
      FUNCTION F(Z)
C
C   Return the residual in the equation for the effective surface roughness.
C
      COMMON ZO(10),ALPHA(10),HO,D,H,N
      H=HH(HO,Z,D)
      ARG1=ALOG(H)
      ARG2=ARG1+H/HO
      ARG=ARG2-ALOG(Z)
      F=1./(ARG*ARG)
      DO 10 I=1,N
      ARG=ARG2-ALOG(ZO(I))
   10 F=F-ALPHA(I)/(ARG*ARG)
      RETURN
      END
C*************************************************************************
C
      SUBROUTINE RESIST(ZOE,ELP,RA,R1,R2)
```

```
C
C   Calculate normalized aerodynamic resistances.
C
      COMMON ZO(10),ALPHA(10),HO,D,H,N
      DIMENSION RA(10)
      C=2.5
      ARG1=ALOG(H)+H/HO
      DO 10 I=1,N
      ARG=ARG1-ALOG(ZO(I))
   10 RA(I)=C*ARG*ARG/(ARG1-ALOG(ZOE))
      R1=C*(ARG1-ALOG(ZOE))
      HPC=HO**1.25*ZOE**-0.25
      IF(HPC.GE.ELP) HP=ZOE**0.2*ELP**0.8
      IF(HPC.LT.ELP) HP=HO+SQRT(D*(ELP-HPC))
      R2=C*(HP/HO+ALOG(HP)-ALOG(ZOE))-R1
      RETURN
      END
C*****************************************************************************
C
      FUNCTION HH(HO,Z,D)
C
C   Calculate the height of a boundary layer at a given fetch.
C
      HC=HO**1.25*Z**-0.25
      IF(HC.GE.1.) HH=Z**0.2
      IF(HC.LT.1.) HH=HO+SQRT(D*(1.-HC))
      RETURN
      END
```